

Max-Planck-Institut für Biochemie
Abteilung Membran- und Neurophysik

Genetically Targeted Staining of Cells with Voltage Sensitive Dyes using an Ecto-Enzyme

Marlon Jakob Hinner

Vollständiger Abdruck der von der Fakultät für Chemie
der Technischen Universität München zur Erlangung des akademischen Grades eines

Doktors der Naturwissenschaften

genehmigten Dissertation.

Vorsitzender: Univ.-Prof. Dr. O. Nuyken
Prüfer der Dissertation: 1. Hon.-Prof. Dr. P. Fromherz
2. Univ.-Prof. Dr. T. Bach
3. Univ.-Prof. Dr. M.-E. Michel-Beyerle, i.R.

Die Dissertation wurde am 22.12.2004 bei der Technischen Universität München eingereicht
und durch die Fakultät für Chemie am 8.03.2005 angenommen.

Abstract

Fast Voltage Sensitive Fluorescent Dyes are membrane-bound, optical probes of membrane potential. They are used to measure voltage transients in nerve cells. Recording signals from individual cells in tissue requires selective staining of these cells. In this work, a novel approach to this unsolved issue is presented. It relies on non-binding dye precursors that are locally activated to bind to cell membranes by the hydrolytic action of a selectively overexpressed, membrane bound enzyme.

Based on the structure of the common voltage sensitive hemicyanine dye Di-4-ASPBS, a number of dyes with additional alcohol residues were synthesized. These were introduced either at the hydrophilic headgroup appendix or at the lipophilic tail of the amphiphilic dyes. By further reaction of the alcohol moieties to phosphate groups, potential dye precursors for enzyme induced binding were obtained.

It was shown that phosphorylation of the headgroup appendix reduced membrane binding by a factor of 16 to 22 for various dyes. Phosphorylation at the lipophilic tail reduced binding drastically by a factor of 1000 to 10000.

An enzymatic assay revealed that all phosphate containing dyes were quantitatively hydrolysed to the respective alcohols by Alkaline Phosphatase from the Human Placenta (PLAP). Using this reaction, fluorescent dye binding activation to model membranes was studied with soluble PLAP and small lipid vesicles, giant lipid vesicles or red blood cells.

To obtain a membrane-bound and plasma-membrane targeted construct of PLAP, the gene of a fusion protein of soluble PLAP and an artificial membrane anchor was cloned. This construct was overexpressed in the adherent mammalian cell lines HEK293 and MDCK, and its correct targeting and functionality was ascertained by immunocytochemical and histochemical methods.

Incubation of phosphatase expressing cells with dye precursors led to staining of their cell membrane by enzymatic activation of dye binding. Selective staining of phosphatase-expressing cells was successfully implemented when transfected and non-transfected cells were cultured together and incubated with precursor dye.

In accordance with a theoretical model of the reaction, the prerequisites of selective staining were a very strong membrane binding of the produced dye and a sufficiently large difference in binding strength compared to the precursor dye.

Contents

1	Introduction.....	1
1.1	Current Neurobiology	1
1.2	Voltage Sensitive Dyes – A Tool in Need of Improvement	1
1.3	Enzyme Induced Selective Staining.....	3
1.4	Thesis Overview.....	4
2	Modified Voltage Sensitive Dyes and their Membrane Interaction	7
2.1	Synthesis and Spectroscopic Properties	7
2.2	Lipid Binding.....	13
2.3	Electrostatic Influence on Binding.....	22
2.4	Membrane Permeation.....	25
2.5	Orientation of Tail-Modified Dye in Membranes.....	28
2.6	Materials and Methods.....	30
3	Enzyme Induced Staining of Membranes by a Soluble Enzyme	37
3.1	Enzymatic Hydrolysis of Phosphorylated Dyes.....	37
3.1.1	Soluble PLAP Accepts all Dye Substrates	37
3.1.2	Hydrolysis Kinetics of Di-4-ASPMP measured by ITC	39
3.2	Enzyme Induced Staining of Liposomes.....	40
3.3	Enzyme Induced Staining of Giant Vesicles.....	44
3.4	Enzyme Induced Staining of Erythrocyte Membrane	46
3.5	Materials and Methods.....	48
4	Genetic Targeting of an Enzyme to the Plasma Membrane.....	51
4.1	Background	51
4.2	Plasma Membrane Targeting Signal for the Construction of Chimeras	53
4.2.1	Design of the Construct ArtPlasMA.....	53
4.2.2	Gene Synthesis of ArtPlasMA.....	55
4.3	Chimera of ArtPlasMA and PLAP (ArtPlasMA AP).....	57
4.3.1	Immunocytochemical Detection – Western Blotting.....	58
4.3.2	Immunocytochemical Detection – Immunofluorescence.....	59
4.3.3	Histochemical Detection.....	62
4.3.4	Activity Determination of HEK293 Stably Expressing ArtPlasMA AP	62
4.4	Conclusion.....	64
4.5	Materials and Methods.....	66

5	Cell Activated Staining with a Voltage Sensitive Dye	71
5.1	Enzyme Induced Staining on Stably Phosphatase Expressing HEK293	71
5.1.1	Di-10P-ASPBS	71
5.1.2	Di-12P-ASPBS	73
5.2	Enzyme Induced Staining on Stably Expressing HEK293 vs. Native Cells	74
5.2.1	Di-10P-ASPBS	74
5.2.2	Di-12P-ASPBS	74
5.2.3	Staining and Destaining after Removal of the Dye Precursor	76
5.3	Enzyme Induced Staining: Profiles of Dye Diffusion	77
5.3.1	Di-10P-ASPBS	77
5.3.2	Di-12P-ASPBS	77
5.4	Enzyme Induced Staining on MDCK Transiently Expressing Phosphatase.....	80
5.5	Model of Enzyme Induced Staining	82
5.6	Discussion	84
5.7	Materials and Methods.....	89
6	Final Conclusion and Outlook.....	91
7	Appendix	95
7.1	Additional Experiments	95
7.1.1	A Study on Gene Synthesis: LCR vs. PCR and the Origin of Mutation ..	95
7.1.2	Comparison of an Artificial and a Natural Targeting Signal	110
7.2	Expanded Background	117
7.2.1	Lipids and Vesicles	117
7.2.2	Human Alkaline Phosphatases	119
7.3	Tables	121
7.3.1	Human and Yeast Codon Usage	121
7.3.2	Oligonucleotides used for the Synthesis of <i>ArtPlasMA</i>	121
7.3.3	Oligonucleotides used for the Synthesis of <i>AsglypMA</i>	122
7.3.4	Oligonucleotides used for the Synthesis of <i>ArtPlasMA sine TM</i>	122
7.4	Vector Maps	123
7.5	Abbreviations.....	124
7.5.1	General Abbreviations.....	124
7.5.2	Nomenclature of the Dyes	125
8	Literature.....	127

1 Introduction

1.1 Current Neurobiology

The study of the human brain's function is undoubtedly one of the most fascinating fields of science today. Finding out why human beings act the way they do has always been a fundamental question. In the last decades, however, the elucidation of complex neurobiological processes seems to have come into grasp. The truly multidisciplinary effort of all natural sciences, engineering and informatics has helped us to understand the basic neuronal principles of sensory transduction, perception and motion. The experimental size scale under study ranges from single proteins to cells, to areas of the brain or even the whole nervous system. Naturally, the methods employed have to be well adapted to the studied problem, and new insights have been gained by the development of new methods and their application in neurobiology. Prominent examples are the patch-clamp technique, positron emission tomography and the modern techniques of molecular and cell biology. Although much has been learned, more complex problems such as memory, learning or behavior are still not well understood. The development and the improvement of techniques that allow the study of neuronal ensembles is therefore a necessary and promising task.

1.2 Voltage Sensitive Dyes – A Tool in Need of Improvement

Voltage Sensitive Fluorescent Dyes are powerful probes to directly study neuronal processes. Signal transmission in nerve cells takes place by the unidirectional propagation of changes in the cell's membrane potential. Due to their amphiphilic nature, the so-called "fast" class of voltage sensitive dyes integrates into cell membranes and exhibits a change in fluorescence that reflects changes in the local membrane potential. The exceptionally large charge shift in the chromophore of these dyes upon excitation (and emission) interacts with the electric field across the membrane, leading to electrochromic ("Stark effect") shifts in the dye spectra.^{1,2} For most dyes, the fluorescence is also modulated by solvatochromic effects.² Prominent examples of Fast Voltage Sensitive Dyes are depicted in Figure 1. The most

sensitive dye known so far is ANNINE 6.^{1,2} Using two-photon excitation, it shows fractional changes in fluorescence of up to 70 % for a 100 mV change in membrane potential.³

Voltage Sensitive Fluorescent Dyes have been successfully used in cultured nerve cells and nerve tissue.⁴⁻⁶ The main advantage of these *optical recording* probes over classical electrophysiological techniques is their high spatial resolution. The number of electrodes that can be placed in a neuron or a tissue preparation is limited by the available space – let alone the difficulty in handling multiple electrodes. The spatial resolution that is achieved with voltage-sensitive dyes is, in principle, only limited by the resolution and sensitivity of the dyes, optics and recording equipment.

Although Voltage Sensitive Dyes have been known for many years, their decisive breakthrough has yet to come. The first exemplary measurement was published as early as 1968 by Tasaki and coworkers⁷ which used the dye 8-Anilino-naphthalenesulfonate (8-ANS, Figure 1). In the following decades, the groups of Cohen, Grinvald, Loew and Fromherz improved the dye sensitivity and recording technique, and the origin of fluorescent voltage sensitivity was elucidated.^{1,2,8-14} However, Voltage Sensitive Dyes are still not established as a standard, widely used technique, in contrast to the alternative method of Calcium-Imaging. This is due to limitations of the technique imposed by pharmacological side effects and phototoxicity, sensitivity, photostability, and unselective staining.

The latter limitation originates from the fact that common extracellular application of the dyes leads to the staining of all cells in a preparation. As a consequence, voltage transients of individual neurons in tissue cannot be measured. It is technically infeasible to resolve the membrane fluorescence of the widely ramified structure of a single neuron closely

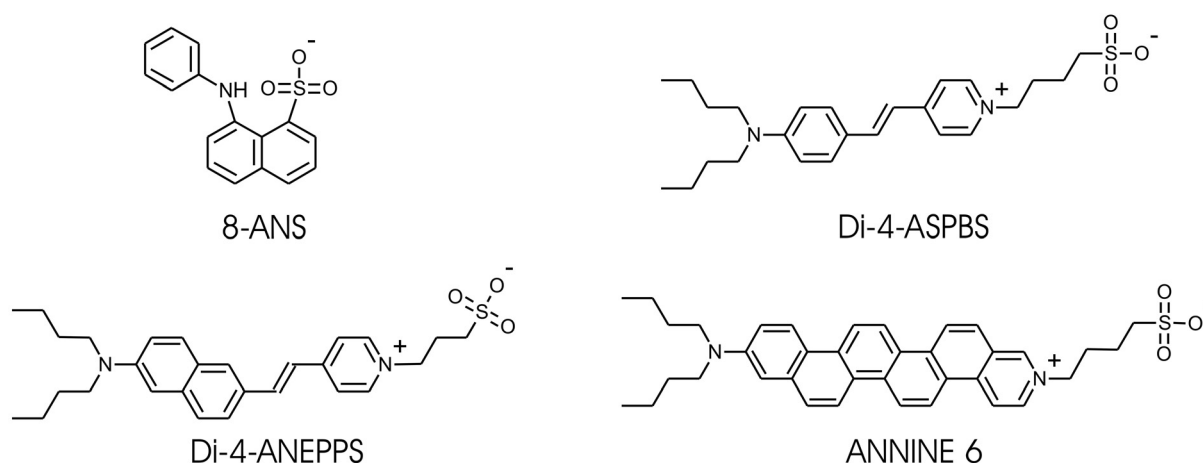


Figure 1. Fast Voltage Sensitive Fluorescent Dyes.

surrounded by other stained cells. Significant progress would be achieved if a satisfactory method for selective staining of individual neurons or groups of neurons were available. So far, intracellular application of dyes has been considered.^{15,16} With this method, however, intracellular structures are stained with the concomitant effects of background fluorescence and phototoxicity. In addition, slow intracellular diffusion may lead to incomplete staining. Attempts using genetically encoded fluorescent proteins with intrinsic voltage sensitivity have had modest success hitherto.^{17,18}

1.3 Enzyme Induced Selective Staining

In this thesis, a completely novel technique for selective staining is proposed and explored. The envisaged method relies on extracellular application of an organic precursor dye and its local activation at a selected cell by a genetically encoded enzyme. Such activation could rely on an induction of fluorescence quantum yield, of voltage sensitivity or on an induction of the interaction with the membrane. The latter approach is particularly attractive because the crucial chemical structure of the voltage-sensitive chromophore would not be affected by enzymatic activation. In the envisaged concept shown in Figure 2, a nerve cell in brain tissue is genetically induced to express a membrane-bound enzyme with its active site facing the extracellular space. This ectoenzyme cleaves off a polar group of a weakly binding, water soluble precursor dye such that the overall lipophilicity of the dye is enhanced. As a consequence, the voltage-sensitive dye binds selectively to the adjacent cell membrane.

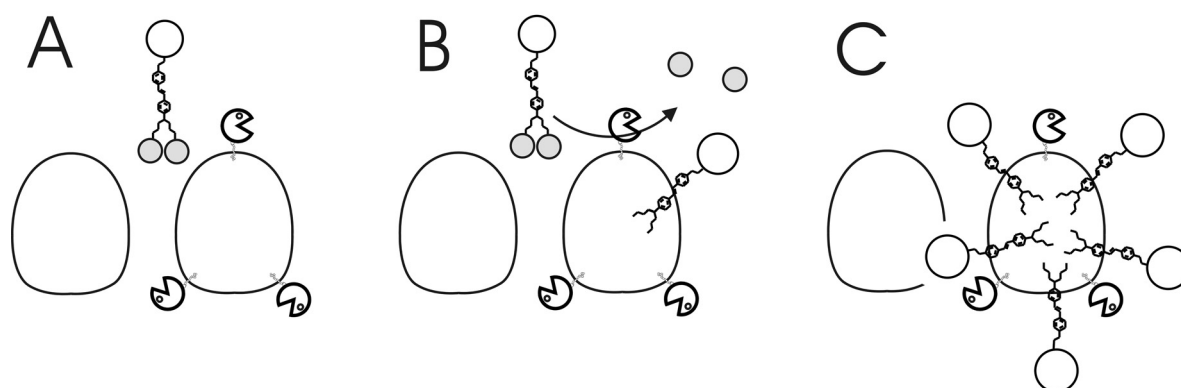


Figure 2. Concept for enzyme induced selective staining of cells. (A) The two components are a voltage sensitive dye derivatized with an enzymatically cleavable polar group (represented by gray circles) and an ectoenzyme expressed on the surface of a selected cell in a tissue symbolized by two cells. The polar headgroup of the dye is depicted as a white circle. (B) The dye is hydrolysed by the ectoenzyme. Upon cleavage of the polar group, the dye binds to the membrane. (C) Cleaved dye accumulates in the membrane of the cell where it was produced.

1.4 Thesis Overview

The feasibility of enzyme induced selective staining has been tested in detail. The main results of the work are described in Chapters 2-5. As far as possible, the chapters are organized as independent subunits of the work. For this reason, every chapter contains its own Materials and Methods section.

Chapter 2 deals with the synthesis and physicochemical properties of dye precursors that could exhibit enzymatically inducible membrane binding. In the test system, the simple voltage sensitive styryl hemicyanine Di-4-ASPBS (cf. Figure 1) was modified by the addition of one or more phosphate groups. A number of new dye phosphates and their corresponding hydrolysis products, the dye alcohols, were examined with regard to spectroscopy, membrane binding and membrane permeation.

Chapter 3 describes enzyme induced membrane binding with soluble enzyme. First, the susceptibility of the dye precursors to hydrolysis by soluble alkaline phosphatase from the human placenta (PLAP) was explored. Exploiting the increase in the dyes' membrane binding strength upon enzymatic hydrolysis, enzyme induced binding in solution was implemented with liposomes. Then, the staining method was tested with individual giant lipid vesicles and red blood cells.

In Chapter 4, the genetic targeting and stable anchoring of PLAP at the extracellular side of the plasma membrane of transfected cells is described. To that end, a special DNA construct encoding a 22 Leucine membrane targeting signal and anchor was fabricated by gene synthesis. The construct, termed *ArtPlasMA*, additionally contains standard epitope tags to facilitate immunochemical detection, and a multiple cloning site that allows the construction of sandwich fusion proteins. Such a fusion protein or *chimera* was produced with PLAP, and the resulting protein *ArtPlasMA AP* was overexpressed in HEK293 cells and characterized in regard to size, subcellular localization and activity by immunochemical, histochemical and spectroscopic methods.

In Chapter 5, all previously described elements are combined to implement *Genetically Targeted Staining of Cells with Voltage Sensitive Dyes using an Ecto-Enzyme*. Tail modified dye precursors were incubated with cells stably or transiently transfected with *ArtPlasMA AP*, and the hydrolysis reaction taking place at the plasma membrane was followed by fluorescence microscopy. The time course of staining was rationalized with a reaction-diffusion model.

In the final Chapter 6, conclusive remarks and a detailed outlook to further optimization of the method, as well as its possible applications, are presented.

The appendix contains tables, abbreviations, vector maps and an expanded background section with additional information on *Lipids and Vesicles* and *Alkaline Phosphatases*.

In addition, two sections in the appendix describe additional work performed, of which the first deals with the origin of mutations in gene synthesis and the second describes further experiments with the membrane anchor construct *ArtPlasMA* and a slightly modified construct termed *AsglypMA*, which contains a natural targeting signal in place of the 22 Leucine sequence.

This work relied on many helping hands, and the last page gives credit to the invaluable cooperation and advice that I received. I want to especially emphasize that the synthesis of the dyes was performed by Gerd Hübener and his assistants. Still, the synthetic routes to the dyes are crucial to this work and are therefore included in the Materials and Methods section of Chapter 2.

Parts of this work have been published prior to completion of the thesis.¹⁹

2 Modified Voltage Sensitive Dyes and their Membrane Interaction

In this section, the syntheses, spectroscopic properties and binding to lipid membranes of several voltage sensitive dyes of the hemicyanine type are described. These are derivatives of Di-4-ASPBS^{13,20} (for nomenclature, cf. section 7.7.1) which have been modified by the addition of one or more polar hydroxyl or phosphoric acid ester residues. The phosphate containing dyes are potential precursors for the enzyme induced staining of membranes. The phosphate residue was chosen for two reasons: (i) It possesses a high polarity due to its two negative charges in moderately alkaline solution, with acidity constants of phosphate monoesters being $pK_{a1} \approx 1$ and $pK_{a2} \approx 6$.²¹ A strong decrease in membrane binding strength should depend on a strong polarity of the introduced residue. (ii) Activation, i.e. conversion into the more strongly membrane bound form, could rely on alkaline phosphatase. This enzyme has a broad range of substrate specificity,²² increasing the chance that it might accept modified voltage sensitive dyes as substrates. Furthermore, it has been found that alkaline phosphatase can be overexpressed in transgenic mice without obvious toxic effects.²³

The additional aspects of membrane permeation, solubility and orientation in the membrane are also addressed shortly. Results and discussion are provided together in each subsection.

2.1 Synthesis and Spectroscopic Properties

Dyes used in this work. The parent compound of all the dyes synthesized for this work is Di-4-ASPBS (Figure 3, dye **1**). Di-4-ASPBS was either modified at the polar head group or at the hydrophobic tail. In both cases, also the length of the aliphatic chains at the lipophilic tail was varied. At the polar head, the sulfonate group of Di-4-ASPBS was exchanged by one or two alcohol groups (dyes **2**, **5**, **7**) to which phosphate groups (dyes **3**, **6**, **8**) or a diphosphate

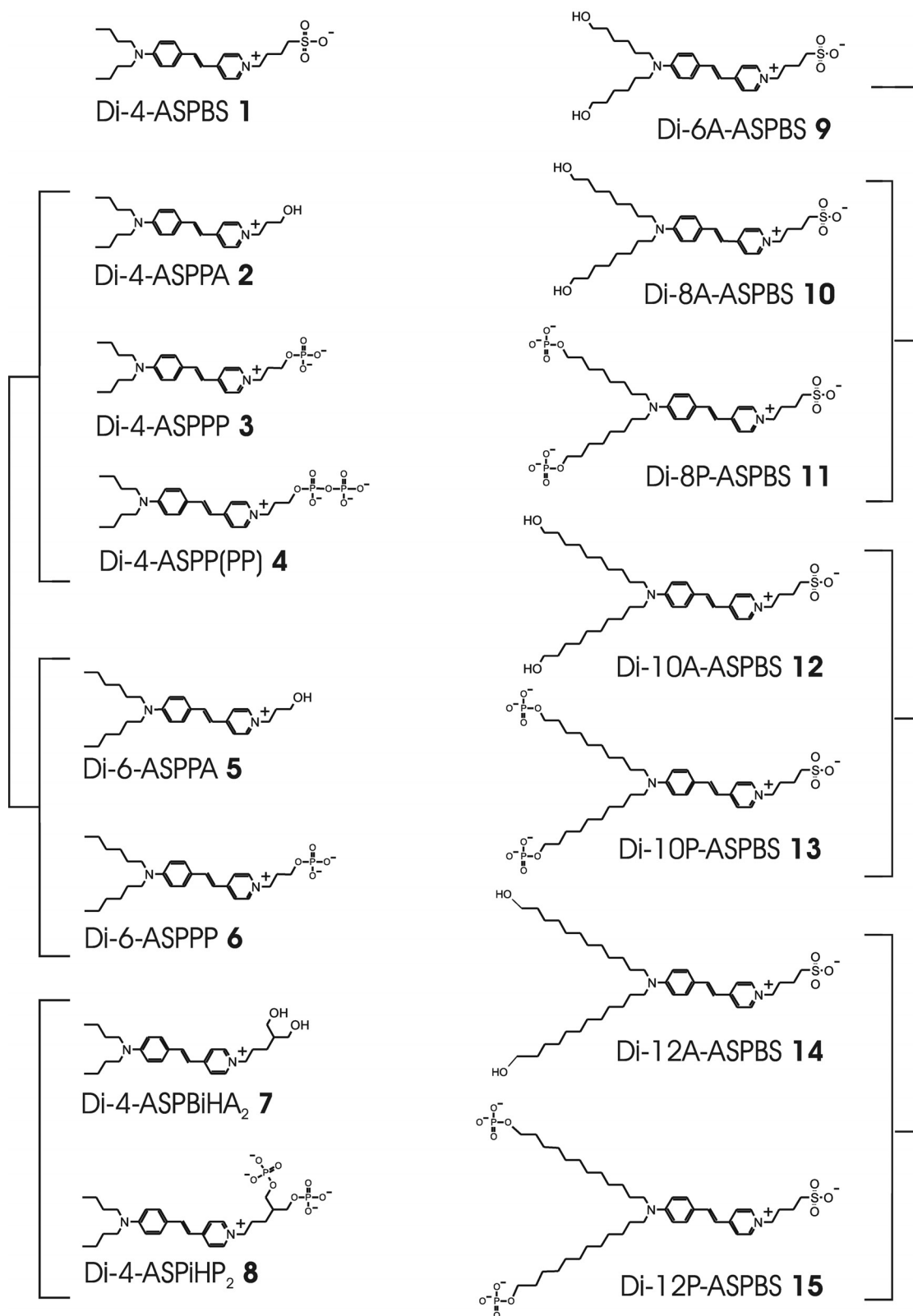


Figure 3. Dyes synthesized for and used in the presented thesis. The dyes are derivatives of the voltage sensitive hemicyanine Di-4-ASPBS (dye 1). They were modified at the hydrophilic headgroup appendix (dyes 2 to 8) or at the lipophilic tail (dyes 9 to 15). An alcohol group was introduced serving as a linker to a polar phosphate or diphosphate group. The relatedness of the dyes is indicated by brackets. The dyes are numbered consecutively. Their short names are oriented towards the nomenclature in ref.¹² (see also section 7.7.1).

group (dye **4**) were coupled. At the terminus of each of the aliphatic chains at the tail of the dyes an alcohol moiety was introduced (dyes **9**, **10**, **12**, **14**). Further derivatization led to the respective monophosphoric acid esters (dyes **11**, **13**, **15**).

In general, the dyes containing the alcohol functions were made in analogy to the synthesis of Di-4-ASPBS.²⁰ 4-bromoaniline was doubly alkylated at the aniline-nitrogen with the appropriate alkyl or hydroxyalkyl moiety and coupled to 4-vinylpyridine in a Palladium-catalyzed Heck reaction. Subsequently, the headgroup was introduced. Finally, the dye alcohols were further reacted to the corresponding phosphate compounds. The synthesis of the dyes was carried out by Dr. Gerd Hübener and his assistants, and it is described in detail in the Materials and Methods section.

The identity and purity of the dyes was proven by Nuclear Magnetic Resonance (NMR) and mass spectrometry and for most dyes also by elementary analysis.

Spectroscopy. An example of fluorescence excitation and emission spectra in aqueous solution and when bound to lipid is shown for Di-4-ASPPA and Di-4-ASPPP in Figure 4. The spectroscopic properties of the dyes are analogous to their parent compound Di-4-ASPBS as summed up in Table 1.

The maxima of absorption in aqueous buffer were around 480 nm (fluorescence emission around 630 nm) with an extinction coefficient around $3.9 \times 10^4 \text{ M}^{-1} \text{ cm}^{-1}$. In the less polar solvent ethanol, the maxima of absorption were red-shifted to around 495 nm. This solvatochromism originates from a change of the molecular dipole moment upon electronic excitation and its interaction with the polarizable environment, i.e., the solvent. With increasing solvent polarity, all hemicyanine dyes exhibit a symmetrical blue-shift of excitation energies and red-shift of emission energies.²⁴ This symmetrical shift has led to the deduction that in bulk solvents, the solvation energies of ground and excited state are nearly equal.²⁴ This is not true for dyes bound to membranes, since in that case the dyes are located at the membrane/water interface and the solvent shell exhibits a strongly anisotropic polarity. The solvation energy of the ground state is high, since the positive charge is located close to the polar interface. The excited state is destabilized by poor solvation compared to solvation in water, since the charge is shifted into the apolar interior of the lipid membrane. This is reflected by the spectroscopic data of lipid-bound dyes, which compared to the measured values in water exhibit similar fluorescence excitation, but strongly blue-shifted fluorescence emission (600 nm) maxima.

Some of the dyes showed deviations in some of the spectroscopic properties:

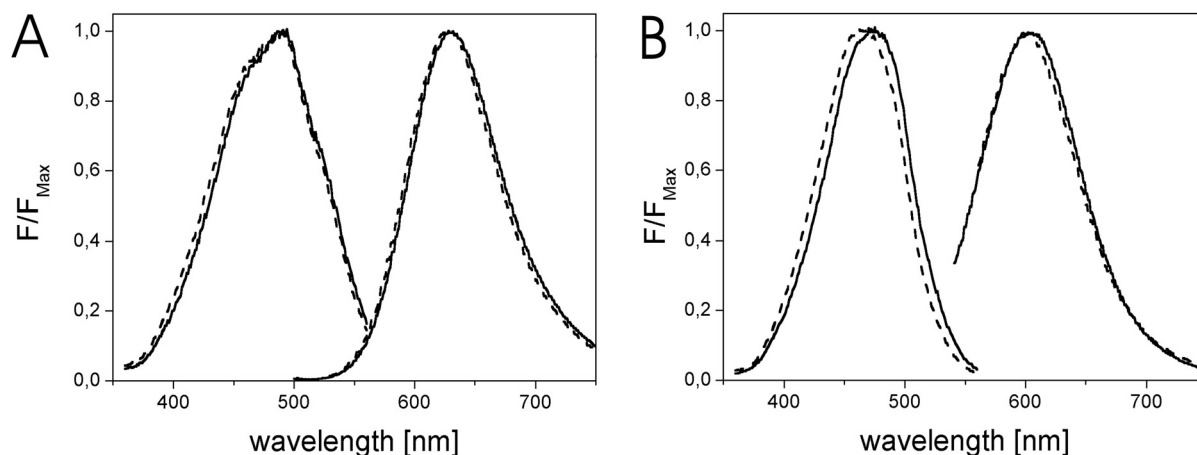


Figure 4. Fluorescence excitation and calibrated emission spectra (λ_{488nm}^{exc}) for Di-4-ASPPA (solid lines) and Di-4-ASPPP (broken lines). Excitation spectra were recorded with emission wavelengths of 630 nm in aqueous solution and 600 nm in lipid suspension, respectively. A. Spectra in aqueous solution at 5 μ M dye concentration. B. Spectra in lipid suspension at 0.5 μ M dye concentration. The lipid concentrations were 22 mM for Di-4-ASPPP and 1 mM for Di-4-ASPPA.

	$\lambda_{max}^{abs} [nm]$ H ₂ O	$\epsilon \times 10^4$ [M ⁻¹ cm ⁻¹]	Solubility at 4°C	$\lambda_{max}^{abs} [nm]$ EtOH	$\epsilon \times 10^4$ [M ⁻¹ cm ⁻¹]	$\lambda_{max}^{exc} [nm]$ H ₂ O	$\lambda_{max}^{em} [nm]$ H ₂ O	$\lambda_{max}^{exc} [nm]$ lipid	$\lambda_{max}^{em} [nm]$ lipid
Di-4-ASPBS ^a	478	3	8 μ M	495	5	-	635	465	597
Di-4-ASPPS ^a	482	4		492	5	-	635	467	595
Di-6-ASPPS ^a	468	4		496	6	-	635	467	595
Di-4-ASP Dicat	495	-	>1mM	506	-	-	640	-	-
Di-4-ASPPP	479	4.0	>1mM	492	4.7	490	629	464	601
Di-4-ASPPA ^b	482	3.9	\approx 1mM	499	5.3	490	631	475	604
Di-6-ASPPP	479		>1mM	493	5.0	492	627	466	599
Di-6-ASPPA	469	-	35 μ M	498	5.2	489	632	470	600
Di-4-ASPiHP ₂	476	3.7	>1mM	486	4.3	488	627	458	605
Di-4-ASPiHA ₂	481	3.9	0.2mM	499	5.1	490	630	475	606
Di-6A-ASPBS ^b	482	-	<1mM		-	490	630	477	610
Di-8P-ASBPS ^c	484	-	>1mM	492	-	491	630	-	-
Di-8A-ASPBS	483	-	6 μ M	505	-	491	632	478	608
Di-10P-ASBPS	485	4.1	>1mM	493	-	491	631	480	608
Di-10A-ASPBS ^d	456	-	3 μ M	496	n.d.	460 ^d	634	475	606
Di-12P-ASPBS	485		>1mM	496		494	630	465	604
Di-12A-ASPBS ^d	454		<0.1 μ M	496		457 ^d	690	459	597

Table 1. Spectroscopic properties of Di-4-ASPBS and derivates. Extinction coefficients are given for the dyes where elementary analyses were obtained and solubility in the respective solvent was sufficient. Lipid concentrations were adjusted to guarantee dye binding (cf. Table 2). ^aData from ref.¹². ^bExact solubility could not be determined since dye particles did not sediment. ^cSpectra in 22 mM lipid suspension were identical to spectra in aqueous environment, indicating no binding of the dye. ^dThe fluorescence excitation spectra were very broad. ^eIn ethanol, the fluorescence excitation and emission maxima of Di-12P-ASPBS and Di-12A-ASPBS were identical with fluorescence excitation at 494 nm and emission at 630 nm.

The dyes Di-6-ASPPS, Di-6-ASPPA, Di-10A-ASPBS and Di-12A-ASPBS exhibited a blue-shift of the absorption maximum in aqueous buffer by up to 25 nm. For Di-12A-ASPBS, the fluorescence emission maximum of the dye in water was changed as well: It was dramatically red-shifted to 690 nm and the spectrum was broadened (not shown). Both absorption and fluorescence changes were very likely due to the formation of dimers or higher aggregates, since all of the affected dyes are only very scarcely water soluble. In ethanol, these dyes are well soluble, and no relevant spectral shifts relative to the more water-soluble dyes occurred (Table 1).

In general, while absorption spectra (not shown) were of an “ideal” shape following a *log-normal*-distribution²⁵ with a single maximum, this was not the case for excitation spectra (Figure 4A). These either exhibited shoulders or were very broad, indicative of the spectra being a superposition of subspecies with slightly differing fluorescence excitation behaviour.

It is noteworthy that in aqueous buffer and ethanol, the absorption as well as the fluorescence emission maxima of the dyes were dependent of the charge z at the headgroup of the dye (Figure 5). The spectra were increasingly blue shifted in the order Di-4-ASP-propyl(trimethyl-)ammonium (Di-4-ASP Dication, $z = +1$), Di-4-ASPPA/Di-4-ASPiHA₂ (both $z = 0$), Di-4-ASPBS ($z = -1$), Di-4-ASPPP ($z = -2$) and Di-4-ASPiHP₂ ($z = -4$). With the exception of Di-4-ASP Dication, the shifts were linearly dependent on headgroup charge. In the relatively unpolar solvent ethanol, the shifts were much more prominent than in aqueous buffer. Fluorescence emission was less affected than absorption.

Within the framework of the monopole-dipole model of solvatochromism,²⁴ the observed spectral shifts can be ascribed to an intramolecular Stark effect. In this model, the solvatochromism of hemicyanine dyes is described by the interaction of only the chromophore with the solvation shell. The solvation of the charged headgroup is not changed upon excitation or emission. However, the headgroup of charge ze_0 interacts with the dipole moments of ground and excited state $\mu = e_0\delta/2$ (δ distance of charge shift upon excitation, e_0 elementary charge). According to eq 1, the energy E of the interaction is dependent on the distance d between the charge and the dipole, and it is dependent on the permittivity ϵ_r of the medium, relative to the permittivity of the vacuum ϵ_0 . In this equation, E is expressed in wavenumbers ($\tilde{\nu} = E/hc$, with h Planck’s constant, c speed of light in the vacuum).

$$\Delta\tilde{\nu}_{Stark} = \frac{ze_0 \times \delta e_0}{4\pi\epsilon_r\epsilon_0 d^2} \frac{1}{hc} \quad (1)$$

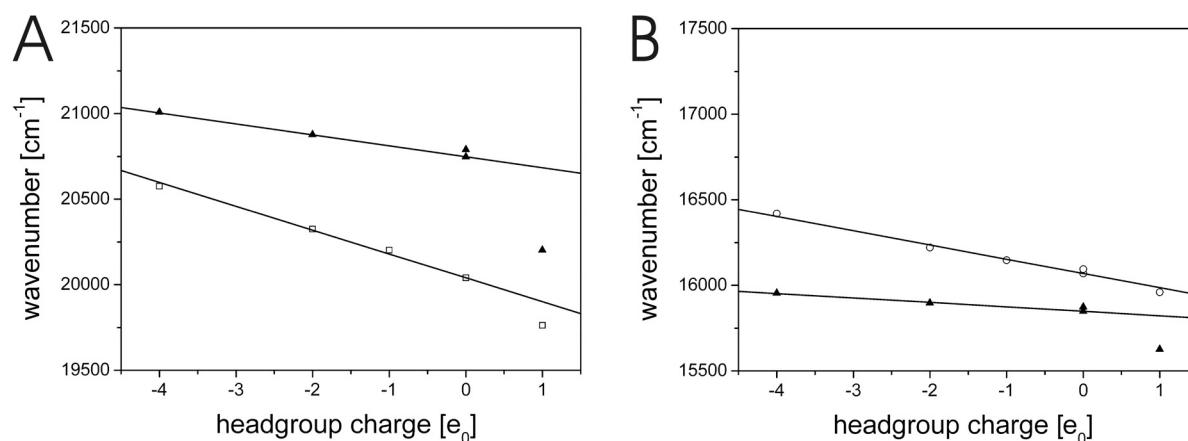


Figure 5. Intramolecular Stark effect. Absorption (A) and fluorescence emission (B) maxima of dyes with different headgroup charges in ethanol (circles) and aqueous buffer (triangles). The following dyes were investigated: Di-4-ASPiHP₂ ($z = -4$), Di-4-ASPPP ($z = -2$), Di-4-ASPBS ($z = -1$), Di-4-ASPiHA₂, Di-4-ASPPA (both $z = 0$) and Di-4-ASP propyl(trimethylammonium) ($z = +1$). The solubility of Di-4-ASPBS in water was not sufficient to reliably obtain data. Absorption maxima were evaluated by the proprietary software of the spectrometer. Fluorescence emission maxima were obtained from a log-normal²⁵ fit of the spectra. The data was fitted according to an intramolecular Stark effect (eq 1) and the obtained shifts were plotted relative to the absorption and fluorescence maxima of Di-4-ASPPA (solid lines).

For Di-4-ASPBS, $\delta = 0.217nm$ as obtained by quantum chemical calculations.²⁴ The observed spectral shifts of absorption in water ($\epsilon_r = 80$) and ethanol ($\epsilon_r = 25$) were in good accord with eq 1 inserting a distance between charge and dipole moment of $d_{abs}^{H_2O} = 0.7nm$ and $d_{abs}^{EtOH} = 0.85nm$, respectively. The calculated charge shifts are plotted in Figure 5A relative to the absorption maximum of Di-4-ASPPA which contains an uncharged headgroup (solid lines). The obtained distances are within a very reasonable range: For the fully stretched Di-4-ASPBS, the calculated distance between the sulfonate and the centre of the chromophore amounts to $d \approx 1nm$ using characteristic bond lengths and angles. Smaller distances are possible due to the flexibility of the spacer between pyridinium and the charged headgroup appendix.

The shifts in fluorescence emission maxima were decreased compared to the shifts in absorption (Figure 5B). Using d as the free parameter, the experimental data was in accord with eq 1 for both solvents at $d_{em} = 1.1nm$ (Figure 5B, solid lines). This implies that the distance between the charged headgroup and the dipole in the excited state increases after excitation and relaxation of the solvent shell, e.g. by stretching the linker to its full length.

The red shifts of excitation and emission observed with Di-4-ASP Dication are far too large to be explained by an intramolecular Stark effect in terms of the monopole-dipole model. Obviously, changes in the intramolecular and solvent reorganization energies as well as changes in solvation energies are dominant for this dicationic derivate.

For the tail modified dyes, there is no clear trend in absorption maxima between those containing phosphate and those containing alcohol groups, indicating that there is no specific interaction between the chromophore and the phosphate groups in this case.

Solubility. The solubility in aqueous buffer of voltage sensitive dyes is an important parameter, since the notorious insolubility of the larger dyes like ANNINE 6 or Di-8-ANEPPS makes it difficult to obtain reproducible and strong membrane stainings. In addition, good solubility is the prerequisite for the application in intracellular staining methods. Tris-NaCl buffer was given to each dye in order to obtain 1 mM solutions, and in the cases where the dye did not dissolve completely at 4°C, the amount of dye in solution was measured by UV/Vis-Spectroscopy. According to the data in Table 1, all dyes containing phosphate moieties as well as the doubly positively charged Di-4-ASP Dication are soluble >1 mM. The non-phosphorylated dyes were much less soluble, and the solubility decreased with the length of the alkyl chain and it was increased when the dye carried a net charge. For example, the solubility of the tail-modified dyes decreased from 0.5mM for Di-6A-ASPBS to <0.1µM for Di-12A-ASPBS, and the cationic Di-4-ASPPA exhibited a vastly higher solubility than the zwitterionic Di-4-ASPBS.

2.2 Lipid Binding

The basic structural component of cell membranes are double layers of amphiphilic lipids like the phosphatidylcholines (cf. section 7.3.1 Lipids and Vesicles). Due to their amphiphilic nature, Voltage Sensitive Dyes of the styryl hemicyanine type insert into lipid membranes. It has been found that the binding of such dyes to lipid membranes follows a partitioning law,²⁶ in agreement with the membrane binding of amphiphiles in general.²⁷ For dyes carrying a net charge, an additional consideration of electrostatic effects that can be treated by the Gouy-Chapman theory^{28,29} is necessary. For low dye concentrations and/or low binding constants electrostatic effects are negligible, and they will be omitted here, but this issue will be treated in section 2.3.

There are quite a number of methods available to assess the binding strength of proteins, peptides or small organic molecules to lipid bilayers, most important of which are Isothermal Titration Calorimetry,³⁰⁻³² Gel Filtration³³, Ultracentrifugation methods of Sucrose Filled Lipid Vesicles,³⁴ Quenching³⁵ and other spectroscopic methods (cf. the extensive review by Santos et al.³⁶). The favourite model system for water/membrane transfer is n-octanol/water

partitioning,³⁷ which, however, has the disadvantage that it is not applicable without restrictions to charged (cf. e.g.³⁸) and amphiphilic (cf. e.g.³⁹) compounds.

Spectroscopic methods are to be preferred if the (macro-)molecule of interest exhibits a change in spectroscopic properties upon binding, such as a change in fluorescence intensity, lifetime or anisotropy. When styryl hemicyanines bind to lipid bilayers, their quantum yield of fluorescence is enhanced. Di-4-ASPBS, for example, shows a 36-fold increase in fluorescence quantum yield upon transfer from water to lecithin membranes.⁴⁰ This is the basis for the technique used in this work, namely fluorescence titration.²⁶

Theory. With respect to the overall concentrations in the dispersion $c_{D,b}$ and $c_{D,f}$ of bound and free dye, the partition equilibrium can be expressed in terms of the lipid concentration c_L and a binding constant of the dye K_D as $c_{D,b} = K_D c_L c_{D,f}$.²⁶ Note that this relation has the form of a mass action law, but does not imply that there is a 1:1 molecular association of dye and lipid molecules.²⁶ With the total dye concentration $c_D = c_{D,b} + c_{D,f}$ one obtains eq 2.

$$c_{D,b} = \frac{1}{1 + (1/K_D c_L)} c_D \quad (2)$$

In fluorescence lipid titration, a constant, low amount of dye is given to various concentrations of a dispersion of large lipid vesicles ($\varnothing \approx 100nm$) and fluorescence is measured. According to eq 2, the relative amount of bound dye increases with the lipid concentration. Due to the increased fluorescence of bound dye, the overall fluorescence of the dispersion increases. With the low and high specific fluorescence intensities $f_{D,f}$ and $f_{D,b}$ of free and bound dye, the total fluorescence intensity is $F_D = f_{D,f} c_D + (f_{D,b} - f_{D,f}) c_{D,b}$. Considering eq 2, it increases with the concentration of lipid according to eq 3.²⁶

$$F_D = c_D \left[f_{D,f} + \frac{f_{D,b} - f_{D,f}}{1 + (1/K_D c_L)} \right] \quad (3)$$

Dispersions of large lipid vesicles ($\varnothing \approx 100nm$) were made from palmitoyl-oleoyl-phosphatidylcholine (POPC) with lipid concentrations ranging over five orders of magnitude. Dye was generally added to a concentration of 0.5 μM and fluorescence was measured. Figure 6 shows typical measurements for the types of dyes mainly used in this work. These are Di-4-ASPPP and Di-4-ASPPA, modified at the hydrophilic head (Figure 6A), and Di-10P-ASPBS

and Di-10A-ASBPS, modified at the lipophilic tail (Figure 6B). For comparison, the binding curve for the parent compound Di-4-ASPBS is included in Figure 6A. Other dyes examined include variants of these dyes with different aliphatic chain lengths as well as those with branched headgroups or diphosphoric acid ester residues (cf. Figure 3). The data was fitted with eq 3 as shown in Figure 6 assuming that only the outer vesicle monolayer is stained, using an effective lipid concentration $c_{L,eff} = c_L / 2$. Asymmetry of staining was demonstrated for Di-4-ASPBS in black lipid membranes where it was a prerequisite for voltage sensitivity.⁴¹ The results of the fits are summed up in Table 2 for all dyes.

Limitations. Before proceeding to a discussion of the data, the limitations of the technique of fluorescence lipid titration shall be briefly mentioned. Note that the reproducibility of the measurement of high binding constants is rather poor. This probably originates from competing processes like lipid solubilization and aggregation/disaggregation of the dyes, as well as from adsorption of the lipid to the reaction and storage vessels³⁴ which is not negligible at low lipid concentrations. Since equilibration is generally slow with strongly binding dyes, long incubation times and ultrasonication are necessary.²⁶ This possibly intensifies negative side effects of lipid solubilization and adsorption. Also, the concentration ratio of bound dye and lipid is high at large binding constants, possibly leading to fluorescence quenching. The data of Di-12A-ASPBS was therefore obtained at a reduced dye concentration of 50 nM. For weakly binding dyes such as Di-10P-ASPBS, only a limited amount of data points can be obtained and the data is possibly influenced by light scattering of the turbid sample at high lipid concentrations. The fitted binding constants of weakly binding dyes must therefore be considered as approximate (Figure 6B).

Note also that fitting the lipid titration data for the charged Di-6-ASPPA with eq 3 leads to a large underestimation of the true binding constant due to the strong influence of electrostatic effects (cf. section 2.3). This dye is therefore not included in the discussion of this section.

Phosphate at the headgroup. Let us first take a look at the binding constants of the dyes Di-4-ASPPP and Di-4-ASPPA with the modification at the headgroup appendix and at Di-4-ASPBS for comparison. The average binding constants are $K_A = 17920 \pm 360 M^{-1}$ for the alcohol (n=5), $K_S = 7500 \pm 440 M^{-1}$ for the sulfonate (n=2) and $K_P = 1140 \pm 140 M^{-1}$ for the phosphate (n=7). The binding constant decreases when the dye bears a negatively charged headgroup.

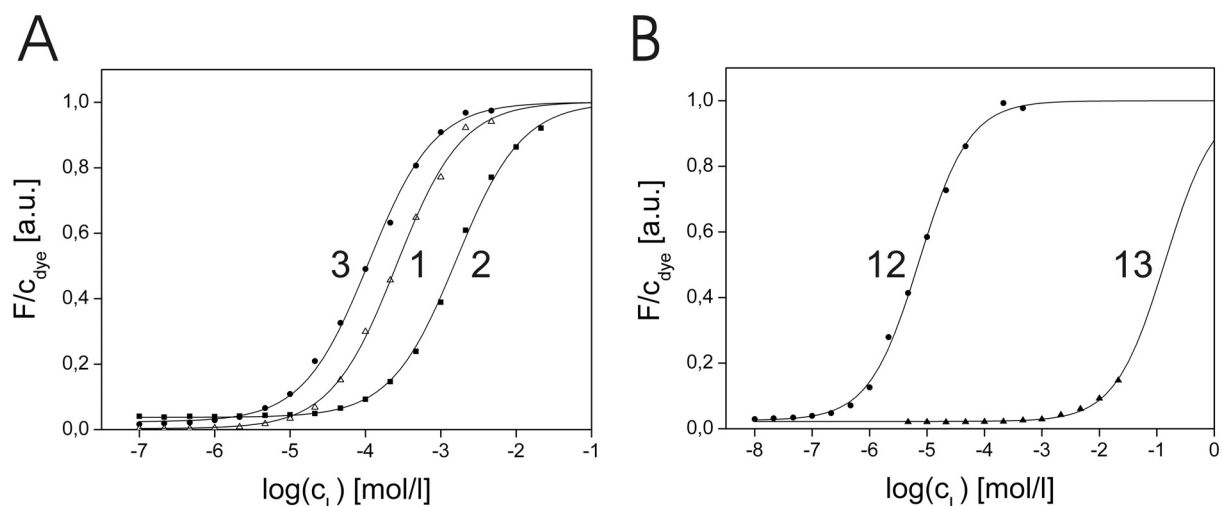


Figure 6. Fluorescence Titration with lipid. The ratio F/c_D of fluorescence intensity and total concentration of dye versus the logarithm of the lipid (POPC) concentration c_L in a dispersion of lipid vesicles. (A) Typical measurements for Di-4-ASPBS (1), Di-4-ASPPP (2) and Di-4-ASPPA (3); (B) Typical measurements for Di-10A-ASPBS (13) and Di-10P-ASPBS (12). The data are fitted by a partitioning equilibrium with a molecular binding constant K_D and specific fluorescence intensities $f_{D,f}$ and $f_{D,b}$ of free dye in water and bound dye in lipid. For the sake of clarity, the data were normalized to $f_{D,b} = 1$ for each dye.

Dye	K_D [M^{-1}]	standard deviation	n
Di-4-ASPBS	7500	440	2
FM1-43 ^a	11500	-	-
Di-4-ASPB Dication	10400	-	1
Di-4-ASPPA	17920	360	5
Di-4-ASPPP	1140	140	7
Di-4-ASPP(PP)	890	-	1
Di-6-ASPPA ^b	190000	22000	2
Di-6-ASPPP	26200	19200	3
Di-4-ASPB _i HA ₂	15600	650	2
Di-4-ASPB _i HP ₂	700	40	2
Di-6A-ASPBS	280	80	2
Di-8A-ASPBS	10000	2800	2
Di-8P-ASPBS	<10	n.a.	2
Di-10A-ASPBS	250000	1.0×10^5	3
Di-10P-ASPBS	27	14	2
Di-12A-ASPBS ^c	3000000	1.5×10^6	2
Di-12P-ASPBS	2100	240	2

Table 2. Binding constants for a variety of Di-4-ASPBS derivatives measured by fluorescence lipid titration. Experiments were made at 0.5 μ M dye concentration. The data for each dye was fitted by eq 3. ^aData from ref.⁴². ^bThe true binding constant at infinite dilution is severely underestimated due to strong electrostatic influence (cf. section 2.3). ^cThe measurements were made with a dye concentration of 50 nM (cf. text).

There is an increment of the binding energy between sulfonate and alcohol of $\Delta(\Delta G_{SA}) = -RT \ln(K_S / K_A) = 2.2 \text{ kJ/mol}$ as well as for phosphate and alcohol $\Delta(\Delta G_{SA}) = -RT \ln(K_P / K_A) = 6.8 \text{ kJ/mol}$. This effect can be assigned to a changed resolution of the polar headgroup when the dye binds to the membrane. The polar headgroup is brought into the water/membrane interface with its lower polarity as compared to bulk water.⁴³ It may be expected that thereby its solvation energy is reduced and that this effect is more significant for a headgroup bearing a net charge. Neglecting as a first approximation the resolution of dipoles and of higher multipoles in the headgroup, the increment of resolution energy ΔG_{ion}^{resolv} of the charged moiety is compared to the result of the Born relation.⁴⁴ This relation yields the resolution energy for an ion of radius a and charge ze_0 that is brought from bulk water (dielectric constant $\epsilon_W = 80$) to the interfacial region with an effective dielectric constant ϵ_i (eq 4).

$$\Delta G_{ion}^{resolv} = \frac{z^2 e_0^2}{8\pi\epsilon_0 a} \left(\frac{1}{\epsilon_i} - \frac{1}{\epsilon_W} \right) \quad (4)$$

When the experimental increment of the binding energy is identified with the Born energy $\Delta(\Delta G_{SA}) = \Delta G_{ion}^{resolv}$, one may estimate the local polarity. For the sulfate group with $z = 1$ and $a = 0.28 \text{ nm}$ given by atomic ion radii,⁴⁵ an effective dielectric constant $\epsilon_i = 47$ is obtained, and for the phosphate with $z = 2$, $a = 0.29 \text{ nm}$ a value of $\epsilon_i = 51$. These values agree well with each other and indicate that indeed the charge plays the dominant role in the change of the binding constants, and that the contributions of the pyridinium and the headgroup appendix charge are independent and not mutually cancelled out. This view is supported by the binding constants of FM1-43 taken from ref.⁴² and the measured value of the similar dye Di-4-ASP Dication; Both of these dyes are derivatives of Di-4-ASP, with a positively charged propyl(triethyl-)ammonium (FM1-43) or propyl(trimethyl-)ammonium headgroup (Di-4-ASP Dication), respectively. Although these dyes are doubly positively charged, their binding constants are close to the value for the zwitterionic Di-4-ASPBS.

The relatively high polarities, as compared to a value of $\epsilon_i = 32$ found for lipid pH indicators,⁴³ indicate a rather peripheral location of the charged groups at the membrane/water interface.

The dye Di-4-ASPiHP₂ has two phosphate appendices attached to a symmetrical, branched dye headgroup. The measured binding constants of the dyes are $K_{A_2} = 15600 \pm 650 M^{-1}$ ($n = 2$) and $K_{P_2} = 700 \pm 40 M^{-1}$ ($n = 2$), corresponding to an increment in binding energy of $\Delta(\Delta G_{P_2A_2}) = 7.7 kJ/mol$. According to the Born model with $\epsilon_i = 51$, the differences in the energy of resolution $\Delta(\Delta G_{P_2A_2}) = \Delta G_{ion}^{resolv}$ would have been expected to be about twice the difference between Di-4-ASPPP and Alcohol, i.e. $2 \times 6.8 kJ/mol = 13.6 kJ/mol$. This discrepancy could be explained by a more peripheral localization of the charged appendices due to the longer aliphatic chain ($\approx 0.2 nm$) at the headgroup. The observed free energy increment would then, as calculated by eq 4, correspond to an effective dielectric constant of $\epsilon_{if} = 61$ at the location of the appendices, a reasonable value. Note, however, that the result for Di-4-ASPBHP₂ needs to be treated with care since the elementary analysis was not in perfect accord with the expected values.

The dye Di-4-ASPP(PP) is similar to Di-4-ASPPP, but it contains a diphosphate appendix at its headgroup and is therefore triply charged. With a binding constant of $890 M^{-1}$, the increment in binding energy relative to Di-4-ASPPA amounts to $\Delta(\Delta G_{(PP)A}) = 7.4 kJ/mol$ and is only slightly increased compared to the pair Di-4-ASPPP/Di-4-ASPPA. In this case as well, the more peripheral location of the charges ($\approx 0.29 nm$, the radius of the phosphate group) may account for this effect. If one tentatively assigns a radius of $0.36 nm$ to the diphosphate group (the radius of a sphere with the double volume of a phosphate group with $a = 0.29 nm$), the observed increment in binding energy correlates to an effective dielectric constant of $\epsilon = 60$.

The dyes described so far exhibit a rather small shift in binding strength upon the (virtual) removal of the polar appendix. The results show that the strategy of introducing more than one polar group at the headgroup does not increase this shift substantially.

Phosphate at the tail. A far greater increment of binding strength between dye phosphate and alcohol was achieved by modifying the hydrophobic *tail* of the dyes. The *phosphorylated* dye precursor is then no longer a true amphiphile, since both head and tail exhibit a high

polarity. The dye with *hydroxyl* residues at the tail is still amphiphilic, and the increased polarity of the tail can be counterbalanced by a longer, more lipophilic alkyl chain. Still, the hydroxyl residues at the tail might compromise the alignment of the chromophore with the membrane normal that is necessary for effective voltage sensitivity. This issue was therefore also investigated, and the corresponding experiment is described in section 2.5.

The dyes Di-10P-ASPBS and Di-10A-ASPBS exhibit binding constants of $K_{10P} = 27 \pm 14 M^{-1}$ and $K_{10A} = 2.5 \times 10^5 \pm 1.0 \times 10^5 M^{-1}$, respectively. The difference in binding strength therefore amounts to almost four orders of magnitude, much higher than for the dyes modified at the hydrophilic headgroup appendix. The resulting difference in binding energy is $\Delta(\Delta G_{10P/10A}) = 22.6 \text{ kJ/mol}$ or 11.3 kJ/mol per phosphate group. For the dyes Di-12P-ASPBS and Di-12A-ASPBS, the binding constants amounted to $K_{12P} = 2100 \pm 240 M^{-1}$ and $K_{12A} = 3.0 \times 10^6 \pm 1.5 \times 10^6 M^{-1}$. The increment in binding energy is $\Delta(\Delta G_{12P/12A}) = 17.9 \text{ kJ/mol}$ or 9.0 kJ/mol per phosphate group, significantly lower than for the Di-10P/A-ASPBS pair. This discrepancy will be discussed at the end of this section. The exact increment in binding energy for the dyes Di-8P-ASPBS and Di-8A-ASPBS can not be evaluated due to the small binding constant of Di-8P-ASPBS, but its minimal value is $\Delta(\Delta G_{8P/8A}) \geq 18 \text{ kJ/mol}$, in accord with what was found for the longer homologues.

A quantitative interpretation of the binding increments in terms of the Born model is not feasible since localization and charge of the dye phosphate in the membrane interior are not known. As an orientation: The resolution energy of even a single charge with $a = 0.29 \text{ nm}$ from water to the interior of the membrane with $\epsilon_{\text{mem}} = 2$ would be far higher with 120 kJ/mol as calculated by eq 4.

There is more information to be extracted from the data of Table 2, namely the contributions of methylene and alcohol groups to the overall binding constant. Di-12A-ASPBS and Di-12P-ASPBS are not regarded here and will be treated below.

In the homologous series Di-6A-ASBPS to Di-8A-ASBPS to Di-10A-ASBPS there is an increment of binding energy of 8.9 kJ/mol between the first two dyes, and one of 8.0 kJ/mol between the second two. On average, this corresponds to a free energy of transfer $\Delta G_{aq \rightarrow mem, CH_2} = 2.1 \text{ kJ/mol}$ per additional methylene group, in strong agreement with the value of $\Delta G_{aq \rightarrow mem, CH_2} = 2.4 \text{ kJ/mol}$ found for the homologous Di-X-ASPBS series.²⁶ The correlation with n-octanol/water partitioning data is rather high, with the contribution of a

methylene group to the transfer free energy being 3.0 kJ/mol for alkanols and 3.5 kJ/mol for alkanes (values computed from the data in ref.⁴⁶). This data also reflects the finding of the present study that the increment per methylene group is smaller for alkanols than for alkanes. Within one class of compounds, however, the contributions of the methylene group and the alcohol functions to the overall hydrophobicity are additive and independent of each other. (ii) One can also calculate the contribution of the alcohol moiety itself from the increment in binding energy between Di-4-ASPBS and the extrapolated value for Di-4A-ASPBS which lies at 9.4 M^{-1} . The free transfer energy of an alcohol group in exchange for a terminal hydrogen group is therefore $\Delta G_{aq \rightarrow mem, OH} = 8.3 \text{ kJ/mol}$, in good agreement with n-octanol/water partitioning measurements: The free energy difference of partitioning between n-pentane and pentane⁴⁶ $\Delta G_{aq \rightarrow oct, OH, OH} = 11.3 \text{ kJ/mol}$. Note that solvation in an amphiphilic solvent like n-octanol depends not only on the bulk properties like polarity, but also on the discrete structure of the solute and the solvent. Still, the n-octanol/water system seems to be a rather fitting model, especially when compared to water/hexadecane partitioning, where an evaluation of the data (not shown) for a series of alkanes and alkanols⁴⁷ yielded $\Delta G_{aq \rightarrow hd, OH} = 23.0 \text{ kJ/mol}$. The good agreement in addition provides further evidence that the partitioning model between water and membrane as opposed to a discrete binding sites model is feasible for amphiphiles.

Let us now again take a look at the binding constants of Di-12A-ASPBS and Di-12P-ASPBS. These were not included in the discussion of the preceding paragraph due to some unexpected effects.

Di-12P-ASPBS. The increase in binding energy of Di-12P-ASPBS relative to Di-10P-ASPBS is 10.8 kJ/mol , or 2.7 kJ/mol per additional methylene group. This lies well above the values of the Di-X-ASPBS and the Di-XA-ASPBS series, and might reflect a change in the mode of binding: Since for the tail-phosphorylated dyes, headgroup and tail exhibit comparably high polarities, the geometry of binding might change from “tail-first” to a “head-first” or sideways incorporation into the membrane. In this case, linear relationships between tail length and binding energy can no longer be expected. However, in contrast to the binding data for Di-12P-ASPBS, the data of Di-10P-ASPBS is not very reliable due to the limited amount of data points. If it is assumed that the true increment in binding energy is 2.1 kJ/mole per methylene group as found for the Di-XA-ASPBS series, and taking the measured binding constant of Di-12P-ASPBS as a basis, the resulting binding constant of Di-10P-ASPBS is

70 M^{-1} . In this case, the increment in binding energy between Di-10A-ASPBS and Di-10P-ASPBS would amount to 20.3 kJ/mol or 10.1 kJ/mol per phosphate group.

Di-12A-ASPBS. The increment in binding energy of Di-12A-ASPBS relative to Di-10A-ASPBS is only 6.1 kJ/mol or 1.5 kJ/mol per additional methylene group. This behavior correlates with experiments on the Di-X-ASPBS series mentioned above, where a decrease in the binding energy per additional methylene was found for dyes with high binding constants as well.²⁶ Whether the measured value reflects the true molecular binding constant or whether the measurements are corrupted by secondary effects, like fluorescence quenching, lipid solubilization, lipid adsorption, or micellation of the dye, cannot be judged without further experiments.

Although the difference in the binding increment per methylene group for Di-12A-ASPBS/Di-10A-ASPBS compared to the average value of 2.1 kJ/mol is rather small, the ratio of binding constants $K_{12A/10A} = 12$ is significantly smaller than the expected average value measured for the dyes with shorter tails, which amounts to $K_{(n+2)A/nA} = 30$. This indicates that there is a limit to how far the binding constant of tail-modified dyes can be increased. If this were the case, it would be problematic for the further development of enzyme induced staining and it must be further explored.

Calculation of K_D for tail modified dyes. Due to the relative independence of the contribution of different moieties in the dye tail to the overall binding constant, it is possible to provide a general formula for the estimation of the binding constant of an arbitrary ASPBS-dye derivatized at the tail, with y alcohol and z phosphate groups and x being the number of methylene groups relative to Di-4-ASPBS (eq 5). In this formula, the contribution of a phosphate group to the overall binding energy is -10.1 kJ/mol , i.e. it is assumed that the contribution of a methylene group is equal for hydroxylated and phosphorylated dyes and that the measured binding constant of Di-10P-ASPBS was underestimated.

$$K_{Dye} = 7500 \text{ M}^{-1} \times \exp(2100x - 8300y - 10100z) / (8.31 \times 298) \quad (5)$$

This equation is useful to interpolate values of dyes of intermediate alkyl chain lengths.

2.3 Electrostatic Influence on Binding

As mentioned above, the binding of charged amphiphiles is modified by electrostatic effects, since a high density of bound dye will electrically charge the membrane and lead to repulsion of like charges or attraction of opposite charges. The Gouy-Chapman theory²⁹ has been applied to the evaluation of Isothermal Titration Calorimetry (ITC) binding data with success.^{42,48,49} In the case of the doubly positively charged FM1-43, however, the Gouy-Chapman theory applied to binding data at high concentrations (measured by ITC) did not reproduce binding data at very low concentrations measured by fluorescence lipid titration unless it was assumed that $z = 1$. Nevertheless, since e.g. the dyes Di-X-ASPPP and Di-X-ASPPA ($X = 4,6$) as well as Di-XP-ASPBS ($X = 8, 10, 12$) used in this work carry charges, and since a treatment of lipid titration data by the Gouy-Chapman theory has so far not been attempted in the literature, the basic principles of how charges influence dye binding and an evaluation of fluorescence lipid titration data shall be introduced here. A simple, but crude estimation at which concentrations and binding constants a treatment without electrostatic effects is justified is also provided.

When electric charge effects are taken into regard, the effective free dye concentration at the membrane/water interface $c_{D,f}$ is modified by the surface potential via the Boltzmann relation to $c_{D,f} \exp(-ze_0\psi_0/k_B T)$, with charge of the amphiphile z , elementary charge e_0 , Boltzmann constant k_B and membrane surface potential ψ_0 .^{28,29} Accordingly, eq 2 changes to

$$c_{D,b} = \frac{1}{1 + (1/K_D c_L e^{-\frac{ze_0\psi_0}{k_B T}})} c_D \quad (6)$$

The surface charge density σ , taking into regard the different specific areas per molecule for lipid A_L and amphiphile A_D , is:²⁸

$$\sigma = \frac{ze_0 c_{D,b}}{c_L A_L} \frac{1}{1 + \frac{c_{D,b} A_D}{c_L A_L}} \quad (7)$$

The surface potential ψ_0 is dependent on the ionic strength of the solution, and it is linked to σ via eq 8, where ϵ_r is the dielectric constant of water, ϵ_0 is the permittivity of free space, c_i

the concentration of the i th electrolyte in the bulk aqueous phase in mol/l, and z_i the signed valency of the i th species.

$$\sigma^2 = 2000\varepsilon_0\varepsilon_r RT \sum_{i=1}^n c_i \left(e^{-\frac{z_i e_0 \psi_0}{k_B T}} - 1 \right) \quad (8)$$

By fluorescence lipid titration, values for $c_{D,b}$ or $c_{D,f}$ cannot directly be obtained, since the combined fluorescence intensity of both species is measured. Eq 3 can be rewritten in the following form, with F being the fluorescence at the lipid concentration c_L :

$$\frac{F - f_{D,f}c_D}{f_{D,b} - f_{D,f}} = \frac{1}{1 + \left(1/K_D c_L e^{-\frac{z e_0 \psi_0}{k_B T}} \right)} c_D \quad (9)$$

This form, when compared to eq 3, shows that $c_{D,b}$ can be substituted by a term that contains the experimentally observable value F . With ψ_0 being a function of $c_{D,b}/c_L$ according to eqs. 7 and 8, this equation can now be numerically evaluated with free parameters $f_{D,f}$, $f_{D,b}$ and K_D to fit the experimental data. In practice this was done by numerically computing the dependence of $c_{D,b}/c_L$ on ψ_0 for the given ion concentrations (0.1 M Na^+ , 0.02 M Tris^+ , 0.12 M Cl^-) and approximating this dependence by a hyperbolic function which was then used in conjunction with eq 9. The specific area of the dye A_D was assumed to be the same as A_L . The result of this fit was $\psi_0 = (0.131 \times c_{D,b}/c_L)/(0.405 + c_{D,b}/c_L)$

Figure 7 shows fluorescence lipid titration measurements of the dye Di-4-ASPPA at the concentrations 0.5 μM , 2 μM and 10 μM . With rising concentration, the binding curve is shifted to the right, and there is a striking deviation from the ideal sigmoid shape for $c = 10 \mu\text{M}$ at lower lipid concentrations while all curves are congruent at high lipid concentrations. The reason for this becomes clear immediately when one takes into regard that the surface charge density σ is highest at the lower lipid concentrations, where $c_{D,f}$ is close to the total dye concentration, while it decreases as the free dye concentration is depleted due to binding to the lipid surface. If one attempts to fit the data with eq 3, the apparent binding constants are 19500 (0.5 μM), 16800 (2 μM) and 8500 (10 μM ; Figure 7A). Taking charge effects into regard, the fitting of the same data yielded binding constants of

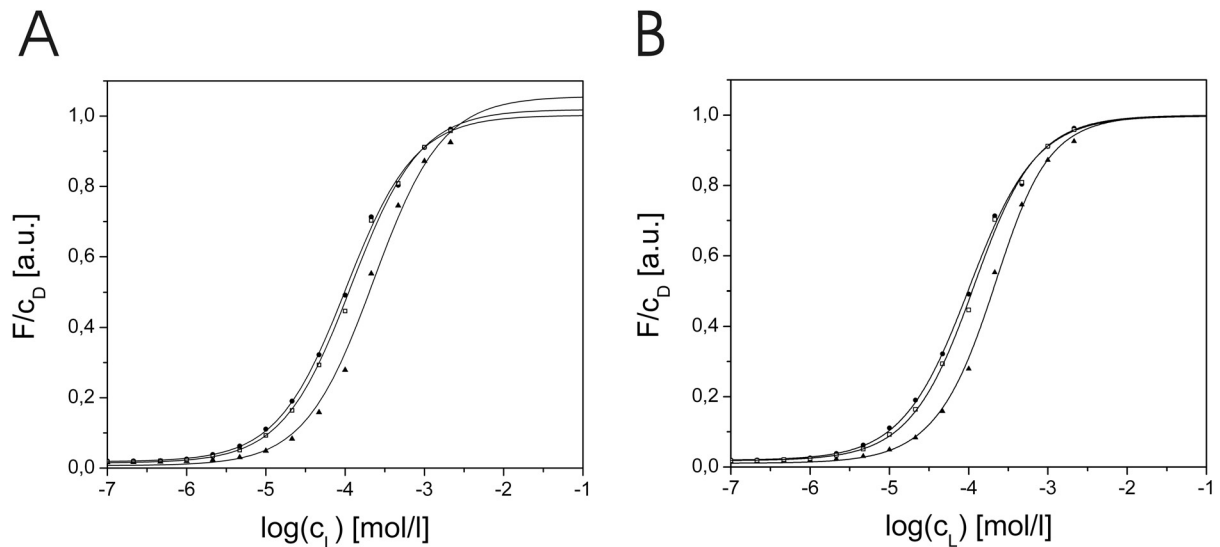


Figure 7. Concentration dependence of fluorescence lipid titration binding experiments with the positively charged dye Di-4-ASPPA. Titration was performed with dye concentrations 0.5 μM , 2 μM and 10 μM (from left to right). All data are normalized to $f_{D,b}$ as fitted by eq 9. (A) Fit of the data disregarding electrostatic effects using eq 3. (B) Fit of the data including electrostatic effects by using eq 9 in conjunction with the dependence of $c_{D,b}/c_L$ on ψ_0 as computed by Gouy-Chapman theory.

21000 M^{-1} , 21600 M^{-1} and 16900 M^{-1} for dye concentrations 0.5 μM , 2 μM and 10 μM , respectively (Figure 7B). The Gouy-Chapman formalism is therefore quite capable to describe the dependence of the data on concentration and the concomitant electrostatic effects. It can also explain the characteristic deviation from the ideal sigmoid shape that is observed for the binding curves of a charged amphiphile as compared to uncharged amphiphiles.

At the point of inflection of the sigmoid curve, $K_D = 1/c_L$. At this lipid concentration, $c_{D,b}/c_L = K_D c_D / 2$. By inserting this into the hyperbolic fit of the relation between ψ_0 and $c_{D,b}/c_L$, one obtains an expression for the dependence of ψ_0 on the binding constant K_D and the total dye concentration at $c_L = 1/K_D$ and ion concentrations 0.1 M Na^+ , 0.02 M Tris^+ , 0.12 M Cl^- .

$$\psi_0 = \frac{0.131 K_D c_D}{0.810 + K_D c_D} \quad (10)$$

The apparent binding constant of singly charged amphiphilic dyes obtained by fitting the data with eq 3 deviates from the “true” binding constant approximately by a factor of $\exp(-ze_0\psi_0/k_B T)$. In order to keep the error below 10 % (i.e. $\exp(-ze_0\psi_0/k_B T) \geq 0.9$), the product $K_D c_D$ must be smaller than 0.017 for singly charged species at the given ion concentrations. For an error <1%, $K_D c_D$ must be smaller than 0.0016. For example, at a

concentration of 0.5 μM dye, the binding constant should not exceed 34000 M^{-1} (10 % error) or 3200 M^{-1} (1 % error). These estimations show that disregarding electrostatic effects for most of the dyes was perfectly justified, but that the binding of Di-6-ASPPA is heavily influenced by electrostatic effects since $K_{\text{DCD}} = 0.0475$ for the measured binding constant. An evaluation of the data for Di-6-ASPPA by eq 9 was not possible since the quality of the data was not sufficient.

2.4 Membrane Permeation

The rate at which molecules can cross lipid membranes is of great importance e.g. for pharmaceutical compounds (see e.g.⁵⁰), and a stable asymmetrical staining is prerequisite for voltage sensitive dyes. The halftime of permeation $t_{1/2}$ can be in the order of seconds or of days, depending on the nature of the respective compound and on the mode of transport, which can occur by means of passive diffusion, facilitated transport or active transport.⁵¹ The latter two are special cases which apply to most membrane lipids, but only to few non-natural compounds. In the case of membrane-bound molecules, this diffusion process is termed *flip-flop*. By passive diffusion, non-charged compounds can generally cross the membrane easily with $t_{1/2} < 1$ min (e.g. diacylglycerol).⁵¹ The same holds true for weak acids and bases, i.e. charged compounds in equilibrium with their neutral form, since they permeate the membrane quickly in their uncharged form⁵² (e.g. fatty acids, phosphatidic acid). In contrast, membranes are generally only weakly permeable for permanently charged compounds. Phosphatidic acid in its charged form, for example, has been found to exhibit $t_{1/2} = 12.6$ days. It has been reported that cations are in general 50 to 200 times less permeable than anions. This has been ascribed to the ability of anions to form short lived aggregates which are shuttled across the membrane.⁵³

An indirect, qualitative method to assess membrane permeability of fluorescent, membrane bound dyes is to incubate cells with dye and to record the change in intracellular fluorescence compared to the plasma membrane fluorescence. Although one cannot distinguish between flip-flop and the subsequent transfer of the dye from the plasma membrane to internal membranes, this method yields some interesting results.

The outcome of this experiment for the dyes Di-4-ASPPP, Di-4-ASPPA, Di-8A-ASPBS and Di-10A-ASPBS is shown in Figure 8. Di-8P-ASPBS and Di-10P-ASBPS did not exhibit any appreciable membrane fluorescence. Di-12A-ASPBS behaved similarly to Di-10A-ASPBS. For comparison, the parent compound of the dyes, Di-4-ASPBS, and one of the most

sensitive dyes known to date, ANNINE 5,¹ are included in the figure. All experiments were performed on the fibroblastic cell line HEK293⁵⁴ in Tris-NaCl-Glucose buffer pH 8.1 at room temperature. The same cell line was also used in further experiments (see the following sections). Performing the experiments in medium (DMEM) with or without the addition of fetal calf serum (FCS, 10 %) had no pronounced influence (data not shown), proving that the observed behavior was not an artifact introduced by an electrolyte or pH-dependent effect.

All dyes with hydrophobic butyl tails showed a strong intracellular staining already three minutes after addition of the dye, the zwitterionic dye Di-4-ASPBS seemingly being internalized more slowly than the charged dyes Di-4-ASPPA and Di-4-ASPPP. The dyes ANNINE 5, Di-8A-ASPBS and Di-10A-ASPBS exhibited a stable plasma membrane fluorescence that was still dominant after 30 minutes. Three conclusions can be drawn: (i). The RH364 related dyes with butyl chains are all relatively quickly translocated, no matter whether they are permanently charged (Di-4-ASPPA), zwitterionic (Di-4-ASPBS) or charged but in equilibrium with a zwitterionic form (Di-4-ASPPP). (ii). The other dyes show a stable plasma membrane staining, which correlates with their overall size due to a larger chromophore (ANNINE 5) or a longer tail (Di-8/10A-ASPBS). 3. This effect is not solely dependent on the overall hydrophobicity since Di-8A-ASPBS is much less permeable than Di-4-ASPPA even though it has a smaller binding constant (cf. Table 2).

Although a definite understanding of the mechanism of flip-flop is lacking,⁵⁵ the size dependence of translocation has been documented for other compounds such as the voltage sensitive dyes Di-8-ANEPPS vs. Di-4-ANEPPS⁵⁶ as well as the dyes DiI-C18 vs. DiI-C12 in planar black lipid membranes⁵⁷ and for anthroyl fatty acids in liposomes of egg phosphatidylcholine.⁵⁵ In the latter study, a 200fold higher rate of flip-flop for a C11-fatty acid was found as compared to a C18-fatty acid, although this finding is still a matter of debate.^{58, a} In these studies, no mechanistic explanation is provided. The experiments described in this thesis suggest that the *size* and not the overall hydrophobicity of the amphiphilic compound is the main parameter governing the rate of transbilayer movement.

^a A different group found the flip-flop rate to be immeasurably fast (<5 ms), with the desorption rate being the rate limiting constant of fatty acid diffusion across bilayers. In this report, a strong decrease of the *desorption rate* with chain length was found.

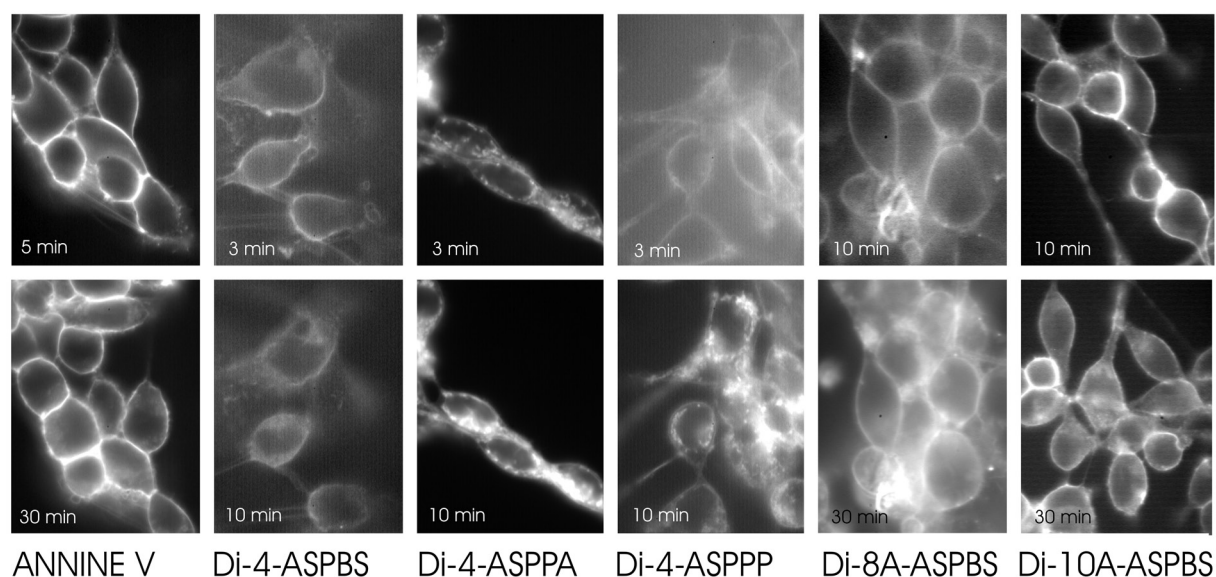


Figure 8. Internalisation of Voltage Sensitive Dyes by HEK293 cells. Microscope fluorescence images (excitation around 450 nm, emission at >510 nm) of HEK293 cells incubated with dyes in Tris-NaCl-Glucose buffer. The images are normalized to the respective maximum intensity.

It is nevertheless surprising that the charged Di-4-ASPPA crosses cell membranes so easily. This might be due to the relatively wide delocalization of the charge at the chromophore. However, Di-4-ASPPP and Di-4-ASPBS show a similar behaviour, even though the additional charges are relatively uncoupled from the charge at the chromophore as the binding data (see above) as well as the fluorescence spectra in lipidic environment suggest (Table 1). It might be speculated that stable (unstable) plasma membrane staining is also a result of a selective exclusion (inclusion) of some dyes from membrane areas that are internalized during endocytosis. Specific binding to cell surface proteins might also play a role, as investigations of the binding to proteins of the Voltage Sensitive Dye RH421⁵⁹ and the report that hemicyanine dyes exhibit no lateral diffusion in membranes indicate.⁶⁰ After all, many cells are quite active in endocytosis, and especially fibroblasts (like the HEK293 cells) have been estimated to internalize more than 200% of their entire surface area every hour under physiological conditions.⁶¹ Although the rate of endocytosis is surely smaller at room temperature, the stability of membrane staining with e.g. ANNINE 5 is difficult to explain. For the further optimization of existing voltage sensitive dyes, detailed experiments on membrane permeation and internalization might prove valuable.

The rate of membrane permeation or flip-flop might well be one of the reasons why many voltage sensitive dyes exhibit different sensitivity on different cell preparations (see, e.g.⁶²). In addition, the voltage sensitivity increases with the length of the chain e.g. for RH160 (with

butyl chains) and its shorter homologues.¹³ This might be attributed to slower flip-flop and a decreased concentration and therefore background fluorescence of dye in the buffer. Increasing the chain length in ANNINE 5 and 6 might increase their effective voltage sensitivity and further reduce their membrane permeability.

2.5 Orientation of Tail-Modified Dye in Membranes

Electrochromic voltage sensitivity (“Stark effect”) originates from the interaction of the dipole moments of the ground and excited state of a Voltage Sensitive Dye with the electric field across the membrane.² The magnitude of this interaction therefore depends on the alignment of the dipole moments with the membrane normal. To test whether the alcohol groups at the lipophilic dye tail severely compromise this defined orientation of the dye alcohol in the membrane, images of stained giant vesicles and HEK293 cells were made with a confocal microscope. Since the laser beam is polarized, one can obtain information on the relative orientation of the dye transition dipole moment in the membrane by cutting through a z-section of the cell or giant vesicle.³ This method is preferable to a direct proof of the voltage sensitivity of the Di-4-ASPBS derivate, since these dyes show only weak sensitivity.

Figure 9 shows inverted images of giant vesicles and HEK293 cells stained with the dyes DiIC₁₈(3), ANNINE 5 and with Di-10A-ASPBS. DiIC₁₈(3) (“DiI”) is known to be oriented close to parallel to the membrane surface,⁶³ while voltage sensitive dyes of the hemicyanine type like ANNINE 5 have been reported to be oriented close to parallel to the membrane normal.^{59,64}

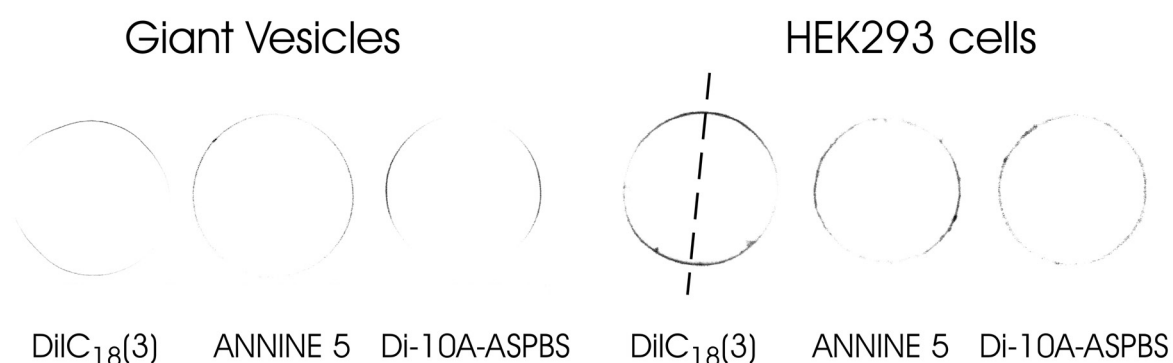


Figure 9. Test of dye orientation in membranes. Inverted laser scan fluorescence images (excitation 488 nm line of an argon ion laser, emission around 610 nm) of (A) giant vesicles and (B) mitotic HEK293 cells. The cell membranes were labeled with Di-10A-ASPBS or with dyes of known chromophore orientation relative to the membrane surface: ANNINE 5 (perpendicular) and DiIC₁₈(3) (parallel). The direction of laser light polarization is indicated by a dashed line.

In accordance with this orientation, the maximum of fluorescence for DiIC₁₈(3) was in the plane of polarization, while it was perpendicular to this plane for ANNINE 5. Like ANNINE 5, Di-10A-ASPBS had its maximal fluorescence also in the plane perpendicular to the plane of polarization, providing proof that the dye is oriented in a manner that does not compromise its electrochromic voltage sensitivity.

Note that mitotic, i.e. loosely attached and therefore spherical HEK293 cells were chosen for this assay in order to allow for a clear interpretation.

2.6 Materials and Methods

Chemicals. The purity of all chemicals other than those used for synthesis was at least p.a.: Tris (Roth, Karlsruhe, Germany), acetonitrile (YMC Europe, Schermbeck, Germany), Sephadex LH20, DEAE Sepharose (Pharmacia, Peapack, NJ, USA), K_2CO_3 , Na_2SO_4 , $ZnSO_4 \times 7H_2O$, $CaCl_2 \times 2H_2O$, ethyl acetate, heptane, ethanol, trichloromethane, methanol, CH_3COOH , triethylamine, palladium diacetate, diethyl ether, silica gel 60 (0.040-0.063 mm), LiChroprep RP-18 (25-40 μm), iodine, $MgCl_2 \times 6H_2O$, trifluoroacetic acid (TFA), saccharose, (Merck, Darmstadt, Germany), dimethyl formamide (DMF), 4-vinylpyridine, dimethylchlorophosphate, 8-chloro-octan-1-ol, 10-chloro-decan-1-ol (Aldrich, Munich, Germany), diethanolamine (DEA), *para*-nitrophenylphosphate (*p*-NPP), methane sulfonic acid, tri-*o*-toluoylphosphine, 1,4 butane sultone, 1-bromopropanol, pyridine, dimethylsulfide, phosphoric acid (Fluka, Munich, Germany), 25 % NH_3 (Riedel de Haen Germany, Seelze), 6-chlorohexan-1-ol (Lancaster Germany, Frankfurt am Main), 12-bromododecan-1-ol (TCI Europe, Bedford, United Kingdom), KCl, NaCl, poly-L-lysine MW 150000-300000 (SIGMA, Munich, Germany). Purified water was obtained with a Milli-Q system (Millipore Germany, Schwalbach).

Dye. Di-4-ASPBS **1** was synthesized as described in the literature.²⁰ Di-4-ASPPA **2** (1-[γ -hydroxypropyl]-trans-4-[*p*-(di-*n*-butylamino)styryl]-pyridinium bromide) was obtained by reaction of trans-4-[*p*-(di-*n*-butylamino)styryl]pyridine (Di-4-ASP) with 1.5 mole equivalents of 1-bromopropanol (100°C, 2 h). Subsequent precipitation of the product from methanol with diethyl ether and digestion in ethyl acetate yielded Di-ASPP alcohol as a red solid. It was purified by column chromatography (SiO_2 , $CHCl_3$:MeOH:H₂O 50:20:4) and identified by NMR and mass spectrometry: ¹H-NMR (400 MHz, $CDCl_3$) δ ppm 8.97 (d, 2H, ³J=5.2 Hz), 7.785 (d, 2H, ³J=5.2 Hz), 7.58 (d, 1H, ³J=15.6 Hz), 7.48 (d, 2H, ³J=7.8 Hz), 6.81 (d, 1H, ³J=15.6 Hz), 6.62 (d, 2H, ³J=7.8 Hz), 4.80 (s, br, 2H), 4.44 (s, br, 1H), 3.71 (t, 2H, ³J=5.0 Hz), 3.32 (s, br, 4H), 2.27 (t, 2H, ³J=5.0 Hz), 1.58 (s, br, 4 Hz), 1.36 (q, 4H, ³J=7.0 Hz), 0.96 (t, 6H, ³J=7.0 Hz); EIMS m/z 367.2 M⁺ ($C_{24}H_{35}N_2O^+$ requires 367.6).

The first step of the synthesis of Di-4-ASPPP **3** (1-[γ -phosphatopropyl]-trans-4-[*p*-(di-*n*-butylamino)-styryl]-pyridinium betaine) leads to Di-4-ASPP dimethylphosphate by reaction of **2** with 1.6 mole equivalents dimethylchlorophosphate in pyridine (16 h, room temperature). After evaporation of the solvent, the red intermediate product was purified by chromatography on a silica column ($CHCl_3$:MeOH:H₂O 60:20:1). The phosphate was deprotected with 5 mole eq dimethylsulfide and 17 mole eq methanesulfonic acid by stirring overnight at room temperature. Upon neutralization with 25 % NH_3 , the colorless solution turned red. After evaporation, the red product was purified by column chromatography (SiO_2 , $CHCl_3$:MeOH:H₂O 50:20:4; Sephadex LH 20, MeOH). It was identified by NMR and mass spectrometry: ¹H-NMR (400 MHz, MeCN) δ ppm 8.60 (s, br, 2H), 7.72 (s, br, 2H), 7.50 (d, 1H, ³J=15.5 Hz), 7.355 (d, 2H, ³J=7.8 Hz), 6.71 (d, 1H, ³J=15.5 Hz), 6.51 (d, 2H, ³J=7.8 Hz), 4.525 (s, br, 2H), 3.925 (s, br, 2H), 3.20 (s, br, 6H, O-H, N-CH₂), 2.17 (s, br, 2H), 1.445 (s, br, 4H), 1.26 (m, 4H), 0.87 (t, 6H, ³J=7.2 Hz); ³¹P-NMR (162 MHz, $CDCl_3$) δ ppm 4.59; EIMS m/z 447.2 M⁺ ($C_{24}H_{36}N_2O_4P^+$ requires 447.5).

The corresponding diphosphate Di-4-ASPP(PP) **4** (1-[γ -diphosphatopropyl]-trans-4-[*p*-(di-*n*-butylamino)styryl]-pyridinium betaine) was obtained via (1-[γ -bromopropyl]-trans-4-[*p*-(di-*n*-butylamino)styryl]-pyridinium bromide), an analogue of **2** with a bromide residue instead of a hydroxyl group.

Di-4-ASP²⁰ (typically 1.6 mmol) and 1,3 dibromopropane (20 mole eq) were stirred at 100 °C for 2h. Upon cooling Et₂O was added and the resulting precipitate was purified by chromatography (SiO₂, CHCl₃:MeOH:H₂O 50:20:4). Yield 76.3 %, red solid m.p. 71 °C (dec.), ¹H-NMR (400 MHz, CDCl₃) δ ppm 9.05 (d, 2H, ³J = 6.5 Hz), 7.79 (d, 2H, ³J = 5.6 Hz), 7.60 (d, 1H, ³J = 15.8 Hz), 7.49 (d, 2H, ³J = 8.9 Hz), 6.82 (d, 1H, ³J = 15.8 Hz), 6.63 (d, 2H, ³J = 8.5 Hz), 4.90 (t, 2H, ³J = 6.9 Hz), 3.51 (t, 2H, ³J = 6.0 Hz), 3.34 (t, 4H, ³J = 7.7 Hz), 2.65 (quint, 2H, ³J = 6.5 Hz), 1.60 (m, 4H), 1.37 (m, 4H), 0.97 (t, 6H, ³J = 7.3 Hz); EIMS *m/z*: 429.2 and 431.2, (M⁺, C₂₄H₃₄BrN₂⁺ requires 430.45). This intermediate product (typically 0.2 mmol) was dissolved in dry acetonitrile and evaporated *in vacuo* to remove water traces. This procedure was performed twice. Then tris(tetrabutylammonium)hydrogen pyrophosphate (1.6 mole eq) and acetonitrile were added. The solution was stirred for 2 d at room temperature, the solvent was reduced to 1/5th and Et₂O was added. The resulting precipitate was dissolved in 1-2 ml of 25 mmol NH₄HCO₃ and was passed through a column containing weak anion-exchange resin (DEAE Sepharose) using 75 mmol NH₄HCO₃. The eluent was lyophilized and the product purified by chromatography (Sephadex LH20, MeOH). Yield 4.5 %, red solid m.p. 71°C (dec.), ¹H-NMR (400 MHz, CD₃OD) δ ppm 8.70 (d, 2H, ³J = 6.8 Hz), 7.93 (d, 2H, ³J = 6.8 Hz), 7.79 (d, 1H, ³J = 15.9 Hz), 7.57 (d, 2H, ³J = 8.9 Hz), 7.03 (d, 1H, ³J = 15.9 Hz), 6.72 (d, 2H, ³J = 8.9 Hz), 4.64 (t, 2H, ³J = 6.5 Hz), 4.03 (m, 2H), 3.40 (m, 4H), 2.27 (m, 2H), 1.61 (m, 4H), 1.41 (m, 4H), 0.99 (t, 6H, ³J = 7.3 Hz); ³¹P-NMR (400 MHz, MeOH) δ ppm -7.1 (d, 1P), -8.2 (d, 1P); EIMS *m/z*: 527.2 (M+1, C₂₄H₃₆N₂O₇P₂ requires 526.52). The corresponding triphosphate could not be obtained in pure form due to disproportionation reactions to the diphosphate and higher polyphosphates.

Di-6-ASPPA **5** (1-[γ-hydroxypropyl]-trans-4-[*p*-(di-*n*-hexylamino)styryl]-pyridinium bromide) was synthesized in analogy to **2**, but using the starting material Di-6-ASP as synthesized in analogy to the literature.²⁰ This compound was heated for 2 h at 80-100°C with 15 mole eq 3-bromopropanol. Upon cooling, the product was precipitated as a red oil by addition of Et₂O. Pure product was obtained by chromatography (SiO₂, CHCl₃:MeOH:H₂O 50:20:4) and subsequent digestion with ethyl acetate, m.p. 152 °C, yield 40.6 %, ¹H-NMR (400 MHz, CDCl₃) δ ppm 8.95 (d, 2H, ³J = 6.1 Hz), 7.77 (d, 2H, ³J = 5.1 Hz), 7.58 (d, 1H, ³J = 15.8 Hz), 7.49 (d, 2H, ³J = 8.1 Hz), 6.80 (d, 1H, ³J = 15.8 Hz), 6.63 (d, 2H, ³J = 7.1 Hz), 4.80 (t, 2H, ³J = 6.5 Hz), 3.74 (t, 2H, ³J = 5.1 Hz), 3.35 (t, 4H, ³J = 7.7 Hz), 2.26 (m, 2H), 1.64 (s, 8H), 1.33 (s, 8H), 0.91 (t, 6H, ³J = 6.6 Hz); EIMS *m/z*: 423.4, (M⁺, C₂₈H₄₃N₂O⁺ requires 423.67).

Di-6-ASPPP **6** (1-[γ-phosphatopropyl]-trans-4-[*p*-(di-*n*-hexylamino)styryl]-pyridinium betaine) was synthesized in analogy to **3**. **5** was reacted with 1.5 mole eq of dimethylchlorophosphate in a low amount of pyridine (4 h at 60°C, then overnight at room temperature). After evaporation and chromatography (SiO₂, CHCl₃:MeOH:H₂O 50:20:4) a mixture of mono- and dimethylated products was isolated and the protective groups of the dimethylphosphate residue were removed as described above for **3**. The product was isolated by chromatography (SiO₂, CHCl₃:MeOH:H₂O 50:20:4) and subsequent digestion with ethyl acetate. Yield (8.5 %, 2 steps), red solid, m.p. 103 °C (dec.), ¹H-NMR (400 MHz, CD₃OD) δ ppm 8.58 (d, 2H, ³J = 6.9 Hz), 7.93 (d, 2H, ³J = 6.9 Hz), 7.81 (d, 1H, ³J = 15.9 Hz), 7.58 (d, 2H, ³J = 9.0 Hz), 7.05 (d, 1H, ³J = 15.9 Hz), 6.72 (d, 2H, ³J = 9.0 Hz), 4.57 (t, 2H, ³J = 6.7 Hz), 3.91 (m, 2H), 3.40 (t, 4H, ³J = 7.6 Hz), 2.27 (m, 2H), 1.62 (m, 4H), 1.36 (m, 12H), 0.93 (t, 6H, ³J = 6.9 Hz); ³¹P-NMR (400 MHz, MeOH) δ ppm 3.2 (s); EIMS *m/z*: 503.4, (M+1, C₂₈H₄₄N₂O₄P requires 503.64).

Di-4-ASPBi-HA₂ **7** (4-{(E)-2-[4-(Di-butylamino)phenyl]vinyl}-1-[5-hydroxy-4-hydroxymethyl-pentyl]pyridinium bromide) was obtained by stirring Di-4-ASP and 1 mole eq 2-(3-bromopropyl)propane-1,3-diol for 2 d, using nitromethane as a solvent. (2-(3-bromopropyl)propane-1,3-diol was synthesized in analogy to the analogous chloro compound⁶⁵ starting from diethyl(3-bromopropyl)malonate,⁶⁶ yield 72.5 %, oil). The solvent was evaporated and the residue was purified by chromatography (SiO₂, CHCl₃:MeOH:H₂O 50:20:4) and by precipitation (MeOH/ethyl acetate). Yield 10.6 %, red solid m.p. 130 °C (dec.), ¹H-NMR (400 MHz, CDCl₃) δ ppm 8.92 (d, 2H, ³J = 6.7 Hz), 7.78 (d, 2H, ³J = 6.7 Hz), 7.57 (d, 1H, ³J = 15.8 Hz), 7.48 (d, 2H, ³J = 8.9 Hz), 6.80 (d, 1H, ³J = 15.8 Hz), 6.61 (d, 2H, ³J = 8.9 Hz), 4.63 (t, 2H, ³J = 7.2 Hz), 3.66 (d, 4H, ³J = 6.5 Hz), 3.31 (t, 4H, ³J = 7.6 Hz), 2.11 (m, 2H), 1.77 (m, 1H), 1.57 (m, 4H), 1.52 (m, 2H), 1.36 (m, 4H), 0.96 (t, 6H, ³J = 7.3 Hz); EIMS *m/z*: 425.4 (M, C₂₁H₄₁N₂O₂⁺ requires 425.6).

Di-4-ASPBi-HP₂ **8** (4-{(E)-2-[4-(Di-butylamino)phenyl]vinyl}-1-[5-phosphoryl-4-phosphorylmethyl-pentyl]pyridinium betaine) was obtained via 4-{(E)-2-[4-(Di-butylamino)phenyl]vinyl}-1-[5-dimethylphosphoryl-4-dimethylphosphorylmethyl-pentyl]pyridinium bromide. The latter was obtained by dissolving **7** in pyridine and adding 6 mole eq of dimethylchlorophosphate at 0°C and stirring at room temperature overnight. Upon evaporation the product was chromatographed (SiO₂, CHCl₃:MeOH:H₂O 50:20:4). The crude intermediate product (yield 22%) still containing impurities was used for the next step without further purification. Deprotection was performed as described above. The product was purified by chromatography (SiO₂, CHCl₃:MeOH:H₂O 50:20:4), subsequent digestion with ethyl acetate and recrystallisation (MeOH/Et₂O). Yield 17 %, red solid m.p. 70 °C (dec.), ¹H-NMR (400 MHz, CD₃OD) δ ppm 8.62 (d, 2H, ³J = 6.9 Hz), 7.94 (d, 2H, ³J = 6.6 Hz), 7.80 (d, 1H, ³J = 15.9 Hz), 7.57 (d, 2H, ³J = 8.9 Hz), 7.04 (d, 1H, ³J = 15.9 Hz), 6.72 (d, 2H, ³J = 8.9 Hz), 4.45 (t, 2H, ³J = 7.2 Hz), 3.93 (m, 2H), 3.83 (m, 2H), 3.42 (t, 4H, ³J = 7.6 Hz), 2.13 (m, 2H), 2.03 (m, 1H), 1.63 (m, 4H), 1.54 (m, 2H), 1.39 (m, 4H), 0.99 (t, 6H, ³J = 7.3 Hz); ³¹P-NMR (400 MHz, MeOH) δ ppm 3.48 (s); EIMS *m/z*: 585.2 (M+1, C₂₇H₄₂N₂O₈P₂ requires 584.6).

In the following, a generalized recipe for the synthesis of the tail modified dyes **9**, **10**, **12** and **14** and for the corresponding phosphorylated dyes **11**, **13** and **15** is given.

Starting from 6-chlorohexan-1-ol, 8-chlorooctan-1-ol, 10-chlorodecan-1-ol and 12-bromododecan-1-ol, the respective ω-iodoalkanoles 6-iodohexan-1-ol, 8-iodooctan-1-ol, 10-iododecan-1-ol and 12-iodododecan-1-ol were synthesized according to literature.⁶⁷⁻⁷⁰

In general, the 4-Di-ω-hydroxyalkylaminobromoanilines were obtained by alkylation of *p*-bromoaniline with 2.5 mole eq ω-Iodoalkyl-1-ol (typically 200 mmol) in DMF containing 2.5 mole eq K₂CO₃. The mixture was stirred at 120 °C for 48 h; If necessary, further ω-Iodoalkyl-1-ol and K₂CO₃ were added until the reaction was complete. The solution was allowed to cool to room temperature and was then distributed between EtOAc and water. The organic layer was washed with brine, dried (Na₂SO₄) and evaporated. Subsequent chromatography performed as indicated provided pure products: 1-Bromo-4-(di-6-hydroxyhexylamino)benzene: (SiO₂, EtOAc/heptane 5:1), oil, yield 25 %, ¹H-NMR (400 MHz, CD₃OD) δ ppm 7.21 (d, 2H, ³J = 9.2 Hz), 6.56 (d, 2H, ³J = 9.2 Hz), 3.55 (t, 4H, ³J = 6.5 Hz), 3.27 (t, 4H, ³J = 7.5 Hz), 1.55 (m, 8H), 1.39 (m, 8H); EIMS *m/z*: 373.8, 371.8 (M+1, C₁₈H₃₀BrNO₂ requires 372.3). 1-Bromo-4-(di-8-hydroxyoctylamino)benzene: (SiO₂, EtOAc/heptane 1:1), oil, yield 33.1 %, ¹H-NMR (400 MHz, CD₃OD) δ ppm 7.19 (d, 2H, ³J = 9.1 Hz), 6.52 (d, 2H, ³J = 9.1 Hz), 3.54 (t, 4H, ³J = 6.5 Hz), 3.22 (t, 4H, ³J = 7.5 Hz), 1.52 (m, 8H), 1.33 (m, 16H); EIMS *m/z*: 430.4, 428.4 (M+1, C₂₂H₃₈BrNO₂ requires 428.4). 1-Bromo-4-(di-10-hydroxydecylamino)benzene: (SiO₂,

EtOAc/heptane 1:2), oil, yield 27 %, ¹H-NMR (400 MHz, CD₃OD) δ ppm 7.20 (d, 2H, ³J = 9.1 Hz), 6.54 (d, 2H, ³J = 9.1 Hz), 3.53 (t, 4H, ³J = 6.5 Hz), 3.24 (t, 4H, ³J = 7.5 Hz), 1.51 (m, 8H), 1.32 (m, 24H); EIMS *m/z*: 486.4, 484.4 (M+1, C₂₆H₄₆BrNO₂ requires 484.6). 1-Bromo-4-(di-12-hydroxydodecylamino)benzene: (SiO₂, EtOAc/heptane 1:2), oil, yield 38.3 %, ¹H-NMR (400 MHz, CD₃OD) δ ppm 7.22 (d, 2H, ³J = 9.0 Hz), 6.56 (d, 2H, ³J = 9.0 Hz), 3.6 (t, 4H, ³J = 6.5 Hz), 3.19 (t, 4H, ³J = 7.5 Hz), 1.54 (m, 8H), 1.34 (m, 32H); EIMS *m/z*: 542.4, 540.4 (M+1, C₃₀H₅₄BrNO₂ requires 540.7).

These compounds were coupled to 4-vinylpyridine in a Heck reaction as described.²⁰ In short, a mixture of 1-Bromo-4-(di- ω -hydroxyalkylamino)benzene (typically 20 mmol), 4-vinylpyridine (1.2 mole eq), palladiumdiacetate (0.001 mole eq), tri-*o*-tolylphosphine (0.02 mole eq) and 20 mL of dry triethylamine was heated at 110 °C for 48 h in an autoclave that was flushed with argon. Upon cooling the solvent was evaporated and the crude product was dissolved in EtOAc. Insoluble components were removed by filtration. The solution was washed twice with water, dried (Na₂SO₄) and evaporated. Chromatography (SiO₂, EtOAc/MeOH 5:1) provided the E/Z mixtures (yields 70.4 % (hexyl), 45.3% (octyl), 60.0% (decyl), 32% (dodecyl)).

These intermediate products were then further reacted to the final 4-{(E)-2-[4-(di- ω -hydroxyalkylamino)phenyl]vinyl}-1-(4-sulfonatobutyl)pyridinium dyes. A mixture of 4-{(E/Z)-2-[4-(di- ω -hydroxyalkylamino)phenyl]vinyl}-pyridine (typically about 10 mmol) and 40 mole eq 1,4-butane sultone in a low amount of EtOH (around 40 mL for 10 mmol starting material) was stirred at 60 °C for 24 h. Then the solvent was reduced *in vacuo* and Et₂O (typically 100 mL) was added dropwise. The resulting precipitate was isolated by filtration and purified by chromatography (SiO₂, CHCl₃:MeOH:H₂O 50:20:4; then LH 20 (Pharmacia), MeOH).

Analytic data:

9 4-{(E)-2-[4-(Di- ω -hydroxyhexylamino)phenyl]vinyl}-1-(4-sulfonatobutyl)pyridinium: red solid, m.p. 148 °C (dec.), yield 33.2 %. ¹H-NMR (400 MHz, CD₃OD) δ ppm 8.56 (d, 2 H, ³J = 7 Hz), 7.94 (d, 2 H, ³J = 7 Hz), 7.81 (d, 1 H, ³J = 16 Hz), 7.58 (d, 2 H, ³J = 9 Hz), 7.04 (d, 1 H, ³J = 16 Hz), 6.72 (d, 2 H, ³J = 9 Hz), 4.45 (t, 2 H, ³J = 7.3 Hz), 3.56 (t, 4 H, ³J = 6.5 Hz), 3.41 (t, 4 H, ³J = 7.5 Hz), 2.87 (t, 2 H, ³J = 7.3 Hz), 2.14 (m, 2 H), 1.83 (m, 2 H), 1.65 (m, 4 H), 1.56 (m, 4 H), 1.41 (m, 8 H). EIMS *m/z* 533.4 (M+1)⁺, C₂₉H₄₄N₂O₅S requires 532.74.

10 4-{(E)-2-[4-(Di- ω -hydroxyoctylamino)phenyl]vinyl}-1-(4-sulfonatobutyl)pyridinium; red solid, m.p. 75 °C (dec.), yield 37.2 %. ¹H-NMR (400 MHz, CD₃OD) δ ppm 8.55 (d, 2 H, ³J = 7 Hz), 7.93 (d, 2 H, ³J = 7 Hz), 7.81 (d, 1 H, ³J = 16 Hz), 7.56 (d, 2 H, ³J = 9 Hz), 7.04 (d, 1 H, ³J = 16 Hz), 6.71 (d, 2 H, ³J = 9 Hz), 4.45 (t, 2 H, ³J = 7.3 Hz), 3.53 (t, 4 H, ³J = 6.5 Hz), 3.39 (t, 4 H, ³J = 7.5 Hz), 2.86 (t, 2 H, ³J = 7.3 Hz), 2.13 (m, 2 H), 1.82 (m, 2 H), 1.63 (m, 4 H), 1.52 (m, 4 H), 1.37 (m, 16 H). EIMS *m/z* 589.6 (M+1)⁺, C₃₃H₅₂N₂O₅S requires 588.84.

12 4-{(E)-2-[4-(Di- ω -hydroxydecylamino)phenyl]vinyl}-1-(4-sulfonatobutyl)pyridinium; red solid, m.p. 169 °C (dec.), yield 33 %. ¹H-NMR (400 MHz, CD₃OD) δ ppm 8.55 (d, 2 H, ³J = 7 Hz), 7.92 (d, 2 H, ³J = 7 Hz), 7.80 (d, 1 H, ³J = 16 Hz), 7.56 (d, 2 H, ³J = 9 Hz), 7.03 (d, 1 H, ³J = 16 Hz), 6.71 (d, 2 H, ³J = 9 Hz), 4.44 (t, 2 H, ³J = 7.5 Hz), 3.52 (t, 4 H, ³J = 7 Hz), 3.38 (t, 4 H, ³J = 7.5 Hz), 2.86 (t, 2 H, ³J = 7.5 Hz), 2.13 (m, 2 H), 1.82 (m, 2 H), 1.62 (m, 4 H), 1.51 (m, 4 H), 1.34 (m, 24 H). EIMS *m/z* 645.4 (M⁺), C₃₇H₆₀N₂O₅S requires 644.96.

14 4-{(E)-2-[4-(Di- ω -hydroxydodecylamino)phenyl]vinyl}-1-(4-sulfonatobutyl)pyridinium; red solid, m.p. 167 °C (dec.), yield 17 %. ¹H-NMR (400 MHz, CD₃OD) δ ppm 8.55 (d, 2 H, ³J = 7 Hz), 7.94 (d, 2 H, ³J = 7

Hz), 7.81 (d, 1 H, $^3J = 16$ Hz), 7.57 (d, 2 H, $^3J = 9$ Hz), 7.04 (d, 1 H, $^3J = 16$ Hz), 6.71 (d, 2 H, $^3J = 9$ Hz), 4.45 (t, 2 H, $^3J = 7.3$ Hz), 3.52 (t, 4 H, $^3J = 6.5$ Hz), 3.39 (t, 4 H, $^3J = 7.5$ Hz), 2.86 (t, 2 H, $^3J = 7.3$ Hz), 2.13 (m, 2 H), 1.82 (m, 2 H), 1.62 (m, 4 H), 1.51 (m, 4 H), 1.34 (m, 32 H). EIMS m/z 701.8 (M+1)⁺, C₄₁H₆₈N₂O₅S requires 701.07.

The dyes **10**, **12** and **14** were phosphorylated to yield the corresponding precursor dyes (1-(4-sulfonatobutyl)-*trans*-4-[*p*-(di- ω -phosphatodecylamino)styryl]pyridinium betaine) compounds).

The first step of the synthesis of the dye precursors leads to di-(dimethylphosphato-alkyl)-ASPBS by reaction of Di-XA-ASPBS dyes (typically 2.5 mmol) with 3 mole equiv dimethylchlorophosphate in pyridine (16 h, room temperature) and subsequent precipitation by dropwise addition of Et₂O. The crude intermediate product is isolated by filtration, dissolved in methane sulfonic acid and 5 mole equiv of dimethyl sulfide were added to remove the protective groups of the phosphate residues. The mixture was stirred overnight at room temperature. Upon neutralization with 25 % NH₃, the colorless solution turned red. After evaporation, the red product was purified by column chromatography as indicated.

11 (4-{(E)-2-[4-(Di- ω -phosphoryloctylamino)phenyl]vinyl}-1-(4-sulfonatobutyl)pyridinium); purification by chromatography on SiO₂ (MeOH:H₂O 1:1) and LiChroprep RP-18 (25-40 μ m) columns, (MeOH:H₂O 1:1), then digeration with Et₂O. Red solid, m.p. 182 °C (dec), yield 18.8 % (2 steps). ¹H-NMR (400 MHz, CD₃OD) δ ppm 8.54 (d, 2 H, $^3J = 7$ Hz), 7.94 (d, 2 H, $^3J = 7$ Hz), 7.81 (d, 1 H, $^3J = 16$ Hz), 7.57 (d, 2 H, $^3J = 9$ Hz), 7.05 (d, 1 H, $^3J = 16$ Hz), 6.71 (d, 2 H, $^3J = 9$ Hz), 4.44 (t, 2 H, $^3J = 7.5$ Hz), 3.84 (m, 4H), 3.39 (t, 4 H, $^3J = 7.2$ Hz), 2.87 (t, 2 H, $^3J = 7.3$ Hz), 2.13 (m, 2 H), 1.84 (m, 2 H), 1.61 (m, 8 H), 1.32 (m, 16 H). ³¹P-NMR (400 MHz, CD₃OD) δ ppm 2.0 (s). EIMS m/z 749.6 (M+1)⁺, C₃₃H₅₄N₂O₁₁P₂S requires 748.8.

13 (4-{(E)-2-[4-(Di- ω -phosphoryldecylamino)phenyl]vinyl}-1-(4-sulfonatobutyl)pyridinium); purification on LiChroprep RP-18, 25-40 μ m (MeOH:H₂O 1:1), then digeration with Et₂O. Red solid, m. p. 152 °C (dec.), yield 25 % (2 steps). ¹H-NMR (400 MHz, CD₃OD) δ ppm 8.54 (d, 2 H, $^3J = 7$ Hz), 7.94 (d, 2 H, $^3J = 7$ Hz), 7.81 d, 1 H, $^3J = 16$ Hz), 7.57 (d, 2 H, $^3J = 9$ Hz), 7.04 (d, 1 H, $^3J = 16$ Hz), 6.71 (d, 2 H, $^3J = 9$ Hz), 4.44 (t, 2 H, $^3J = 7.5$ Hz), 3.84 (m, 4 H), 3.39 (t, 4 H, $^3J = 7.5$ Hz), 2.87 (t, 2 H, $^3J = 7.5$ Hz), 2.12 (m, 2 H), 1.85 (m, 2 H), 1.61 (m, 8 H), 1.34 (m, 24 H). EIMS m/z 805.4 (M+1)⁺, C₃₇H₆₂N₂O₁₁P₂S requires 804.92.

15 4-{(E)-2-[4-(Di- ω -phosphoryldodecylamino)phenyl]vinyl}-1-(4-sulfonatobutyl)pyridinium; purification on LiChroprep RP-18, 25-40 μ m, (MeOH:H₂O 1:1), then digeration with Et₂O and acetonitrile. Red solid, m. p. 167 °C (dec.), yield 25 % (2 steps). ¹H-NMR (400 MHz, CD₃OD) δ ppm 8.55 (d, 2 H, $^3J = 7$ Hz), 7.94 (d, 2 H, $^3J = 7$ Hz), 7.81 d, 1 H, $^3J = 16$ Hz), 7.58 (d, 2 H, $^3J = 9$ Hz), 7.05 (d, 1 H, $^3J = 16$ Hz), 6.75 (d, 2 H, $^3J = 9$ Hz), 4.45 (t, 2 H, $^3J = 7.5$ Hz), 3.93 (m, 4 H), 3.39 (t, 4 H, $^3J = 7.5$ Hz), 2.87 (t, 2 H, $^3J = 7.5$ Hz), 2.13 (m, 2 H), 1.82 (m, 2 H), 1.63 (m, 8 H), 1.33 (m, 32 H). EIMS m/z 861.6 (M+1)⁺, C₄₁H₇₀N₂O₁₁P₂S requires 861.03.

The stability of the dyes in aqueous solution was checked by Thin Layer Chromatography (TLC). Even after four weeks in Tris-NaCl buffer pH8.1 at 4°C, no degradation or hydrolysis products could be detected.

Elementary analysis. Analyses were carried out by Manfred Barth and assistants from the Inorganic Institute of the Technische Universität München. The results and the best fitting number of solvent molecules are shown in Table 3.

Dye	Batch		C	H	N	P	Br	Br+Cl
Di-4-ASPPP	Hü 947/948 Mix	Found	55.8	8.2	5.5	5.7		
		Calcd. 4*H ₂ O	55.6	8.4	5.4	6.0		
Di-4-ASPPA	SO 21 ger.	Found	67.9	8.0	6.6			
		Calcd.	64.4	7.9	6.3			
Di-6-ASPPA	B814P	Found	66.7	8.6	5.5		14.2	
		Calcd.	66.8	8.6	5.6		15.9	
Di-6-ASPPP	St166	Found	58.9	8.2	4.8	5.2		
		Calcd. 4*H ₂ O	58.6	8.8	4.9	5.4		
Di-4-ASPPiHA ₂	So74P	Found	60.5	7.8	5.3			15.7
		Calcd. 1*H ₂ O	61.9	8.3	5.4			15.3
Di-4-ASPPiHP ₂	So104	Found	47.3	6.9	5.3	7.6		
		Calcd. 5*H ₂ O	46.8	7.9	4.0	8.9		
Di-10A-ASPBS	Hü 991	Found	62.0	8.4	3.8			
		Calcd. 11% inorganic impurities	61.4	8.4	3.9			
Di-10P-ASPBS	So188gs	Found	53.1	7.9	6.7	7.4		
		Calcd. 2*NH ₃	52.2	8.1	6.2	7.5		
Di-12A-ASPBS	So210/1	Found	67.1	9.8	3.8			
		Calcd. 2*H ₂ O	66.8	9.8	3.8			
Di-12P-ASPBS	So221	Found	53.0	8.1	3.1	n.d		
		Calcd. 4*H ₂ O	52.8	8.4	3.0			

Table 3. Elementary analyses of most of the newly synthesized voltage sensitive dyes. The best fitting amount of solvent molecules was inserted to fit the experimental data. In the case of Di-4-ASPPiHA₂, bromine and chlorine were both found as counterions in the analysis and the sum of both halogens was used in the calculation.

Spectroscopy. Absorption spectra were recorded at room temperature with a Varian Cary 3E spectrometer (Mulgrave, Victoria, Australia). Absorption maxima were evaluated by the appending software.

Fluorescence measurements were performed with an SLM Aminco 8100 fluorescence spectrometer (Acton Research, Acton, MA), using an avalanche photodiode in the detection channel (Polytec, Waldbronn, Germany). The bandwidths for excitation and emission were 16 and 36 nm, respectively. All measurements were performed under magic angle conditions. This was done to exclude possible effects of lifetime-dependent spectra on the detected signal due to common polarization in the excitation and emission monochromator. The cuvette holder was kept at a temperature of 25°C (LAUDA RM6 Thermostat). Fluorescence emission maxima were obtained from a log-normal^{1,25} fit of the spectra.

Dye-lipid binding. The binding of the dyes to lipid membranes was determined by fluorescence lipid titration²⁶ with large unilamellar vesicles (LUVs) made of 1-palmitoyl-2-oleoyl-phosphatidylcholine (POPC). The lipid was purchased from Avanti Polar Lipids (Alabaster, AL, USA), Lipoid KG (Ludwigshafen, Germany) and Matreya (State College, PA, USA). The purity of the lipids was checked by 2-dimensional TLC.⁷¹ The vesicles were made by extrusion⁷² in Tris-NaCl buffer (20 mM Tris, 100 mM NaCl, pH 8.1), using an extrusion apparatus and polycarbonate filters with 100 nm pore size (both Avestin Europe, Mannheim, Germany). Vesicle size was determined by quasielastic light scattering using an argon ion laser (Spectra-Physics, Darmstadt, Germany), a photomultiplier (Brookhaven Instruments, Vienna, Austria) and a correlator (ALV-5000, Langen, Germany). The lipid concentration was determined by a chromogenic enzyme assay (Biomerieux, Marcy l'Etoile, France). The standard deviation of three concentration measurements for every vesicle preparation was always below 4 %. Vesicles were stored under argon at 4°C in 15 ml Falcon Centrifuge Tubes (BD Labware Europe, Le Pont de Claix, France) and used within three days.

To measure dye binding constants, 1 mM solutions of the dyes were prepared by ultrasonication in Ethanol (1, 10, 12, 14) or Tris-NaCl buffer (2-9, 11, 13, 15). These stock solutions were diluted in Tris-NaCl buffer to a concentration of 1 μ M. In the same buffer, suspensions of POPC vesicles with concentrations ranging from 100 nM to 10 mM were prepared by dilution of stock solutions. Dye and lipid were pre-thermostated to 25°C. Equal volumes of both were mixed directly before measurement. For the dyes 10, 12 and 14, an additional ultrasonication was necessary to improve reproducibility. The fluorescence emission recorded at 600 nm with excitation at 488 nm was used for the evaluation of the partition coefficients.

Dye internalization assay. HEK293 cell culture was performed as described in section 4.5. The cell medium was removed by suction and replaced by Tris-NaCl-Glucose buffer after washing three times in this buffer. Dye was added to a concentration of 0.03 mM (Di-4-ASPFP, Di-4-ASPPA, Di-4-ASPBS), 0.04 mM (Di-8A-ASPBS), 4 μ M (ANNINE 5, solubilized in 0.3 M HCl) or 1 μ M (Di-10A-ASPBS) and images were made every 10 to 30 sec with the setup used for giant vesicles (cf. section 3.5).

Dye orientation in lipid membrane. Giant lipid vesicles were made by electrosweeling, suspended in Tris-Lipid-Glucose buffer pH 8.1 and adhered to poly-L-lysine treated culture dishes as described in section 3.5. HEK293 cells were cultured as described in section 4.5, and the medium was exchanged for Tris-Lipid-Glucose buffer pH 8.1. In separate experiments, 40 μ l of the dyes ANNINE 5, DiIC₁₈(3) and Di-10A-ASPBS were applied to the medium (4ml) from ethanolic (1 mg/ml DiIC₁₈(3), 1 mg/ml Di-10A-ASPBS) or acidic (1 mg/ml ANNINE 5 in 0.3M HCl) stock solutions. Membrane fluorescence was recorded with a confocal microscope (BX50WI coupled to Fluo200 scanhead and control box; Fluoview 2.0.32 software; all Olympus, Hamburg, Germany) with polarized laser excitation at 488 nm (Stabilite 2017 Argon-ion-laser, Spectra-Physics, Darmstadt, Germany). Fluorescence light was recorded with a high aperture (0.9) water immersion objective (Lum-Plan-FL/IR 60 \times , Olympus) and passed through a band pass filter (610/75 nm). The HEK293 cells chosen for the experiments were mitotic (i.e. loosely attached and therefore round) to facilitate data interpretation. Z-sections were acquired at the approximately maximum diameter of the cells and vesicles.

3 Enzyme Induced Staining of Membranes by a Soluble Enzyme

In this section, the basic experiments elucidating the physicochemical principles of enzyme induced staining of membranes with voltage sensitive dyes are described. First, the susceptibility of the dye phosphates to hydrolysis by soluble alkaline phosphatase from the human placenta (PLAP) in solution was explored. For the dye Di-4-ASPPP, more detailed data about the equilibrium of dye hydrolysis and enzyme kinetic data were determined. Then, the staining of membranes with the help of PLAP was accomplished with the enzymatic reaction taking place in the bulk solution. This exemplary work was performed with Di-4-ASPPP. Results and discussion are described together in each subsection.

3.1 Enzymatic Hydrolysis of Phosphorylated Dyes

3.1.1 Soluble PLAP Accepts all Dye Substrates

The simplest method to check whether PLAP hydrolyses the dye derivatives containing phosphate groups is thin layer chromatography (TLC). For all dye phosphates examined, digestion over night led to complete hydrolysis to the respective alcohol within the limits of detection of TLC (Figure 10A). Note that also the Diphosphate Di-4-ASPP(PP) is accepted as a substrate, in accordance with the fact that alkaline phosphatases in general can also hydrolyze Di-, Tri- and higher polyphosphates.²² For dyes containing two phosphate groups, an incomplete digest was performed to determine whether there was a great difference in the rates of removal for the first or second phosphate group. At the point of time where hydrolysis was stopped, the ratio of Diphosphate : Monophosphate : Alcohol was between 1 : 0.75 : 0.2 and 1 : 1 : 0.5 for all dyes as estimated by evaluation of the brightness of the respective bands. According to a coupled first order reaction model⁷³ with equal rate constants for the first and second step, one would expect ratios of 1 : 0.75 : 0.37 and 1 : 1 : 0.72, respectively

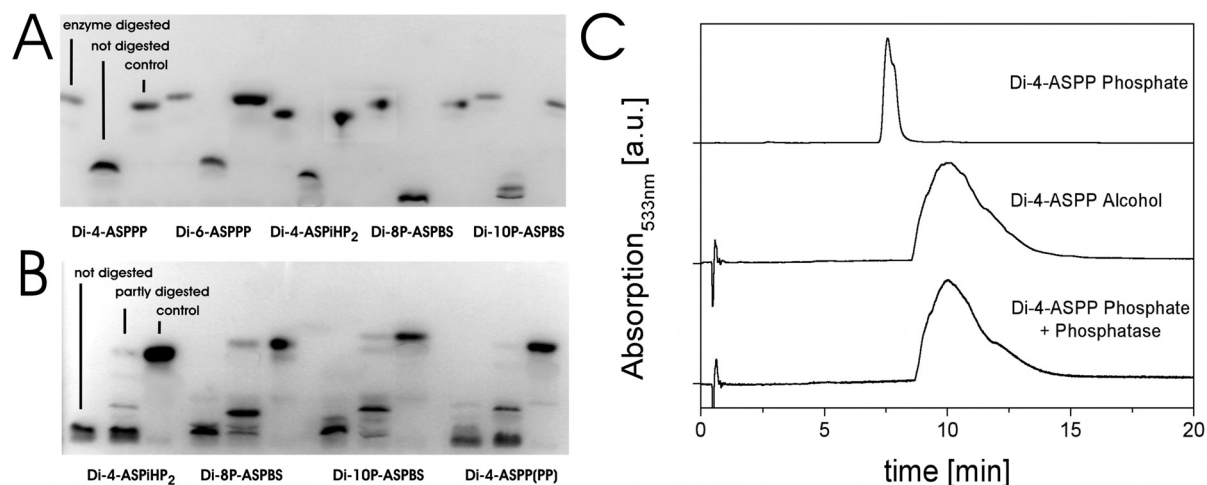


Figure 10. Enzymatic hydrolysis of dye phosphates by PLAP. (A) Complete digest. Inverted fluorescence image of dyes on a SiO₂ TLC plate (solvent MeOH:CHCl₃:H₂O - 50:20:4 (v/v/v)). Dye phosphates at a concentration of 10 μM were incubated overnight at room temperature with PLAP of an activity of 0.18 DEA Units/ml. For each digest, the dye phosphate incubated without PLAP and the corresponding dye alcohol were run on the same plate as a control. (B) Partial digest. The same assay was performed with a reduced incubation time for dyes containing two phosphate groups. Note that some additional bands appear on the TLC plate. These originate from a reaction occurring on the plate after prolonged drying of the applied dye and do not represent originally present impurities. (C) HPLC time traces of Di-4-ASPPP, Di-4-ASPPA and Di-4-ASPPP incubated with enzyme overnight.

(calculation not shown). The data, although admittedly crude, therefore indicates that there are no substantial differences in the rate constants for first and second step.

An alternative quantitative examination of the relative equilibrium concentrations of Di-ASPP Phosphate and the product of hydrolysis, Di-4-ASPP Alcohol, was carried out by High Performance Liquid Chromatography (HPLC). Dye phosphate was incubated with PLAP and the enzyme was subsequently removed by ultrafiltration. The HPLC spectra show that the hydrolysis is quantitative (Figure 10C).

3.1.2 Hydrolysis Kinetics of Di-4-ASPPP measured by ITC

The reaction kinetics of the hydrolysis of Di-4-ASPPP were studied by isothermal titration calorimetry (ITC). The heat production of a chemical reaction per unit time is proportional to the reaction rate, with the molar heat of reaction being the constant of proportionality.⁷⁴ Figures 11B (i) and (iii) show the calorimeter traces of typical measurements of enzymatic hydrolysis and the heat of dilution. The raw data was corrected by subtraction of the baseline which was approximated by a polynomial fit of the lowest applicable order (Figure 11B (ii)). The fully corrected signal of enzymatic hydrolysis was then obtained by subtracting the heat of dilution from the corrected raw signal (Figure 11B (iv)). It was found that the hydrolysis was endothermic by $1.1 \pm 0.2 \text{ kJ/mol}$, a value in a typical range for monophosphoric acid esters.⁷⁵ By calibration with that energy, the initial reaction velocity was evaluated. The precision was limited due to the low substrate concentrations. The initial reaction velocity scaled by the effective enzyme concentration \tilde{c}_E in *PLAP DEA Units/l*^b is plotted in Figure 11A versus the substrate concentration c_P .

To evaluate the data, Michaelis-Menten kinetics were used according to eq 11 with the Michaelis constant K_m , an effective maximum rate constant \tilde{k}_{cat} per DEA Units of PLAP and an effective enzyme concentration \tilde{c}_E .

$$-\frac{dc_P}{dt} = \frac{\tilde{k}_{cat}\tilde{c}_E}{1 + K_m/c_P} \quad (11)$$

The initial velocity $v_0 = -(dc_P/dt)_0$ was fitted by nonlinear regression and yielded $K_m = 10.9 \pm 4.3 \mu\text{M}$ and $\tilde{k}_{cat} = 0.56 \pm 0.12 \text{ nmol/s Units}$ (n=3). The hydrolysis is slow compared to $\tilde{k}_{cat} = 17 \text{ nmol/s Units}$ for the common model substrate *para*-Nitrophenylphosphate (*p*-NPP) at optimal conditions (pH 9.8, 37°C, DEA buffer). However, the reaction conditions with pH 8.1, 25°C, Mg²⁺-free, chosen for stability of vesicles and cells, are quite different. Under these conditions, the rate constant for *p*-NPP hydrolysis was

^b For reasons stated in the Materials and Methods section, the enzyme concentration is expressed in units of activity in Diethanolamine (DEA) buffer containing Mg²⁺ at pH 9.8/37°C.

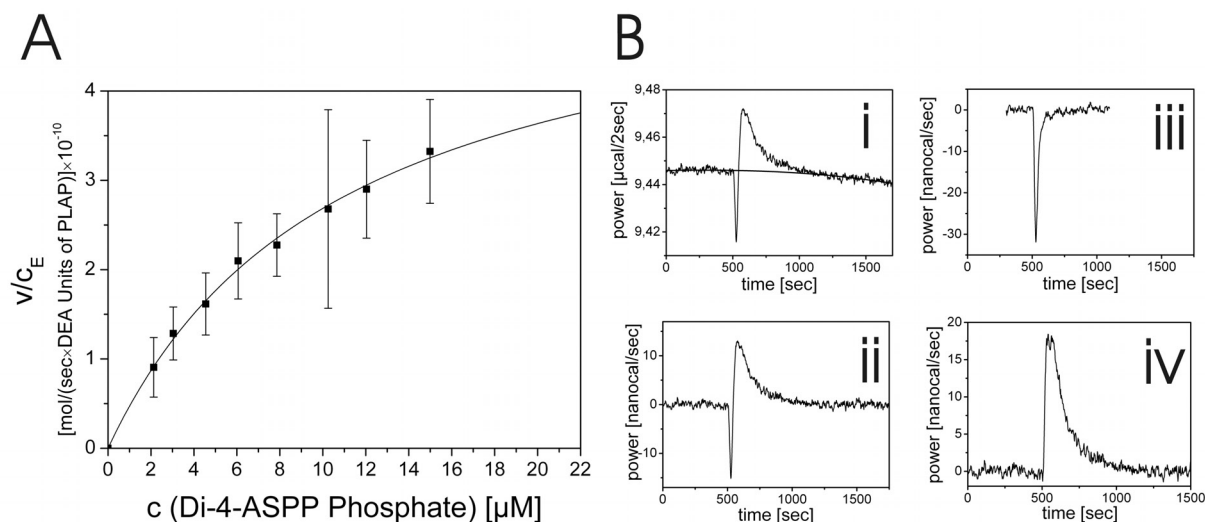


Figure 11. Enzyme kinetics by microcalorimetry. (A) Ratio v_0/\tilde{c}_E of initial velocity of hydrolysis and of effective enzyme concentration versus concentration c_p of the substrate Di-4-ASPPP at 25.0°C. The data are fitted with Michaelis-Menten parameters K_m and \tilde{k}_{cat} . (B) Example for microcalorimeter tracings of reaction heat versus time ($c_p = 6.1\mu M$). (i) Raw data for dye injected into solution containing PLAP with polynomial baseline fit (solid line). (ii) Calorimeter tracing (i) corrected by subtraction of the fitted baseline. (iii) Corrected calorimeter tracing of dye injection into buffer without enzyme. (iv) Calorimeter tracing (ii) corrected by subtraction of the dilution heat (iii). The peak of the curve corresponds to the initial velocity of the enzymatic reaction. The molar heat of reaction is obtained by integration.

$\tilde{k}_{cat} = 0.35 \text{ nmol/s Units}$ (data not shown). Apparently, Di-4-ASPPP is accepted by PLAP as a regular substrate.

3.2 Enzyme Induced Staining of Liposomes

In the next step, the previous experiments were combined. The dye phosphate was hydrolysed by phosphatase in the presence of lipid vesicles. The reaction was observed by the enhancement of fluorescence due to the enhanced binding of the dye alcohol to the lipid. Two examples are shown in Figure 12A. The fluorescence intensity of a vesicle suspension (100 μM lipid) was recorded before and after the addition of the phosphatase with 0.43 μM and 4.31 μM Di-4-ASPPP. From a low level caused by the binding of the substrate, it was enhanced to a sixfold higher level due to binding of the product. This corresponds to the ratio of the fluorescence lipid titration data of alcohol and phosphate at 100 μM lipid (cf. Figure 12B and eq 2). Obviously, the staining of lipid membranes is accomplished by enzymatically induced enhancement of lipophilicity.

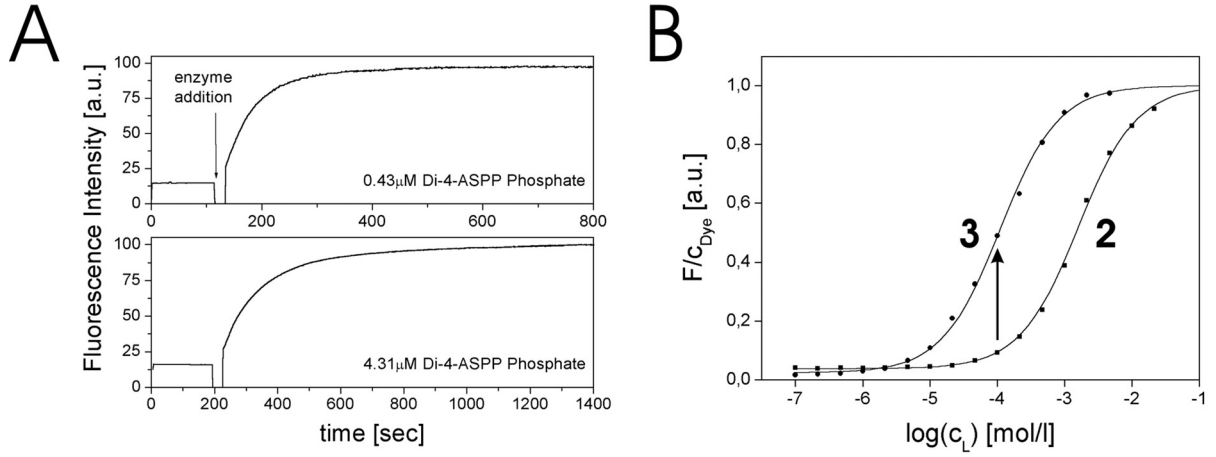


Figure 12. Enzyme induced staining of lipid membrane. (A) Fluorescence intensity versus time of a vesicle suspension (lipid concentration 100 μM POPC) at two concentrations 0.43 μM (top) or 4.31 μM (bottom) for the substrate Di-4-ASPPP. The addition of phosphatase is marked by an arrow. (B) Fluorescence lipid titration curves for Di-4-ASPPP (2) and Di-4-ASPPA (3; cf. Figure 6). The increase in fluorescence intensity as expected for (A) at the used lipid concentration is indicated by an arrow.

To test the correlation of time dependent fluorescence with the kinetic data of hydrolysis as obtained by ITC, an evaluation of the data in terms of the Michaelis-Menten kinetics of hydrolysis coupled to equilibrated water/lipid distribution of substrate and product was performed. Let us first consider the correlation that would be expected from what we know about binding and enzyme kinetics. Both dyes contribute to the total fluorescence, proportional to the concentrations of Di-4-ASPPP c_P and Di-4-ASPPA c_A with $c_{tot} = c_P + c_A$ according to eq 3. The total fluorescence of the suspension before and after the reaction is denoted by F_0 for $c_P = c_{tot}$ and by F_∞ for $c_P = 0$. During the reaction the fluorescence is $F(t) = F_0 [c_P(t)/c_{tot}] + F_\infty [1 - c_P(t)/c_{tot}]$ and the initial velocity of the reaction is obtained from the initial slope of intensity according to eq 12.

$$v_0 = \frac{c_{tot}}{F_\infty - F_0} \left(\frac{dF}{dt} \right)_0 \quad (12)$$

Using eq 12, the kinetic data for vesicle suspensions of 100 μM POPC with 0.17 DEA Units/ml PLAP was evaluated in a concentration range of Di-4-ASPPP from 0.1 μM to 10.7 μM. The initial velocities v_0 scaled by the effective enzyme concentration \tilde{c}_E in PLAP DEA Units / l are plotted versus the dye concentration in Figure 13. The fit of the data by eq 11 resulted in $K_m = 7.3 \pm 0.6 \mu M$ and $\tilde{k}_{cat} = 0.53 \pm 0.2 \text{ nmol/s Unit}$ (n=3).

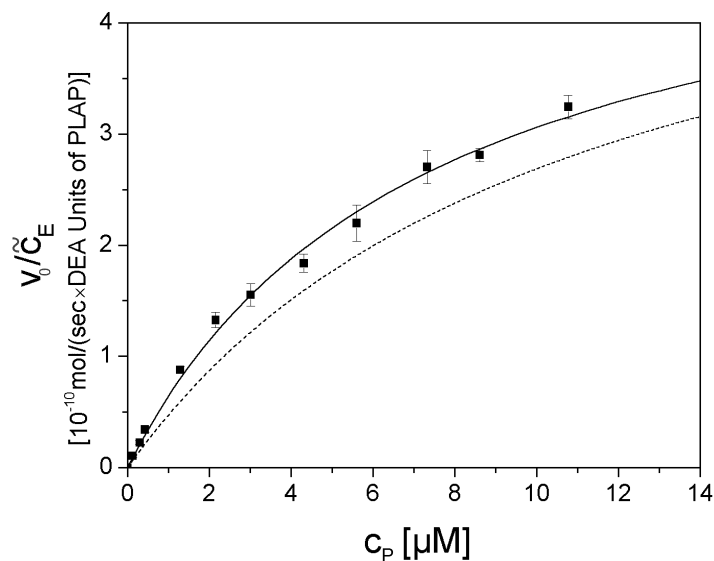


Figure 13. Enzyme kinetics by fluorometry in a vesicle suspension. Ratio v_0 / \tilde{c}_E of initial velocity of hydrolysis and of effective enzyme concentration versus concentration c_p of the substrate Di-4-ASPPP at a lipid concentration of $100 \mu\text{M}$ (25.0°C). The data are fitted with Michaelis-Menten parameters K_m and \tilde{k}_{cat} . The fit obtained from microcalorimetric experiments (Fig. 4) is indicated as a dashed line.

There is good agreement between the enzyme kinetic parameters obtained by the fluorescence measurements in a lipid suspension and those obtained by ITC in a lipid free solution considering the experimental error of the ITC measurements (cf. Figure 11). However, several problems have to be considered in a quantitative evaluation of the enzyme reaction with lipid vesicles by indirect observation of fluorescence: (i) Does hydrolysis originate from free or from lipid bound enzyme? (ii) Is it free or lipid bound substrate that is hydrolysed? (iii) Does binding of the dye to the enzyme contribute to enhanced fluorescence? (iv) Is there an effect caused by changed electrostatics during the reaction – with the membrane being negatively charged by bound Di-4-ASPPP before reaction and being positively charged by bound Di-4-ASPPA after the reaction? (v) Is there an interference caused by the flip-flop dynamics of the product across the membrane? To consider these questions, additional experiments were performed.

(i) *Lipid-bound enzyme.* It was checked whether PLAP interacts with POPC membranes using a sucrose loaded vesicle binding assay. PLAP was incubated with sucrose filled liposomes. After incubation, the liposomes and potentially bound PLAP were removed by ultracentrifugation, and the percentage of bound PLAP was calculated from the residual enzymatic activity of the supernatant. Commonly, this assay yields sigmoidal binding isotherms for proteins,³⁴ similar to fluorescence lipid titration. With PLAP, the assay indicated that between 8 and 20 % of the protein were removed by ultracentrifugation (Figure

14A). There was no significant dependence of the fraction of bound enzyme on the lipid concentration. Conclusively, the observed binding is an artifact introduced by the assay and there is no specific binding of the enzyme to the vesicles, i.e. the observed dye hydrolysis is due to the enzymatic action of *free* enzyme.

(ii) *Lipid-bound substrate*. It was examined whether the reaction rate depends on the fraction of bound substrate that increases with the lipid concentration according to eq 2 (Figure 14B, solid line). The fluorescence kinetics were evaluated with 0.5 μM Di-4-ASPPP at various lipid concentrations as shown in Figure 14B (squares). The reaction rate slows down inversely to the fraction of bound dye. This effect was ascribed to the inaccessibility of bound Di-4-ASPPP to the phosphatase. In the kinetic experiments described above, the inhibiting effect on Di-4-ASPPP hydrolysis was avoided by using a low lipid concentration of 100 μM .

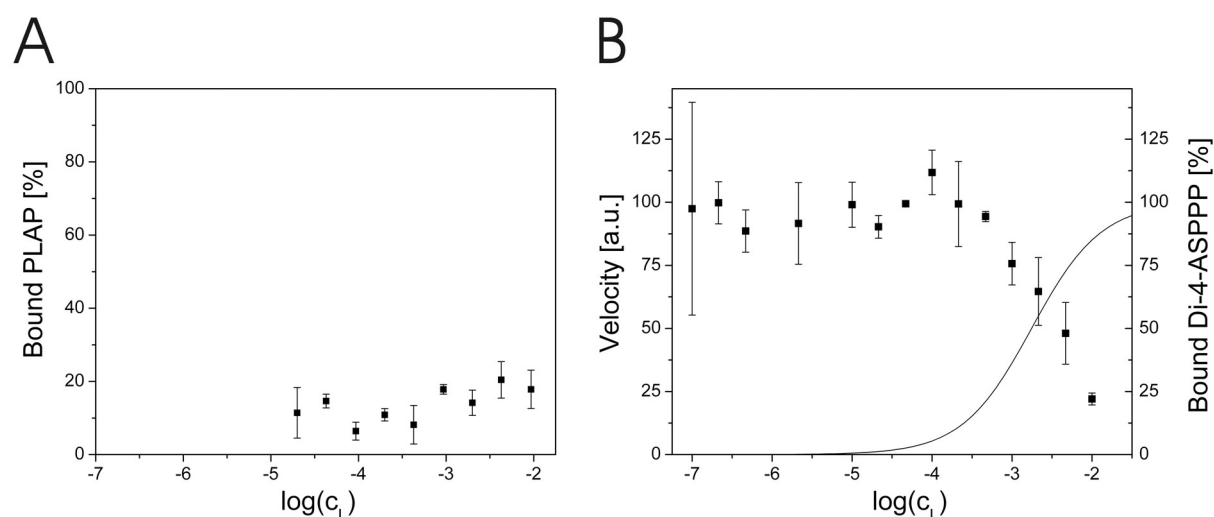


Figure 14. Perturbation of enzyme kinetics by lipid bound enzyme and lipid bound substrate. (A) Percentage of bound enzyme PLAP versus lipid concentration determined by a sucrose loaded vesicle binding assay. The fraction of bound phosphatase is not significant considering the accuracy of the method (see text). (B) Reaction rate of enzymatic hydrolysis for Di-4-ASPPP (solid squares with standard deviation) versus lipid concentration. For comparison, the fraction of lipid bound Di-4-ASPPP as calculated by eq 2 is plotted as a dashed line.

(iii) *Enzyme bound dye*. The initial fluorescence F_0 of enzyme kinetics was measured prior to the addition of enzyme, while the fluorescence increase and the final fluorescence F_∞ were obtained in the presence of enzyme. When PLAP was added to a solution of the product Di-4-ASPPA, the fluorescence of the solution increased due to an enhanced fluorescence quantum yield of dye bound to the surface of protein. It was found that a protein concentration of 0.17 DEA Units/ml PLAP corresponded to a lipid concentration of

approximately 5 μM from experiments in the presence of both lipid and PLAP (data not shown). Thus at the lipid concentration of 100 μM , the effect of dye binding to the protein can be neglected.

(iv) *Electrostatics*. During the course of the reaction, the surface potential of the liposomes changes from a low negative value due to weakly bound phosphate to a higher positive value due to bound alcohol. Considering eq 6, the effect leads to a lower binding constant at high dye concentrations and a sublinear increase of fluorescence with hydrolysis. The role of the phosphate is negligible due to its low binding constant. Electrostatic repulsion of bound alcohol affects the maximum fluorescence F_∞ used in the evaluation of the initial reaction velocity and at high dye concentrations should lead to an overestimation of its value. Considering the good match of fluorescence assay and ITC data, this effect is considered to be negligible.

(v) *Flip-flop*. In the kinetic measurement at the high dye concentration of 4.31 μM in Figure 12A, the fluorescence does not level out at a constant F_∞ but grows with a small constant slope. The effect was observed for dye concentrations above 3 μM . It may be attributed to a slow flip of the dyes to the inner monolayer of the liposome and enhanced binding. The effect was not apparent at lower dye concentrations, because the fluorescence increase due to reaction was much faster than the increase due to flip-flop. In the evaluation of the data, F_∞ was therefore defined by the fluorescence at the time where constant slope was attained.

The discussion of the problems (i) to (v) indicates that adequate enzyme and lipid concentrations must be chosen in the fluorescence assay with liposomes in order to obtain data that reliably reflect enzyme activity in the aqueous phase. Some error may be introduced by electrostatics and flip-flop. Nonetheless, the fluorescence assay can be used as a reliable and sensitive method to test enzymatically activated amphiphilic dyes.

3.3 Enzyme Induced Staining of Giant Vesicles

As a first example of enzyme induced staining of a cell-like system, giant lipid vesicles were chosen ($\varnothing \approx 10 - 40 \mu\text{m}$). Individual vesicles of POPC were incubated with 9.8 μM of the dye phosphate and observed in a microscope with a CCD camera. Figure 15A shows a sequence of images before (Figure 15A, 0 min) and after the addition of the phosphatase. Apparently, the fluorescence of the membrane increases considerably after addition of the enzyme. Figure 15A impressively demonstrates that enzyme induced staining is possible with individual cell-type structures.

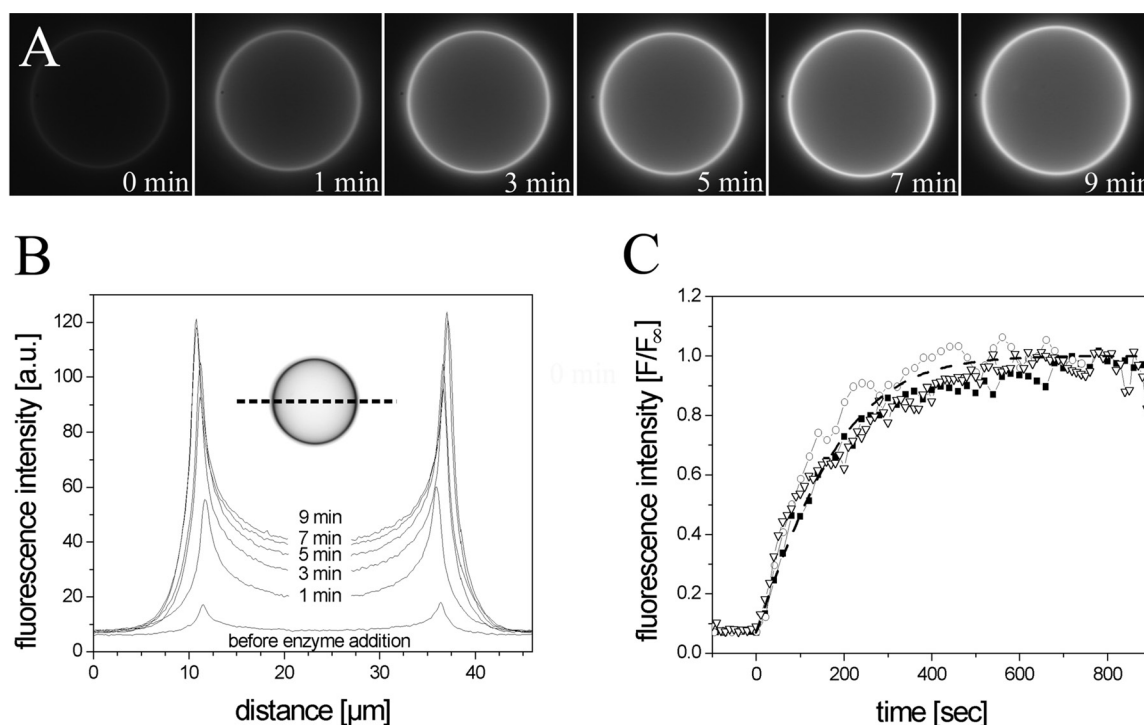


Figure 15. Enzyme induced staining of giant lipid vesicle. (A) Fluorescence image (excitation around 450 nm, emission at >510 nm) of a giant vesicle before (0 min) and after addition of phosphatase (activity 0.18 DEA Units/ml). Di-4-ASPMP was present at a concentration of $9.8 \mu\text{M}$. (B) Profiles of fluorescence intensity across the diameter (approx. $27 \mu\text{m}$) of a vesicle. (C) Normalized fluorescence intensity of vesicle membrane (peak of the profile minus background) versus time for three different vesicles. The dashed line is the fluorescence computed with the enzyme kinetic parameters K_M and \tilde{k}_{cat} from ITC and a scaling factor of fluorescence fitted to the data.

The intensity of a row of pixels of the image was evaluated at the maximum diameter in y -direction as shown in Figure 15B. The profiles exhibited a strong intensity at the maximum diameter of the vesicle and a weaker, “U”-shaped intensity at the center of the vesicle. The fluorescence intensity is a projection of the whole giant vesicle fluorescence (note that the images were not recorded with a confocal microscope). A plot of the maximum intensity minus background versus time is shown for three different vesicles in Figure 15C. The fluorescence intensity was normalized to the mean value of the plateau fluorescence for each experiment. After addition of the enzyme, the fluorescence increased from a constant low value F_0 caused by staining with the phosphate to a high constant value F_∞ due to staining by the alcohol. The ratio of intensities was $F_\infty / F_0 = 9 - 13$.

How does this value correlate with the measured binding constants? The fluorescence intensity in a microscope that is focused on the membrane is dominated by membrane-bound dye, i.e. by the density of bound dye molecules $n_{D,b}$, with little contribution of the solution since the dye is essentially non-fluorescent in the aqueous environment. $n_{D,b}$ is determined by

the concentration of free dye according to the relation $n_{D,b} = K_D c_{D,f} / a_L$ where it may be assumed that $c_{D,f} \approx c_D$ since the number of giant vesicles in the culture dish was very small and hence the solution was not depleted. Considering this relation, it is expected that the ratio of fluorescence intensity before and after the staining process is solely determined by the ratio of the binding constants of the dyes, if excitation and recording of fluorescence are identical for phosphate and alcohol. For liposome suspensions, $K_A / K_P \approx 16$ were measured at low dye concentrations and $K_A / K_P \approx 7$ at a concentration of 9.8 μM (cf. section 2.3). The ratio of the fluorescence intensities $F_\infty / F_0 = 9 - 13$ found with giant vesicles is in good agreement.

During the reaction, the fluorescence is $F(t) = F_0 [c_P(t)/c_{tot}] + F_\infty [1 - c_P(t)/c_{tot}]$. The dynamics of the normalized fluorescence F/F_∞ were computed by inserting the Michaelis-Menten dynamics (eq 11) and integrating it with the parameters determined by ITC. The result is plotted in Figure 15C (dashed line). The perfect agreement with the data shows that staining of giant vesicles is indeed due to enzymatic activation of the precursor dye.

3.4 Enzyme Induced Staining of Erythrocyte Membrane

The plasma membrane of cells consists of a variety of charged and uncharged lipids and of membrane proteins. It is well known that voltage sensitive dyes are able to bind to membrane proteins.⁵⁹ Therefore it must be checked whether an enzyme induced change of headgroup polarity also leads to increased staining of a eukaryote membrane. As noted in section 2.4, Di-4-ASPPP and Di-4-ASPPA rapidly stain internal membranes of eukaryotic cells. Red blood cells, however, have a rather inactive plasma membrane and no internal organelles. For that reason erythrocytes were chosen as a model.

Di-4-ASPPP was added to human erythrocytes attached to a culture dish to a concentration of 9.8 μM . Membrane fluorescence was measured in the same setup as with giant vesicles. Fluorescence was weaker than with giant vesicles, which is attributed to fluorescence quenching by hemoglobin and the smaller size of the erythrocytes. Figure 16A shows an example of a sequence of images of the erythrocyte membrane before and after addition of phosphatase. The fluorescence intensity significantly increased. The experiment proves that the enzyme induced modulation of headgroup polarity is also an effective mechanism of staining for cell membranes.

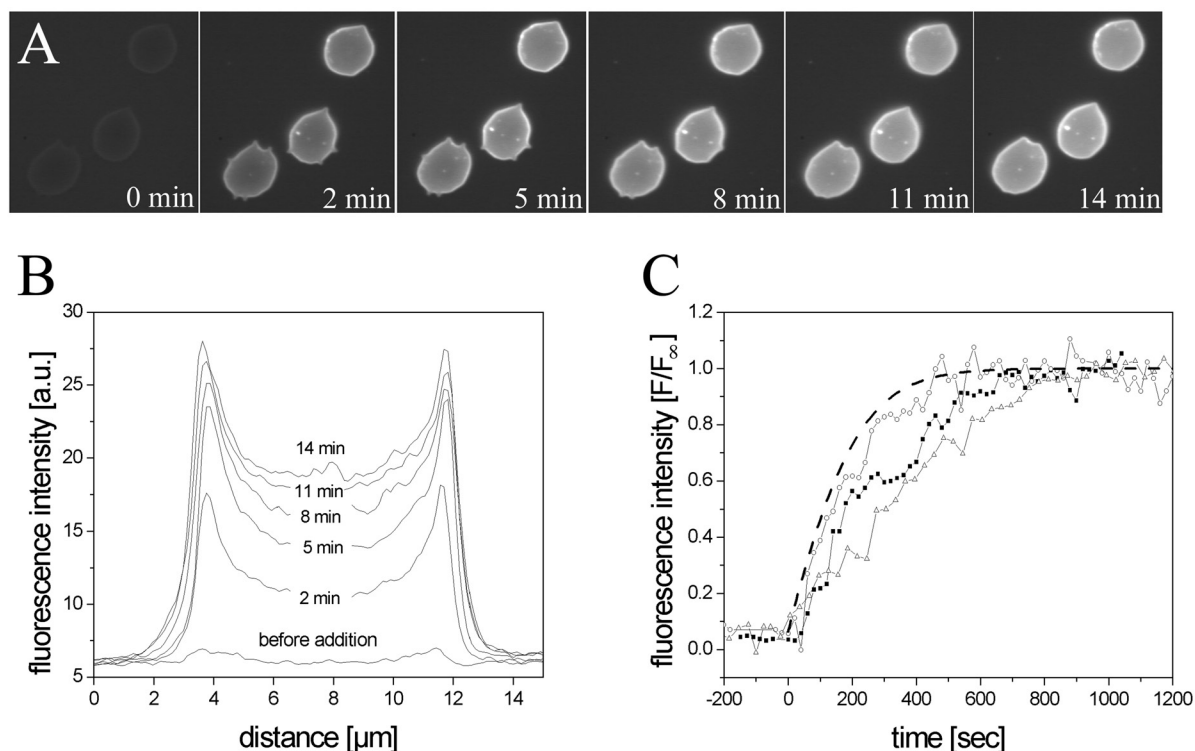


Figure 16. Enzyme induced staining of erythrocyte membrane. (A) Fluorescence image (excitation around 450 nm, emission at >510 nm) of an erythrocyte before (0 min) and after addition of phosphatase (activity 0.18 DEA Units/ml). Di-4-ASPMP was present at a concentration of $9.8 \mu\text{M}$. (B) Profiles of fluorescence intensity across the diameter of an erythrocyte with a diameter of about $8 \mu\text{m}$ on the culture dish. (C) Normalized fluorescence intensity of vesicle membrane (peak of the profile minus background) versus time for three different vesicles. The dashed line is the fluorescence computed with the enzyme kinetic parameters K_M and \tilde{k}_{cat} from ITC and a scaling factor of fluorescence fitted to the data.

Plots of the intensity of a row of pixels cutting through the image of an erythrocyte at its maximum diameter are shown in Figure 16B. The normalized maximum brightness minus the background signal versus time is shown in Figure 16C. The ratio of final and initial fluorescence was $F_\infty/F_0 = 11 - 25$ with an average of 15. These values are similar to the fluorescence enhancement with giant vesicles. Also the fluorescence dynamics during staining that are computed from the Michaelis-Menten kinetics agree fairly well with the experiments as shown in Fig. 9C. However, the variation of the experiments and the deviation from the expected reaction progress is larger than for giant vesicles. It is probable that there is a larger experimental error attributable to the weaker fluorescence and to changes in the shape of the erythrocytes during the measurement.

3.5 Materials and Methods

Enzyme. HPLC was used to determine whether Di-4-ASPPP is a substrate for Alkaline Phosphatase from the Human Placenta (PLAP). The activity of the two batches of the enzyme (SIGMA) was tested with 1 mM *p*-NPP ($\epsilon = 18.5 \times 10^3 \text{ M}^{-1} \text{ cm}^{-1}$) as a chromogenic substrate in DEA buffer (1 M DEA, 1 mM MgCl_2 and 10 μM ZnSO_4 , pH 9.8) at $37.0 \pm 0.3^\circ\text{C}$. The activities obtained were 27.2 ± 0.4 Units/mg and 26.1 ± 0.5 Units/mg. (A Unit is defined as the activity necessary to digest 1 μM *p*-NPP per minute). The purity of the samples was tested by liquid chromatography coupled with mass spectrometry (LCMS; Sciex API 165, Perkin Elmer Instruments, Rodgau-Jügesheim, Germany) with a Nucleosil-100-5 C8 column (Macherey & Nagel, Düren, Germany; solution A: 0.05% TFA in H_2O ; solution B: 0.05% TFA in acetonitrile; gradient: 80% H_2O to 10% H_2O in 15 minutes). It was found that the elution profile was identical for both batches, and that both contained a mixture of various compounds not further identified. The impurity of commercially available PLAP is documented in the literature.⁷⁶ Since the activity per milligram varies between the batches, all concentrations and activities are referred to DEA Units, i.e. the activity that an equal amount of PLAP would have in DEA buffer (pH 9.8, 37°C).

In the HPLC assay, Tris-NaCl buffer containing 55 μM dye and 0.24 DEA Units/ml PLAP was incubated for three hours at room temperature. The enzyme was separated by filtering through a Centricon YM-3 membrane (Millipore, Billerica, MA, USA) with a cut-off at 3 kD. The filtered solution was concentrated to dryness in a vacuum centrifuge at room temperature. The analytes were dissolved in acetonitrile/ H_2O (1:1) and HPLC analysis (Bischoff, Leonberg, Germany) was performed with a C18 Nucleosil column (100-7, Macherey & Nagel, Düren, Germany) and 10 mM phosphoric acid and acetonitrile as eluents (gradient 30% to 70% phosphoric acid in 15 min) with optical detection at 533 nm.

Enzyme kinetics with ITC. Enzyme kinetic measurements were performed with Di-4-ASPPP as a substrate of PLAP by isothermal titration calorimetry (ITC). For this, Tris-NaCl buffer (20 mM Tris, 100 mM NaCl, pH 8.1) without Zn^{2+} and Mg^{2+} was used although most alkaline phosphatases depend on these metals for maximum activity. However, divalent cations bind to lipid membranes and induce their aggregation and fusion.⁷⁷ The pH-value is a compromise between optimal enzymatic activity (at pH 9.8) and compatibility with vesicles and cells. The microcalorimeter (VP-ITC, Microcal, Northampton, MA, USA) was thermostated to 25.0°C , with reference power set to 10 $\mu\text{cal}/\text{sec}$ and a stirring speed of 310 rpm. The sample cell contained a PLAP solution of 0.19 DEA Units/ml activity and the syringe was filled with a 1 mM solution of Di-4-ASPPP. The reference cell contained buffer only. Different amounts of dye were injected into the sample cell in separate experiments to cover a concentration range from 2 μM to 15 μM . To determine the heats of dilution alone, injections were carried out with pure buffer. For both hydrolysis and dilution, the baseline signal was approximated by linear or polynomial functions and subtracted from the raw signal, resulting in a curve with a flat baseline. The dilution signal was subtracted from the signal of the enzymatic reaction to yield the final calorimeter tracing of enzymatic hydrolysis. The molar heat of reaction was obtained by integration. The initial velocities were determined from the average heat of reaction of the first 10 to 30 seconds after the onset of the reaction, using the mean molar heat of reaction as a proportionality constant. Data analysis, including estimates of statistical errors of nonlinear curve fits, was performed with Origin (OriginLab Software, Northampton, MA, USA).

Sucrose Loaded Vesicle Binding Assay. This assay³⁴ was used to study the binding of PLAP to lipid vesicles. Sucrose loaded vesicles were made by extrusion in 20 mM Tris, 176 mM Sucrose, pH 8.1. The outside

buffer was exchanged by 1:4 dilution into sucrose-free Tris-KCl buffer (20 mM Tris, 100 mM KCl, pH 8.1) and ultracentrifugation for 1 h at 100000 g and 25°C (Optima TLX with a TLA-100.3 rotor, 1.5 ml polyallomer microfuge tubes, Beckman Coulter, Fullerton, CA, USA). The pelleted vesicles were resuspended in Tris-KCl buffer and used within the same day. The lipid concentration was determined by a chromogenic enzyme assay (Biomerieux). For the binding assay, sucrose loaded POPC vesicles were diluted to concentrations ranging from 20 μ M to 10 mM. To 550 μ l lipid suspensions, 5 μ l of a PLAP solution of 18.6 DEA Units/ml activity in Tris-KCl buffer were added. After 45 minutes incubation at room temperature the suspensions were centrifuged. To account for protein loss during centrifugation, tubes containing no lipid were added as a reference. The supernatant was removed as completely as possible. The enzymatic activity in the supernatant of solutions with and without lipid was determined by using *p*-NPP as a substrate. 0.2 ml of the supernatant were added to 1.8 ml 1 mM *p*-NPP in Tris-KCl buffer and absorption over time was recorded at 405 nm. The fraction of bound phosphatase was obtained from the ratio (activity of supernatant without lipid - activity of supernatant with lipid)/activity supernatant without lipid.

Enzyme induced staining of liposomes. To observe enzyme induced staining, enzymatic hydrolysis of Di-4-ASPFP was studied in the presence of large unilamellar POPC vesicles (LUVs). Tris-NaCl Buffer was used for the preparation of all solutions. To 550 μ l of a 200 μ M solution of POPC vesicles in a cuvette, an equal volume of Di-4-ASPFP was added to yield concentrations between 0.1 μ M and 10.7 μ M. 10 μ l of PLAP (18.6 DEA Units/ml) were added and the suspension was mixed by pipetting. The cuvette was held at 25°C. Fluorescence (excitation 488 nm, emission 600 nm) was recorded before and after addition of the enzyme with a resolution of 1 sec. Initial velocities were determined from the slope of the first 10 to 20 seconds of the fluorescence traces.

Enzyme induced staining of giant vesicles. Giant POPC vesicles were prepared by electrosweeling⁷⁸⁻⁸⁰. 5 μ l of a 2 mM lipid solution in diethyl ether/methanol (9:1, v/v) were applied to a pair of planar electrodes of indium tin oxide coated with 70 nm of silica. After evaporation of the solvent under reduced pressure (0.1 mbar), 2 ml of 300 mM sucrose were added and giant vesicle formation was promoted by applying AC voltage to the electrodes. After formation was complete, vesicles were transferred to 35 mm polypropylene cell culture dishes (BD Biosciences Europe, Le Pont de Claix, France) and diluted in the same buffer. They were used the same day.

For enzyme kinetic measurements at room temperature, 400 μ l of the giant vesicle stock solution were transferred to a culture dish containing 3600 μ l buffer (20 mM Tris, 100 mM NaCl, 120 mM Glucose, pH 8.1). The dish had been treated overnight with poly-L-lysine (25 μ g/l) to permit the immobilization of vesicles. The giant vesicles were allowed to adhere to the substrate for 15 minutes. Subsequently, 40 μ l of a 1 mM Di-4-ASPFP solution in the same buffer were added. The fluorescence of a selected giant vesicle with a diameter of 10 to 40 μ m was observed using a microscope (Axioskop, Zeiss, Oberkochen, Germany) equipped with a 100 \times water immersion objective and a b/w CCD camera (Sony ICX 285 Chip, Theta System, Gröbenzell, Germany). The light of a high pressure mercury lamp (Zeiss) was passed through a band pass (450/50 nm) and a dichroic mirror (505 nm). The fluorescence was detected through the dichroic mirror and a long pass filter (510 nm). Grey filters were used to reduce light intensity. The microscope was focused on the maximum diameter of the vesicles before and during the experiment. After incubation with the dye for 5 minutes, 40 μ l of PLAP were added from a stock solution with an activity of 18.6 DEA Units/ml. Homogenous distribution was achieved by mild pipetting. Images were recorded every 10 or 20 seconds before and after addition of the phosphatase.

Image acquisition, camera and shutter control as well as image analysis were performed with software written in Labview (National Instruments Germany, Munich).

Enzyme induced staining of red blood cells. Human erythrocytes were prepared according to a slightly modified standard procedure⁸¹. 4 ml of blood of the author of this work were sucked into a tube coated with EDTA (Vacutainer 367861, Becton Dickinson, Meylan, France) and centrifuged for 10 min at 1600 g. The pellet (~1 ml) was washed three times by resuspension and centrifugation for 10 min at 1600 g using 15 ml of a 300 mOsm Tris buffer (50 mM Tris, 110 mM NaCl, pH 7.4). Finally, the pellet was diluted with an equal volume of the same buffer additionally containing 1 mM CaCl₂. Ca²⁺ was added since it was found to increase the number of erythrocytes retaining a round shape under the experimental conditions.

The staining experiments with erythrocytes were similar to those with giant vesicles. 2 µl of the erythrocyte stock solution were spread on the bottom of an untreated culture dish containing Tris buffer with CaCl₂ (20 mM Tris, 100 mM NaCl, 70 mM Glucose, 1mM CaCl₂, pH 8.1). After 30 seconds, erythrocytes not adhered to the substrate were removed by washing twice. The dish was filled with 4 ml buffer. 40 µl of a 1 mM Di-4-ASP-phosphate solution were added. After 5 minutes incubation, 40 µl of PLAP were added from a stock solution with an activity of 18.6 DEA Units/ml. Images were taken every 30 seconds before and after the addition of the enzyme. To minimize UV exposure, erythrocytes were focused under red light before and, if necessary, during the experiment.

4 Genetic Targeting of an Enzyme to the Plasma Membrane

The next step towards selective staining of cells with voltage sensitive dyes by enzyme activation is the expression of the respective enzyme on the surface of the cell of interest itself. To that end, a plasma membrane targeting signal equipped for facilitated construction of fusion proteins between membrane targeting signal and enzymes was designed and synthesized. The present chapter is subdivided into three parts: The first one provides background information on sorting in the cell, the second part describes the design and synthesis of the membrane targeting signal, and the last section addresses the construction and characterization of a sandwich fusion protein of this targeting signal with Alkaline Phosphatase from the Human Placenta (PLAP). Results are discussed in each subsection and in a final conclusion.

4.1 Background

Every mammalian cell contains distinct organelles, for example those of the secretory pathway: endoplasmic reticulum (ER), the *cis*, *medial* and *trans* Golgi compartments and the plasma membrane. These organelles or compartments contain their own sets of proteins which enable them to fulfill their specialized tasks. All protein syntheses start in the cytoplasm (except for a number of proteins synthesized in the mitochondria). So how does a protein know where it belongs, i.e. how does protein sorting take place? The answer is that proteins contain sorting signals. These can either be *signal sequences* which consist of a continuous amino acid sequence, or *signal patches*, where the tertiary protein structure contains the sorting information. An example for the former are membrane targeting signals, which target a protein to the organelles of the secretory pathway.

A membrane targeting signal consists of a continuous, hydrophobic stretch of 7 to 25 amino acids. A ribosome that is active in the synthesis of a protein containing such a signal is transferred to the ER, where synthesis is continued, with the nascent peptide chain being translocated through the ER membrane while the protein is synthesized. This process is

termed *cotranslational translocation*. The targeting signal is then either cleaved off (*signal peptide*) by a specialized enzyme, or it serves as a *membrane anchor*. Although both signal peptide and membrane anchor consist of a stretch of hydrophobic amino acids, the signal peptide sequence is usually shorter (7 to 15 residues), and it must be preceded by small, uncharged residues at positions -3 and -1 (relative to the cleavage site) to allow correct cleaving.⁸² The membrane anchor, with a length of 15 to 25 residues, forms an alpha-helix and through hydrophobic interaction tethers the protein to the membrane, with the protein facing the inside of organelles or the extracellular space with the N-terminal (type I) or C-terminal side (type II). The inner space of the organelles of the secretory pathway (also referred to as *lumen*) and the extracellular space are topologically equivalent since the vesicles transporting proteins to the plasma membrane are fused to the plasma membrane in a fashion that turns them inside-out.

It is also possible that a protein contains a signal peptide as well as a membrane anchor, which is then referred to as a *stop transfer sequence*. By the sequential integration of more than one hydrophobic stretch into the membrane, *multispanning* membrane proteins like e.g. ion channels are formed. Hydrophobic stretches that serve as a membrane anchor independently of a signal peptide are sometimes also referred to as *internal signal sequences* (cf. e.g. ref.⁸³).

The final subcellular localization of the protein is determined by the presence of additional sorting signals. Known sorting signals include the *KDEL* sequence for ER retention⁸⁴ and short C-terminal tyrosine containing motifs which can serve as endocytosis or Golgi retention signals.⁸⁵ It has also been found that short TM-segments are preferentially sorted to the trans-Golgi-Network (TGN).⁸⁶ Although it has been reported that specific signals that enhance the transport from the Golgi to the plasma membrane may exist,⁸⁷ it is commonly believed that onward transport to the plasma membrane happens by default,⁸⁸ provided there exist no specific divergent sorting signals and that the protein can fold properly and thus bypass the ER's quality control system. Accordingly, a protein containing only the cleavable signal peptide is translocated to the ER lumen and, since the lumen topologically correlates to the extracellular space, this protein is ultimately secreted.

A different mode of membrane attachment is the use of glycosyl phosphatidylinositol (GPI) membrane anchors.⁸⁹ These are attached posttranslationally to a protein with an N-terminal signal peptide that additionally contains a C-terminal *glypiation signal*. These signal sequences, which show no homology among different proteins, are cleaved off before

attachment of the GPI anchor. The biological relevance of GPI anchors over membrane anchors is a subject of speculation.

4.2 Plasma Membrane Targeting Signal for the Construction of Chimeras

4.2.1 Design of the Construct *ArtPlasMA*

The amino acid sequence and putative structure of the desired Artificial Plasma Membrane Anchor *ArtPlasMA* is shown in Figure 17A. It contains a hydrophobic stretch of 22 Leucine residues (22L) which serves as a plasma membrane targeting signal and anchor.^{86,90} It is followed by the sequence VQQQ which is supposed to provide a clear border for the hydrophobic region.⁹¹ The main and best known determinant of membrane protein topology is the so-called "positive inside-rule": It has been found that for the majority of membrane proteins the side that contains more positive charges is cytoplasmic.^{90,92} Therefore, four lysine residues precede the N-terminal side of the 22L stretch, which should lead to the N-terminus being cytoplasmic, making *ArtPlasMA* a type II membrane anchor. In addition, the construct contains three standard tags, from which *myc* and *HA* are routinely used for immunochemical detection,⁹³ while the *6His*-tag is especially suited for protein cleanup using nickel-coated beads or column materials. The sequence between membrane anchor and *myc*-tag corresponds to the multiple cloning site in the DNA sequence (see below), preceded by a standard spacer with random coil structure.⁹⁴ Another spacer, two glycine residues, is inserted between *6His*- and *HA*-tag. The purpose of the spacers is to provide room between the different structural parts of the protein so that their folding will not be hindered. Finally, care was taken that none of the known subcellular sorting signals were accidentally included in the protein sequence.

In Figure 17B the corresponding DNA sequence is depicted. The coding sequence (*cds*) was obtained by backtranslation of the amino acid sequence, taking into regard preferred codon usage,⁹⁵ (cf. Appendix 7.3.1) to optimize expression levels. The optimal codon was not used in cases where it was not compatible with desired restriction sites or with the design of the oligos which were used to build up the gene (cf. below). Also, multiple base or sequence repetitions (e.g. (G)₅ or (GTC)₃) were eliminated by using the second best codon in order to

4.2.2 Gene Synthesis of ArtPlasMA

The advent of highly automated oligonucleotide synthesis has made it possible to synthesize wholly artificial genes from scratch. The most straightforward way to do this is by synthesizing both complete strands of the double stranded DNA separately, annealing them and amplifying the full length product by Polymerase Chain Reaction (PCR) with two additional smaller primers binding to the 5' and 3' end of the gene, respectively. With this method, genes of up to 655 bp have been synthesized.¹⁰¹ However, the obtained products had many unwanted mutations which subsequently had to be corrected by other techniques. A more dependable method relies on the assembly of multiple smaller oligonucleotides (length <60 bp) that together comprise both strands of the full length gene. These are chosen in a way that each oligo corresponds to equal parts of the opposing two oligos (Figure 18). Two methods can then be used to join the oligos to the full length gene. In the first technique, the open links between the oligos are closed by a Ligase.^{102,103} This process is predominantly performed in a thermocycler with a thermostable ligase and repeated cycles of denaturing, annealing, and ligating, therefore called Ligase Chain Reaction, *LCR* (Figure 18 right hand side). The alternative is to use PCR, where the oligos serve as both primer and template and the gene is built up stepwise during cycling^{97,104-107} (Figure 18, left hand side). In both cases, the desired full length product is amplified by an additional PCR with two primers binding to 5' and 3' end of the gene to discriminate against unwanted products and to obtain sufficient amounts of material for the following cloning steps.

To synthesize *ArtPlasMA*, the PCR-based method was chosen. The oligos comprising the gene were designed according to the following considerations: (i) 40 bp length, 20 bp overlap with the two opposing primers; (ii) optimized hybridization specificity, i.e. each 20 bp fragment was tested against the whole gene in order to rule out unwanted hybridization to other oligos; (iii) avoidance of stable secondary structures. The stability of the oligo secondary structure was calculated with *mfold*¹⁰⁸ using free base pairing energies determined by SantaLucia.¹⁰⁹ If necessary, the optimal codon was exchanged for the second best codon (see above) to reduce mishybridization or secondary structure stability. The full length construct synthesized by two PCR steps was cloned into the TA-cloning vector pCR2.1¹¹⁰ (cf. map in Figure 38). Ten clones obtained using varying reaction conditions were sequenced, and all contained a number of mutations. No systematic experiments were carried out, but from the available data it could be concluded that there was no significant dependence of the

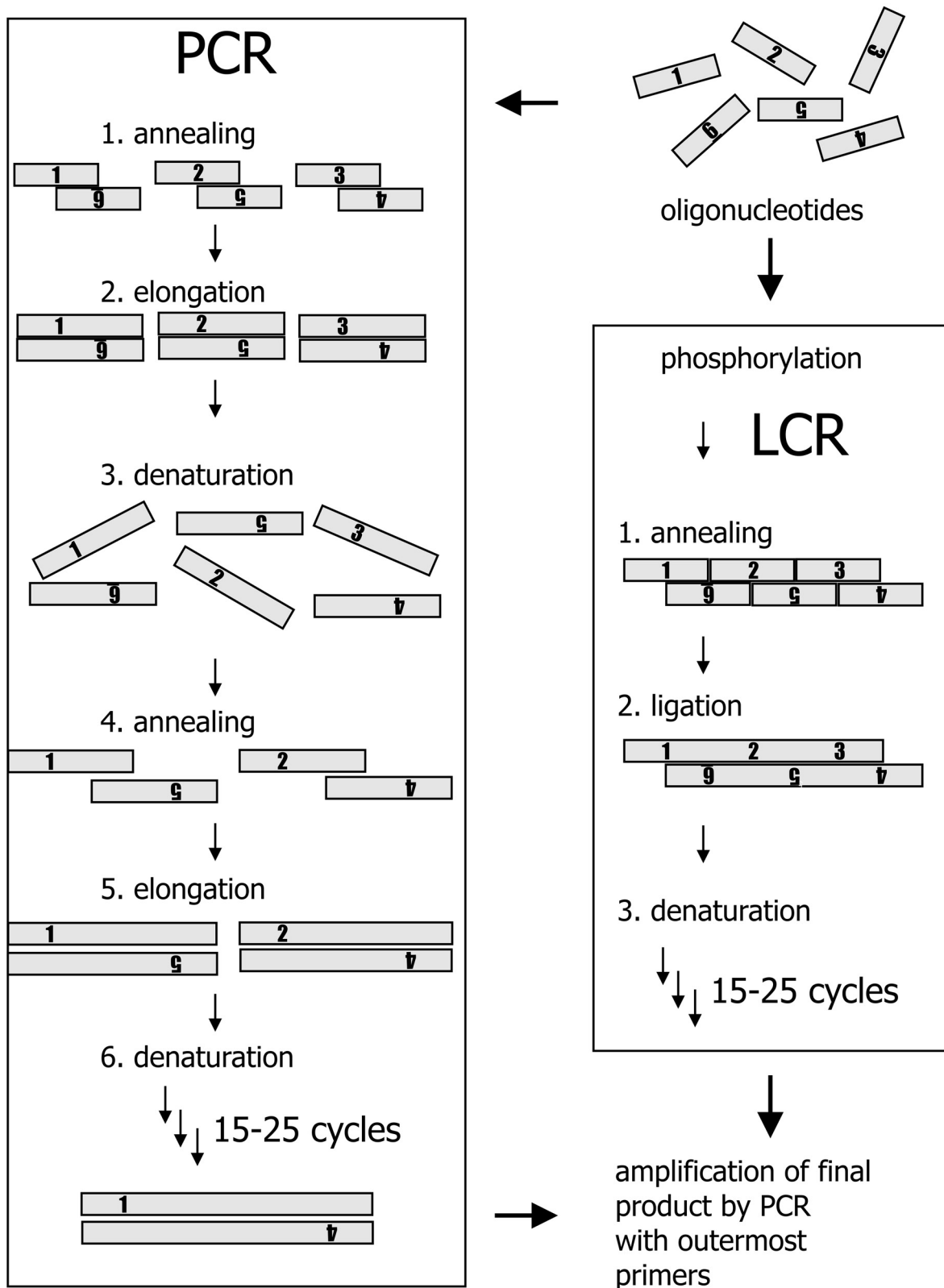


Figure 18. Schematic view of gene synthesis based on polymerase chain reaction (PCR) and ligase chain reaction (LCR) using six oligonucleotides. The oligonucleotides comprise both strands of the gene with overlapping sequences of opposing forward (1-3) and reverse (4-6) primers being half the length of each oligo. The shortest possible way to the full length product is shown. Only the minimally necessary intermediate products are depicted.

error rate on the used Mg^{2+} -concentration, choice of polymerase or choice of PCR-product cleanup. The most striking deviation between sequenced clones and desired sequence were huge deletions (up to 48 bp), that occurred in four clones, and insertions (up to 30 bp), found in three clones. These were located exclusively in the region that codes for the 22 Leucine-stretch. Since this region contains 22 repetitions of the codons CTG and CTC, the mutations were very probably introduced by mishybridization (cf. DNA sequence in Figure 17B). This hypothesis is supported by the fact that in four of the seven mutated clones the reading frame was not shifted, i.e. the number of additional or missing bases was a multiple of three. In other regions of the construct, point mutations and deletions of 1 to 5 bp were observed, but single base pair insertions also occurred. This phenomenon, which was not expected to occur to this extent, and its origin, will be treated in detail in section 7.1.1. One of the clones was acceptable, since it contained only two point mutations and one deletion. One of the point mutations had no effect on the coded protein sequence, while the other changed the first stop codon to a cysteine. Only the deletion was corrected by site directed mutagenesis, since the point mutations were considered to not impair the functionality of the construct. Finally, the construct was subcloned into pcDNA3.

4.3 Chimera of ArtPlasMA and PLAP (ArtPlasMA AP)

The next step was to use *ArtPlasMA* for the targeting of Placental Phosphatase from the Human Placenta (PLAP) to the plasma membrane and its detection. Native PLAP is itself an ectopic, i.e. extracellular space-facing, plasma membrane enzyme bound by a GPI anchor. Although GPI anchored proteins are not integral membrane proteins, they are quite stably attached to the membrane and demand rather harsh conditions to be solubilized.¹¹¹ Nevertheless, the more stable anchoring, the strong overexpression, the possibility of thorough characterization and the possibility to test *ArtPlasMA* for future developments with other enzymes served as motivation to construct a chimera of PLAP and the membrane anchor. The DNA coding for PLAP without the N-terminal signal sequence and the C-terminal glypiation signal^{112,113} (AA 17 to 516) was amplified by PCR and cloned in-frame into pcDNA3 *ArtPlasMA*. HEK293 cells were stably transfected with the construct *ArtPlasMA AP* and 20 clones were analyzed for alkaline phosphatase activity (see below). For the experiments described, the clone exhibiting the maximal and most homogenous activity was chosen.

4.3.1 Immunocytochemical Detection – Western Blotting

A western blot analysis was performed to check the appropriate size of the fusion protein and to test whether the protein is expressed in full length. For western blotting, all membranes of HEK293 stably expressing *ArtPlasMA AP* were isolated. The membrane proteins were separated according to their size by denaturing polyacrylamide gel electrophoresis (SDS-PAGE) and transferred to a nitrocellulose membrane. The nitrocellulose membrane was then incubated with primary antibodies against the epitopes *cmyc* and *HA* and secondary antibodies carrying horse radish peroxidase *HRP*. The secondary antibody was then detected on a lightsensitive film by an enhanced chemiluminescence (*ECL*) reaction of *HRP* with luminol (Figure 19).

The main bands on the blot with *HA* and *cmyc* alike corresponded to a protein of approximately 80 kDa size as determined by calibration with a protein size marker running on the same respective gels. The lane depicting the *cmyc* hybridization contains two additional bands, a very weak one at 112 kDa of unknown origin and one at 74 kDa. The latter one might correspond to a fragment liberated by activity of the leader peptidase, which cleaves signal peptides close to their C-terminal end. Due to the length of the N-terminal sequence preceding the TM-domain and the length of the poly-Leu-sequence, this seems rather improbable (cf. section 4.1). Since the intensity of this band increased with prolonged storage of isolated membranes, it seems more feasible that it resulted from protease digestion.

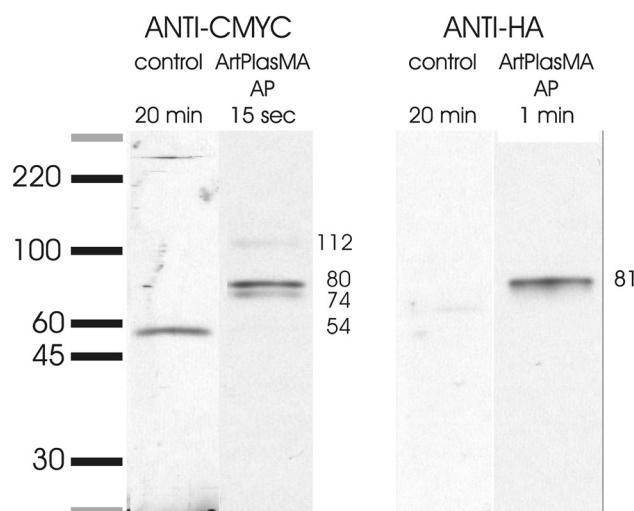


Figure 19. Westernblot analysis of *ArtPlasMA AP* expressed in HEK293 cells with antibodies *anti-HA* and *anti-cmyc* (both SantaCruz, CA, USA). Membranes containing the protein were isolated by crushing stably transfected HEK293 cells in a glass homogenizer and subsequent differential centrifugation. Membrane proteins were then separated according to their size by SDS-PAGE (10%) and transferred to a nitrocellulose membrane by semi-dry blotting. The blotted proteins were incubated with the respective primary antibodies and subsequently with *HRP*-conjugated secondary antibody. They were detected by *ECL*. Untransfected HEK293 cells were used as a control.

The *calculated* molecular weight of the AP module disregarding posttranslational modification is 53 kDa. The apparent weight as determined by SDS-PAGE, however, is 67 kDa.¹¹³ With calculated 9.2 kDa for *ArtPlasMA*, the complete construct *ArtPlasMA AP* should have an apparent molecular weight of 76 kDa, close to the weight of the main band detected in the western blots. At very long exposure times of the film, the human myc protein p67 (PubMed Acc.# BAA01374) was detected at an apparent molecular weight of 54kDa (Figure 19, anti-myc control lane). Apart from p67, membrane proteins of untransfected cells did not show any reaction with either anti-HA or anti-myc antibodies. Note that the marker used only allows for approximate qualitative size determination since it contains proteins conjugated to dyes.

4.3.2 Immunocytochemical Detection – Immunofluorescence

To determine the localization of the construct in the cell and its topology, immunofluorescence experiments were performed. A stable clone was grown on glass coverslips, fixed and incubated with primary antibodies conjugated to fluorescent dyes anti-myc-Fluorescein (*myc-FITC*)^d and anti-HA-Tetramethylrhodamine (*HA-TRITC*). Fixation was performed in 4 % formaldehyde in PBS either with or without additional 0.5% Triton X-100 (w/w). Triton X-100 as a surfactant permeabilizes all cell membranes, providing access of the antibody to the interior of the cell's organelles. Fixation without a surfactant agent (so-called “non-permeabilizing conditions”) leads to a selective permeabilization of the plasma membrane and the membrane of selected organelles, but not the membranes of the organelles which are part of the secretory pathway (see also section 7.1.2).¹¹⁴

An overview of immunofluorescence images is shown in Figure 20. In these experiments, cells were stained with antibodies against epitopes *myc* (Figure 20A), *HA* (Figure 20B) or with both antibodies together (Figure 20C). The green fluorescence of Fluorescein and the red fluorescence of Tetramethylrhodamine were recorded with a microscope equipped with the appropriate filter sets and camera. The experiments were performed with (bottom) or without (top) Triton X-100.

In the experiments performed without Triton X-100, i.e. without permeabilizing the organelles of the secretory pathway, staining with *anti-myc-FITC* (Figure 20A, top) led to a

^d Note that the human myc-protein p67 is not detected under non-denaturing conditions. Accordingly, the native protein does not disturb immunofluorescence experiments.

distinct signal at the plasma membrane of the cells, while staining with *anti-HA-TRITC* (Figure 20B, top) resulted in fluorescence all over the cell, with an especially strong signal in a region close to the cell nucleus, as determined by a co-staining with the DNA-binding blue fluorophore *Hoechst 33258*. The intracellular signal of *anti-HA* at the cell nucleus is so strong that a staining of the plasma membrane can not be discerned. In the co-staining experiment (Figure 20C, top), the fluorescence of *anti-cmyc-FITC* and *anti-HA-TRITC* is not co-localized.

Under permeabilizing conditions, however, the appearance of the immunofluorescence images is identical (Figure 20A and B, bottom). In the co-staining experiments, a perfect co-localization of both fluorescence signals is obvious (Figure 20C). Both plasma-membrane fluorescence and intracellular fluorescence, especially fluorescence at the region close to the nucleus, are strong for both antibodies.

The identity of the intracellularly stained organelle can not be proven without performing co-localization experiments using native organelle specific proteins. Nevertheless, the organelle is quite likely the Golgi-apparatus, as a comparison with immunofluorescence images of Golgi-resident proteins suggests.^{114,115} The visually similar *aggresomes*,^{116,117} which form in cells when the amount of misfolded overexpressed protein exceeds the capacity of normal degradation pathways, are ruled out by the fact that under non-permeabilizing conditions no *anti-cmyc* staining can be discerned. Since aggresomes have been reported to be cytosolic aggregates that contain no membranes, a staining with both antibodies both under permeabilizing and non-permeabilizing conditions would be expected in this case (cf. also immunofluorescence experiments of section 7.1.2).

The results are therefore in agreement with the desired and predicted *type II* orientation of *ArtPlasMA AP* (cf. Figure 17): The C-terminal *cmyc*-epitope has an extracellular topology at the plasma membrane and is luminal in the cell. In experiments without Triton, it is therefore only accessible at the plasma membrane, while it is fully accessible under permeabilizing conditions and colocalized with *HA*. The N-terminal *HA*-epitope is cytoplasmic and therefore fully accessible to the antibody with or without full permeabilization. As the immunofluorescence images suggest, a large fraction of the produced protein is accumulated within the cell.

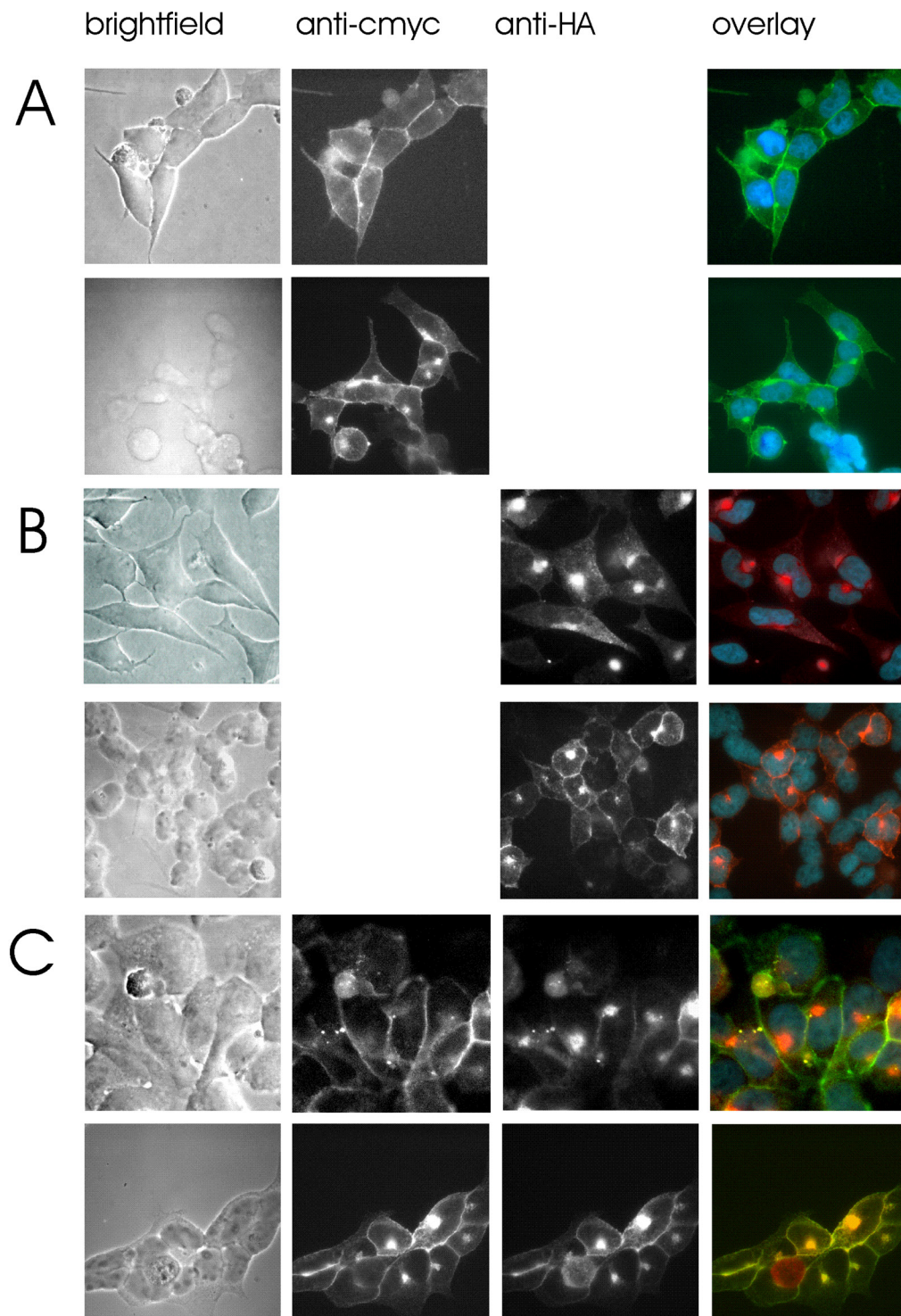


Figure 20. Immunofluorescence of HEK293 cells stably transfected with *ArtPlasMA AP*. Immunofluorescence images of formaldehyde-fixed HEK293 cells incubated with fluorescently labeled antibodies *anti-cmyc-FITC* (A), *anti-HA-TRITC* (B) and both *anti-cmyc-FITC* and *anti-HA-TRITC* (C). Cell nucleus counterstaining was achieved with the dye *Hoechst 33258*. Experiments were performed without (resp. first rows) and with (resp. second rows) Triton X-100 treatment. Fluorescence images were digitally edited by normalization to the maximum intensity and subtraction of background fluorescence. In the overlay of the images, the fluorescence of *anti-cmyc-FITC*, *anti-HA-TRITC* and *Hoechst 33258* is colored green, red and blue, respectively. A colocalization of anti-cmyc and anti-HA results (C) results in a yellow color on the overlay image.

4.3.3 Histochemical Detection

So far, it has been proven that *ArtPlasMA AP* is expressed in full length and that it is an integral, single spanning membrane protein with its N-terminus being cytoplasmic. The most important question, though, is whether it also exhibits alkaline phosphatase activity. This was determined by adding the chromogenic and precipitate-forming phosphatase substrate 5-bromo-4-chloro-3-indolyl-phosphate (*BCIP*) to PFA-fixed transfected cells. When used in conjunction with Nitro-Blue Tetrazolium Chloride (*NBT*) as an electron acceptor, the staining is better localized and develops more quickly.⁹³ HEK293 and MDCK cells were transiently transfected with *ArtPlasMA AP* and color development was observed over time. To distinguish non-transfected from transfected cells, a cytoplasmically expressed construct of Enhanced Green Fluorescent Protein (EGFP) was co-transfected with the construct and used as a transfection marker. This is possible since transfection takes place in an “all or nothing” fashion, i.e. cells either take up all offered plasmids or none.

In HEK293 cells (Figure 21A), transfected cells are strongly stained by the reaction product of *BCIP*-hydrolysis after four minutes, indicating a very strong expression of *ArtPlasMA AP*. Transfected MDCK cells also exhibit phosphatase activity (Figure 21B), which, however, leads to a slower staining than in HEK293 cells, indicating a reduced expression compared to HEK293.

4.3.4 Activity Determination of HEK293 Stably Expressing *ArtPlasMA AP*

In order to facilitate a quantitative approach of enzyme induced binding experiments (see below), a crude estimation of the phosphatase activity of a stable clone of *ArtPlasMA AP* in HEK cells was performed. To ensure a truly monoclonal culture, it was, after a first round of ring cloning, again diluted, picked and propagated.¹¹⁸ In histochemical staining experiments, the clone that exhibited the most homogenous phosphatase activity was chosen for the experiments described in this and all following sections. For activity quantization, defined numbers of cultured cells were suspended in Tris-NaCl-Glucose pH 8.1 buffer, and their hydrolytic activity on *p*-NPP was measured in a UV/Vis-spectrometer. For comparison, the native phosphatase activity of untransfected HEK293 cells was also determined. This approach delivers only a rough estimate with a large uncertainty, due to variations in enzymatic activity, light scattering by the turbid sample and the overall small activity. As controls, the spontaneous rate of degradation of *p*-NPP and the activity of cells crushed

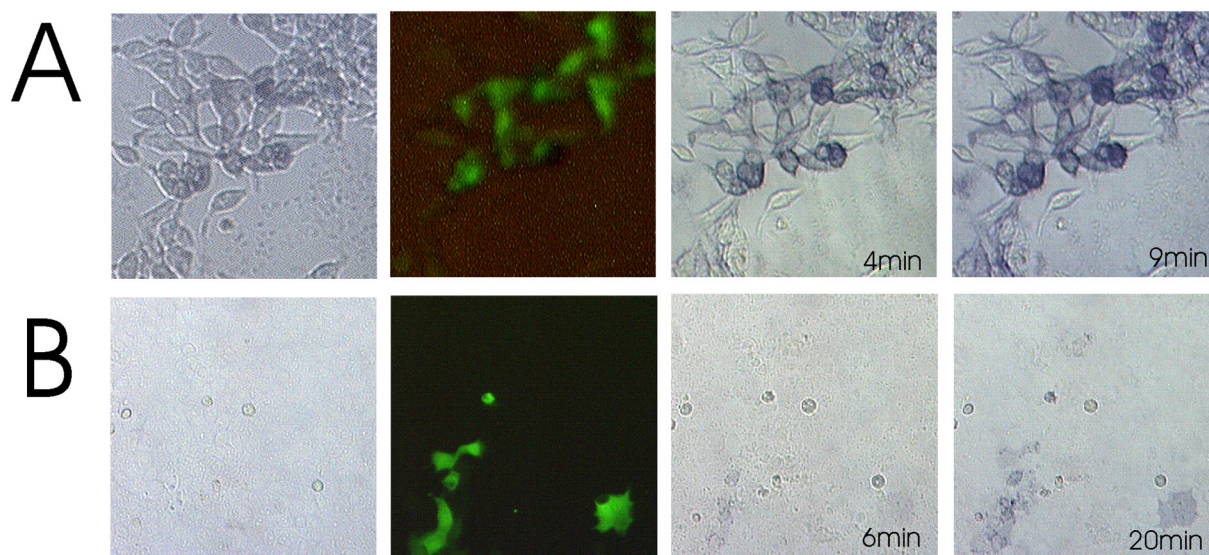


Figure 21. Histochemical staining of HEK293 (A) and MDCK (B) cells transiently transfected with *ArtPlasMA AP*. Cells were incubated with the chromogenic phosphatase detection reagents BCIP and NBT and images were acquired with a color CCD camera (columns 1,3,4). Cytoplasmically expressed EGFP was used as a transfection marker (fluorescence image column 2).

in a glass homogenizer were examined. This was done in order to exclude the possibility that an inevitable low amount of dead and therefore permeable cells compromised the results.

The measured values were transformed to activities per cell in DEA buffer at pH 9.8/37°C with the known relation of activities for soluble PLAP in Tris-NaCl buffer at pH 8.1/25°C and DEA buffer (confer section 3.1.2). By doing this, it was assumed that the buffer dependence of the reaction rate is similar for *ArtPlasMA AP* and soluble PLAP. Stably transfected cells exhibited a phosphatase activity which ranged from 2.3×10^{-7} – 1.1×10^{-6} DEA Units/Cell ($n = 3$) with an average of 5.7×10^{-7} Units/Cell, 70fold higher than that of untransfected cells with an average of 0.08×10^{-7} DEA Units/Cell ($n = 3$, range 2.5×10^{-9} – 2.2×10^{-8} DEA Units/Cell). The activity of crushed cells did not deviate significantly from the values of intact cells. The measured values were significantly higher than the spontaneous degradation of *p*-NPP which corresponded to 0.01×10^{-7} DEA Units/cell. The very broad range of the results underlines the fact that these measurements are only roughly approximate and need to be interpreted with care. This may also reflect differences in expression depending on culture times and conditions of the cells.

It has been reported that *p*-NPP permeates the plasma membranes of intact cells only slowly.¹¹⁹ Alkaline Phosphatase is enzymatically active before it reaches the plasma membrane, but experimental results suggest that it reaches full activity not until it reaches the *trans*-Golgi compartment, i.e. on the last station of the secretory pathway before it reaches the

plasma membrane.¹²⁰ Although a major fraction of *ArtPlasMA AP* is retained in intracellular organelles as shown by immunocytochemistry, the measured enzymatic activity should therefore originate mainly from the plasma membrane bound enzyme.

The density of *ArtPlasMA AP* on the cell surface of the clone can be estimated from the activity per cell. With the radius of a HEK293 cell being about 10 μm , one obtains with the calculated cell surface area an activity of 453 U/m^2 . The activity of soluble PLAP ($\text{MW}_{\text{Monomer}} = 67 \text{ kDa}$) amounts to reported 128 U/mg or $8.6 \times 10^9 \text{ U}/\text{mol}$ in DEA buffer at pH 9.8/37°C.⁷⁶ One therefore obtains with Avogadro's number a density of 3.2×10^{16} *ArtPlasMA AP* monomers per square meter, assuming that the phosphatase chimera has the same activity as soluble PLAP. This corresponds to one dimer in a square with a lateral length of 8 nm, a strongly overestimated density considering that the diameter of the dimeric native enzyme is almost 10 nm.¹²¹ This discrepancy may be due to the following causes: (i) The measured activity may also reflect some of the activity of intracellularly retained phosphatase; (ii) The reported activity of soluble PLAP⁷⁶ might be too low, i.e. the protein was not sufficiently purified; (iii) The activities of soluble and membrane-bound PLAP may differ significantly.

The result of the assay must therefore be taken as an upper limit of the actual enzymatic activity at the plasma membrane. Nevertheless, this experiment shows that the activity of the investigated cells must lie within the maximum attainable range.

4.4 Conclusion

ArtPlasMA AP is expressed in full length as proven by western blotting of the proteins of the membrane fraction. Immunofluorescence experiments show that, within the limits of the technique, it is exclusively oriented as a type II membrane protein. Although a large fraction of the produced protein seems to be accumulated in intracellular organelles, presumably the Golgi compartments, a significant amount of the protein is transported to the cell surface. It is functional in hydrolysis of BCIP, and a crude estimate of the hydrolytic activity indicates that a very high surface density of the functional protein is achieved. PLAP functionality is not destroyed by the presence of additional tags or by the sandwich fusion construction.

The transmembrane (TM) domain of *ArtPlasMA* consists of a 22 Leucine stretch preceded by four positively charged amino acid residues. The information encoded by this sequence contains contradictory signals with regard to the desired type II orientation in conjunction with plasma membrane transport. It has been found that Golgi resident proteins contain TM

domains that are on average five residues shorter than plasma membrane targeted proteins, and that shortening the TM domain of the latter can infer Golgi retention.⁸⁶ On the other hand, short hydrophobic sequences would be favorable to adopt a type II orientation, since long hydrophobic sequences can increase the translocation of the N-terminus across the ER membrane.¹²² This effect can be an even stronger determinant of topology than the positive inside rule. However, a long or a rapidly and stably folded N-terminal structure can negate this effect.¹²² This is likely to be the reason why in the experiments no *ArtPlasMA AP* in type I orientation can be detected.

It is generally believed that anterograde, i.e. onward, transport through the organelles of the secretory pathway occurs by default, i.e. that in the absence of specific retention signals, proteins are ultimately transported to the plasma membrane with the “bulk” protein flow.⁸⁸ The fact that *ArtPlasMA AP* accumulates to a significant extent in intracellular structures could originate from a saturation of the export machinery from the Golgi network to the plasma membrane, as has been reported for an overexpressed secretory protein.¹²³ The intracellular accumulation of *ArtPlasMA AP* might also originate from a high rate of misfolding with subsequent degradation, or it might be due to the construct missing signal sequences necessary for efficient recycling to the plasma membrane after endocytosis.⁶¹ These cases can not be differentiated on the basis of the available data.

Since native PLAP is a secreted or GPI-anchored ectopic protein, it is not too surprising that the exchange of the GPI signal for a transmembrane anchor was successful. In fact, fusions of Alkaline Phosphatases with TM domains have been used successfully for topology studies in prokaryotes, yeast and in a few cases also in higher eukaryotes (see, e.g. ref.¹²⁴⁻¹²⁶). Nevertheless, the high activity of *ArtPlasMA AP* that was achieved is a necessary prerequisite for enzyme induced staining, and as experiments described in the appendix show, a different design of the construct can make a huge difference in expression levels (cf. section 7.1.2: Comparison of an Artificial and a Natural Targeting Signal). The design of *ArtPlasMA* in addition allowed the detailed characterization of *ArtPlasMA AP*, and on this basis, future developments which rely on other enzymes, such as other, faster phosphatases, or enzymes which are not natively present on the plasma membranes of mammalian cells, are now feasible.

4.5 Materials and Methods

PCR, Cloning and expression were performed according to standard procedures unless otherwise indicated.¹¹⁸ Sequencing of DNA constructs was performed by Medigenomix GmbH (Munich, Germany). DNA quantitation was performed with a photometer (GeneQuant II, Amersham Pharmacia Biotech, Buckinghamshire, UK) using microcuvettes.

Organisms. For cloning, the E.coli strains Top10 (genotype F- *mcrA* Δ (*mrr*- *hsdRMS*-*mcrBC*) ϕ 80lacZ Δ M15 Δ lacX74*recA1 araD139* Δ (*ara-leu*)7697 *galU galK rpsL* (Str^R)*endA1nupG*; Invitrogen, Karlsruhe, Germany) or XL-10 Gold (genotype Tet^R Δ (*mcrA*)183 Δ (*mcrCB*-*hsdSMR*-*mrr*)173 *endA1 supE44 thi-1 recA1 gyrA96 relA1lac Hte*[F'*proAB lacI^f ZAM15 Tn10*(Tet^f) Amy Cam^r] (Stratagene Europe, Amsterdam, The Netherlands) were used. For transient and stable transfection, the adherent mammalian fibroblast cell line HEK293 (Human embryonic kidney,⁵⁴ German Collection of Microorganisms and Cell Cultures) and the adherent epithelial cell line MDCK (Madin Darby canine kidney¹²⁷) were employed.

Chemicals and Biochemicals. The eukaryotic expression vector pcDNA3 and the cloning vector pCR2.1 with the TA- or Topo-TA cloning kits were obtained from Invitrogen (cf. maps and features in Figure 38). The following enzymes and kits were used in the work: Restriction enzymes KpnI, NotI and EcoRV (Fermentas GmbH, St. Leon-Rot, Germany), TAQ polymerase, T4 DNA Ligase, dNTPs (Fermentas), Native and Cloned Pfu Polymerase (Stratagene Europe, Amsterdam, The Netherlands) and Site directed mutagenesis kit (Quikchange, Stratagene). Oligonucleotides were synthesized by MWG Biotech (Ebersberg, Germany) in 0.05 μ M quantity. They were purified by a company-proprietary method termed "HPSF" and used as obtained. PCR products were purified by agarose gel electrophoresis and DNA binding columns (Qiaquick Spin columns, Qiagen). Buffers, salts and further chemicals were obtained from SIGMA (Munich, Germany) or Roth (Karlsruhe, Germany) in the appropriate grade of purity.

Gene Synthesis of ArtPlasMA. The gene was obtained by two PCR steps from 14 primers of 40 bp length (cf. section 7.5.2) with a Robocycler Gradient 40 (Stratagene). Varying protocols were tried with no apparent difference, i.e. the error frequency did not seem to depend on Polymerase choice, Mg²⁺-concentration or PCR product cleanup. Here, only the protocol finally leading to the desired product is given. Note, however, that this does not imply that the described approach was better than any other that was tried.

In the first step, the gene was assembled in the buffer supplied for the polymerase containing 2 μ M of each Primer, 1.2mM Mg²⁺, 0.5 mM of each dNTP, and 1.7U/ml Pfu Polymerase. The PCR program consisted of 5 min initial denaturation and 30 cycles of 30 sec denaturation at 94°C, 30 sec annealing at 58°C and 60 sec elongation at 73°C. To amplify the full size product in a second round of PCR, the product was diluted 1:10 in Pfu Polymerase buffer containing 1 μ M of the outermost primers, 50 U/ml Pfu Polymerase, 0.5 mM of each dNTP and 2.5 mM Mg²⁺. PCR parameters were 1 min initial denaturation, 30 cycles of 45°sec at 94°C, 45 sec at 68°C and 60 sec at 73°C with a final elongation step of 10 min at 73°C. The final PCR product was purified by agarose gel electrophoresis and gel elution with the Qiaquick Spin Columns kit. To facilitate cloning into the vector pCR2.1 using the Topo-TA cloning kit., adenosine residues were added using TAQ polymerase at 72°C (1mM dNTPs, 7mM Mg²⁺, 3 U/ml TAQ polymerase in TAQ buffer; reaction time 10 min). Positive colonies were identified by blue-white selection¹¹⁸ and PCR screening with primers Forw2 and Rev2 (cf. section 7.5.2). Ten clones with the approximately correct size were sequenced. The best clone had two mutations and one

deletion at bp 149 (cf. Figure 17). The deletion was corrected by site directed mutagenesis (Quikchange kit) using primers 5'-GCTGCTCCTGCTCCTCGTGCAGCAACAGG-3' and 5'-CCTGTTGCTGCACGAGGAGCAGGAGCAGC-3'. Finally, the construct pcDNA3 *ArtPlasMA* was obtained by subcloning from pCR2.1 into the mammalian expression vector pcDNA3 using the restriction sites *KpnI* and *NotI*.

Cloning of ArtPlasMA AP. A fusion protein was constructed of *ArtPlasMA* and Alkaline Phosphatase from the Human Placenta (PLAP or SEAP, PubMed Acc.# U89940) with its glypiation signal removed. As the source of PLAP DNA, the construct pRC/CMV *AP-ten-m1*¹¹² was used which was a generous gift by Reinhard Fässler. The DNA of PLAP corresponding to bases 17 – 519 of native PLAP was amplified by PCR from *AP-ten-m1* with forward primer 5'-ACCCGGGTGCGCGGC-3' and reverse primer 5'-GGAATCATCCCAGTTGAGGAGG-3' and gel purified (Qiaquick kit, Qiagen). It was blunt cloned into pcDNA3 *ArtPlasMA* using EcoRV and ligating with T4 DNA ligase in the presence of the restriction enzyme, a method sometimes referred to as blunt cut-ligation.¹²⁸ For this reaction, 50 ng plasmid, 200 ng insert, 1 U T4 DNA ligase, BSA, 0.5 mM ATP, 1 U EcoRV and the buffer for the restriction enzyme supplied by the manufacturer were used. The overall volume was 10 µl. Positive colonies were identified by PCR screening with primers Forw2 and Rev2 (cf. 7.5.2) and restriction analysis.

Culture and Transfection. HEK293 and MDCK cells were kept and passaged under standard culture conditions at 37°C and 5% CO₂.¹²⁹ For HEK293 cells, Dulbecco's Minimal Essential Medium (DMEM, #21885-205) containing 10% fetal calf serum (FCS) and L-glutamine (all Gibco BRL, Invitrogen), but not containing antibiotics, was used. MDCK were kept in Eagle Minimum Essential Medium (EMEM, SIGMA, #M-2279) containing 10% FCS, 1% L-Glutamine and 1% NEAA. Transient and stable transfection of HEK293 cells was achieved by the Calciumphosphate method,¹¹⁸ for MDCK cells the Effectene Transfection Reagent (Qiagen) was used according to supplier's instructions (the ratio of buffer:enhancer:effectene was 150:25:8 (v/v/v)). Stable Clones of HEK293 cells expressing *ArtPlasMA AP* were obtained by dilution cloning at an initial antibiotic concentration of 400µg/ml G418 which was reduced to 200µg/ml for further propagation.

Western Blotting of Membrane Proteins. Membranes of HEK293 cells stably transfected with *ArtPlasMA AP* were prepared by swelling in low osmolar buffer (50 mM Tris, 35 mM KCl pH 7.4, protease inhibitors 10µg/ml Pepstatin, 10µg/ml Leupeptin/Aprotenin, 0.1 mM Phenylmethyl-sulfonylfluorid (PMSF)) on ice for 15 minutes, crushing the cells in a dounce homogenizer (B. Braun Biotech, Melsungen, Germany) and isolating the membrane fraction by differential centrifugation. Cell debris and nuclei were removed in a first centrifugation at 700 g for 8 min and the supernatant was subjected to a second centrifugation for 30 min at 15000 g and 4°C (Eppendorf 5417R centrifuge, 700 g = 3000 rpm, 14000 rpm = 15000 g). Membranes were then mixed with loading buffer (Sigma, #S3401-10VL) and subjected to SDS-Polyacrylamide Gel Electrophoresis (SDS-PAGE; 0.9 mA/cm²) according to the protocols described by Laemmli et al.¹³⁰ A molecular weight marker was run on the same gel (Colorburst, Sigma). For electrophoresis Tris-Glycine-SDS buffer pH 8.8 (10 × buffer, Sigma, 2.5 M Tris, 1.92 M lysine, 1 % SDS) was used. 10% separating gels were made at a final concentration of 0.4 M Tris-Cl pH 8.8, 10 % (w/v) acrylamid/N,N-methylenbisacrylamid (AA/Bis) 30:0.8, 0.1% (w/v) SDS, 0.1 % (w/v) APS and 0.1 % (w/v) TEMED (all reagents Roth). 4 % AA:Bis (w/v) stacking gels were made with 0.05 M Tris-Cl pH 6.8, 0.1 % (w/v) SDS, 0.05 % (w/v) APS and 0.1% (w/v) TEMED. The separated membrane proteins on the gel were transferred to a nitrocellulose membrane (BioRad

Germany, Munich, #162-0117) by semi-dry blotting (Tris-Glycine-SDS pH 8.8 containing 20% (v/v) MeOH, 2.5 mA/cm² for 75 min, power source Consort E835, Roth, blot chamber MPI Biochemistry homemade). The membrane was blocked by shaking for 1 h in blocking buffer (PBS pH 7.4 containing 4 % (w/w) milk powder). Membranes were then washed three times for five minutes in TBS-Tween buffer (10 mM Tris-HCl, 150 mM NaCl, 0.05 % Tween-20, pH 8.0) and once in TBS-buffer without Tween. They were then incubated with 1:1000 anti-HA (mouse HA.11 clone 16B12, BabCo, Berkeley, CA, USA; German supplier: Hiss Diagnostics, Freiburg i. Br.) or 1:1000 anti-cmyc (mouse anti-cmyc/9E10-FITC #sc40-FITC, SantaCruz Biotechnologies, CA, USA) antibody in blocking buffer overnight at 4°C. After washing three times in TBS-buffer, incubation with the secondary, horse-radish-peroxidase (HRP) conjugated antibody (goat anti-mouse IgG HRP #sc2005, SantaCruz) was carried out for 90 min at 4°C. The secondary antibody was detected by Enhanced Chemiluminescence (Western Blotting Luminol Reagent sc-2048, SantaCruz) according to supplier's instructions. These consisted of washing three times for five minutes in TBS-Tween buffer (10 mM Tris-HCl, 150 mM NaCl, 0.05 % Tween-20, pH 8.0), once in TBS-buffer without Tween and subsequent incubation with Luminol reagent. Photographic films were obtained from Amersham (Hyperfilm ECL, Buckinghamshire, UK). Film development was carried out in an AGFA curix 60 with AGFA reagents.

Immunofluorescence. HEK293 cells were grown on glass coverslips (Roth). These had been pre-treated by cleansing in detergent at 70°C (Tickopur, Dr. H. Stamm GmbH, Berlin, Germany), hydrophobisation in a gas stream of hexamethyldisilazane for thirty minutes (HMDS, Merck), sterilisation under UV-light for another 30 min and coating with fibronectin (30 µg/ml, overnight, SIGMA). Transfection was performed 24 hours after plating, and cells were processed for immunofluorescence 48 hours after transfection. After washing twice in PBS containing 1 mM MgCl₂, cells were fixed for 30 minutes in 4 % formaldehyde (w/w) in PBS at 4°C. For immunofluorescence under permeabilizing conditions, all buffers additionally contained 0.5 % Triton X-100 (w/w). Cells were then washed twice with blocking buffer (10 % BSA) and incubated at 4°C for ten minutes in the same buffer. Hoechst 33258 dye for nucleus counterstaining and primary antibodies were added at the predetermined optimal concentration (mouse anti-cmyc/9E10-FITC #sc40-FITC 1:300, mouse anti-HA/F7-TRITC #sc7392-TRITC 1:100, both SantaCruz) and the cells were incubated for 2 h at 4°C, washed twice in PBS and mounted on glass slides (Glow Mounting Medium, Energene, Germany). Fluorescence images were made at an Axioskop 2 microscope (Zeiss) with an oil immersion objective (63× Plan Apochromat objective, Zeiss) using Immersol 518N (Zeiss) as immersion oil. The microscope was equipped with filter sets for fluorescence of FITC (band pass 470/20 nm, dichroic 510 nm, band pass 540/30 nm), TRITC (low pass 546 nm, dichroic 580 nm, high pass 590 nm) and Hoechst (band pass 365 nm, dichroic 395 nm, long pass 397 nm). Images were recorded with a CCD-camera (MicroMax, Princeton Instruments, Trenton, NJ, USA) and IPLab software (Scanalytics, Fairfax, VA, USA). A 100 W HBO lamp served as the light source (Attoarc, Zeiss). Further image processing, like level adjustment and overlaying, was done with Photoshop (Adobe Systems Inc., USA).

Histochemistry. Detection of phosphatase activity in HEK293 and MDCK cells was performed with the chromogenic substrate BCIP in conjunction with NBT (Molecular Probes).⁹³ The medium was removed by suction, the cells were washed gently with PBS containing 2 mM MgCl₂, and then fixation was performed with PBS containing 2 mM MgCl₂ and 4 % formaldehyde. After washing in BCIP/NBT detection buffer for 15 min at room temperature (100 mM Tris-HCl, 100 mM NaCl, 50 mM MgCl₂, pH 9.5), the cells were incubated in the

same buffer containing BCIP/NBT. Images were made with the help of a microscope (Olympus BX50WI), colour CCD camera (HITACHI HV-C20) and a PC with frame grabber (PC-Eye2, Eltec Elektronik, Mainz, Germany) and the appending software.

Activity determination. The phosphatase activity of stable clones was quantified by UV/Vis-Spectrometry (Varian Cary 3E spectrometer, Mulgrave, Victoria, Australia) with *p*-NPP as a chromogenic substrate (20 mM Tris, 100 mM NaCl, 70 mM Glucose, pH 8.1). Cells were counted with a haemocytometer (Paul Marienfeld, Lauda-Königshofen, Germany). For comparison, the activity of crushed cells was also quantified (dounce homogenizer, B. Braun Biotech, Melsungen, Germany). Stable clones expressing cytoplasmically expressed EGFP (vector pcDNA3) were used as a control.

5 Cell Activated Staining with a Voltage Sensitive Dye

In this final section, the objective of the work is presented: the staining of cell membranes by voltage-sensitive dyes with the help of an overexpressed, membrane-bound enzyme. For these experiments, the dyes Di-10P-ASPBS and Di-12P-ASPBS were used. With these, the method was implemented on HEK293 cells stably expressing ArtPlasMA AP, and the time course of this reaction was investigated. Then, the selectivity of the reaction for both dyes was explored on a co-cultured mixture of phosphatase expressing and non-expressing cells. To test whether enzyme induced staining also works on other cell lines, the functionality and selectivity of the reaction was then tested on transiently transfected MDCK cells. A simplified mathematical model of the reaction is introduced. Finally, the results are discussed and compared to the predictions of the model.

5.1 Enzyme Induced Staining on Stably Phosphatase Expressing HEK293

A HEK293 clone stably expressing ArtPlasMA AP was incubated in Tris-NaCl-Glucose buffer pH 8.1. Dye precursor was added and fluorescence was recorded. The solution was stirred continuously by pipetting. Cells were seeded at a low density to minimize the overall phosphatase activity in the dish in order to exclude depletion of the precursor dye.

5.1.1 Di-10P-ASPBS

Figure 22A shows a sequence of images before and after the addition of 100 nM Di-10P-ASPBS to a group of four cells. The fluorescence of the cell membranes increased strongly due to conversion of the dye precursor to the strongly binding dye Di-10A-ASPBS and its

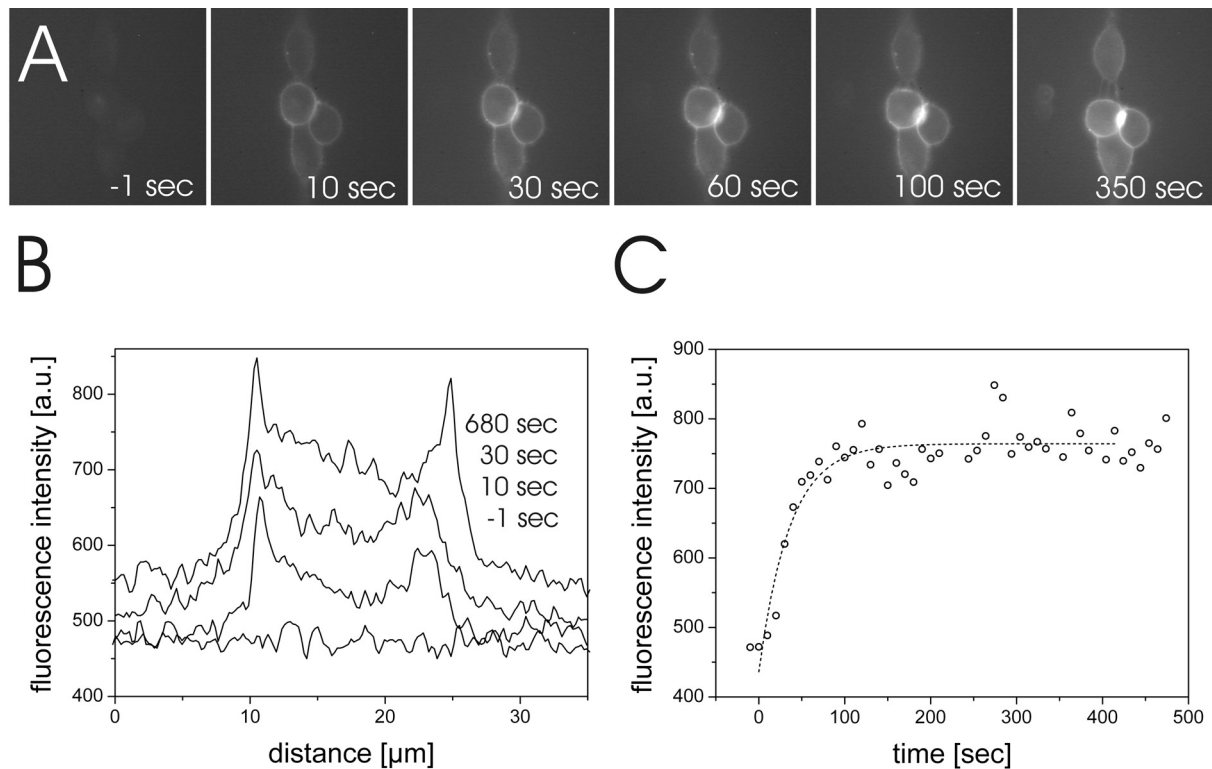


Figure 22. Enzyme Induced Staining on stably phosphatase expressing HEK293 cells with the dye Di-10P-ASPBS. (A) Fluorescence image (excitation around 450 nm, emission at >510 nm) of HEK293 cells before (-1 sec) and after addition of Di-10P-ASPBS at a final concentration of 100 nM. The image brightness was normalized to the same level for all images. Image contrast was enhanced by subtracting background fluorescence. (B) Profiles of fluorescence intensity across the diameter (approx. $15 \mu\text{m}$) of a selected cell. (C) Fluorescence intensity of cell membrane (average of the peaks of the profile) versus time.

subsequent binding to the cell membrane. In non-transfected cells, no fluorescence increase was detected on this time scale (not shown), proving that enzyme induced staining on phosphatase-expressing cells works.

The fluorescence profiles of one of the cells at selected points of time are shown in Figure 22B. A plot of the peak intensity versus time is shown in Figure 22C. In this exemplary measurement, the fluorescence intensity increased during a time span of about 70 seconds and then reached a plateau which stayed constant for the remainder of the experiment. The time course was fitted by the growth function $A(1 - \exp(-t/\tau_{stain})) + B$ (Figure 22C, dashed line). The fitted time constant of the fluorescence increase amounted to $\tau_{stain}^{10P} = 48 \pm 14 \text{ sec}$ ($n = 3$). The average of the plateau fluorescence minus the background was $310 \pm 35 \text{ a.u.}$ (cf. next paragraph).

5.1.2 Di-12P-ASPBS

The same experiment was performed with the dye Di-12P-ASPBS at the same dye concentration of 100 nM (Figure 23). The outcome of the experiment was similar, however the fluorescence intensity minus the background at the plateau and the time constant of staining were higher (compare Figures 22B and 23B; since the experiments described were performed on the same day, using both dyes in an alternating manner, the scale of fluorescence intensity is the same for both dyes). The average fluorescence increase was 800 ± 340 a.u., the average fitted time constant of staining was $\tau_{stain}^{12P} = 108 \pm 18$ sec ($n = 3$).

The membrane surface density of the dye might be quite high. To exclude possible fluorescence quenching from compromising the results, an experiment was performed with 25 nM dye. It exhibited $\tau_{stain}^{12P} = 105$ sec and a reduced staining intensity of 320 a.u. (data not shown). Both values are in rather good accord with the values at 100 nM substrate, indicating no effect of fluorescence quenching.

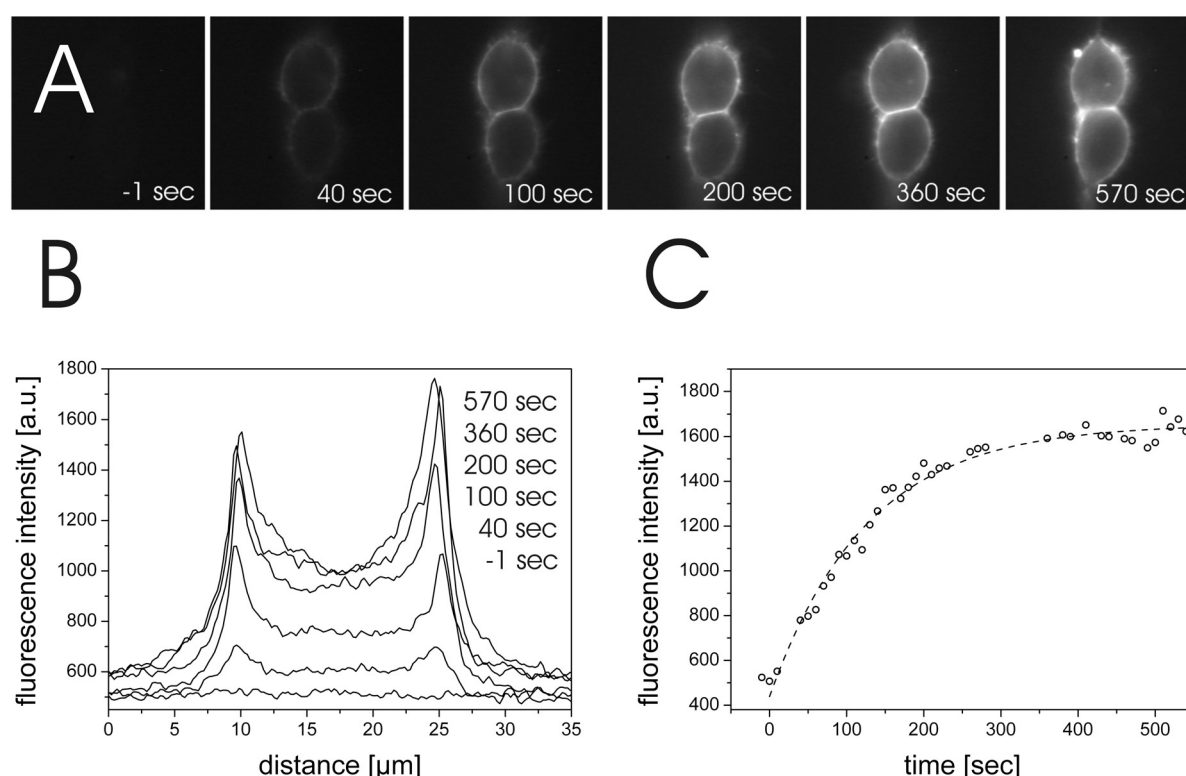


Figure 23. Enzyme Induced Staining on stably phosphatase expressing HEK293 cells with the dye Di-12P-ASPBS. (A) Fluorescence image (excitation around 450 nm, emission at >510 nm) of HEK293 cells before (-1 sec) and after addition of Di-12P-ASPBS at a final concentration of 100 nM. The image brightness was normalized to the same level for all images. Image contrast was enhanced by subtracting background fluorescence. (B) Profiles of fluorescence intensity across the diameter (approx. 15 μm) of a selected cell. (C) Fluorescence intensity of cell membrane (average of the peaks of the profile) versus time.

5.2 Enzyme Induced Staining on Stably Expressing HEK293 vs. Native Cells

In this experiment, the phosphatase expressing HEK293 clone described in the preceding chapter was co-cultured with HEK293 cells exhibiting only native phosphatase activity. In order to facilitate a discrimination between enzymatically active and non-active cells, the non-active clone was stably transfected with a cytosolically expressed construct of Enhanced Green Fluorescent Protein (EGFP).¹³¹ EGFP and the dyes have partly overlapping fluorescence excitation and emission spectra. EGFP has its maximum of excitation at 488 nm while its maximum emission is at 508 nm.¹³¹ Therefore, a different filter set (“B”) leading to red-shifted excitation and emission compared to the one described in the preceding chapter (filter set “A”) was used for selective staining experiments.

5.2.1 Di-10P-ASPBS

Three images illustrating the experiment are depicted in Figure 24A. In the brightfield image, all cells are shown, while the fluorescence image depicts the cells expressing cytosolic EGFP. The last image shows the cells expressing *ArtPlasMA AP* as obtained by “virtual subtraction” of the fluorescence image from the brightfield image.

To these cells, Di-10P-ASPBS was added at a final concentration of 1 μ M. Fluorescence images show an increase in fluorescence of cell membranes over time (Figure 24B). To facilitate an investigation of the selectivity of the reaction, Figure 24C shows the inverted and individually normalized images of Figure 24B. At $t = 50$ sec, a slightly stronger staining of phosphatase expressing cells is discernible. At reaction times >80 sec, all cells were stained to a similar degree. Apparently, the produced dye quickly diffused to the adjacent cells. Enzyme induced staining with Di-10P-ASPBS was not selective.

5.2.2 Di-12P-ASPBS

The same experiment was performed with Di-12P-ASPBS at a final concentration of 400 nM (Figure 25). The logical configuration of the images is the same as in the preceding section. After addition of dye, the membrane fluorescence of phosphatase expressing cells increased strongly. In contrast to the experiment with Di-10P-ASPBS, however, the staining was selective: As Figure 25B and C impressively demonstrate, the cells not expressing phosphatase were only weakly stained during the time course of the experiment. The experiment clearly shows that selective staining is possible with Di-12P-ASPBS as a precursor.

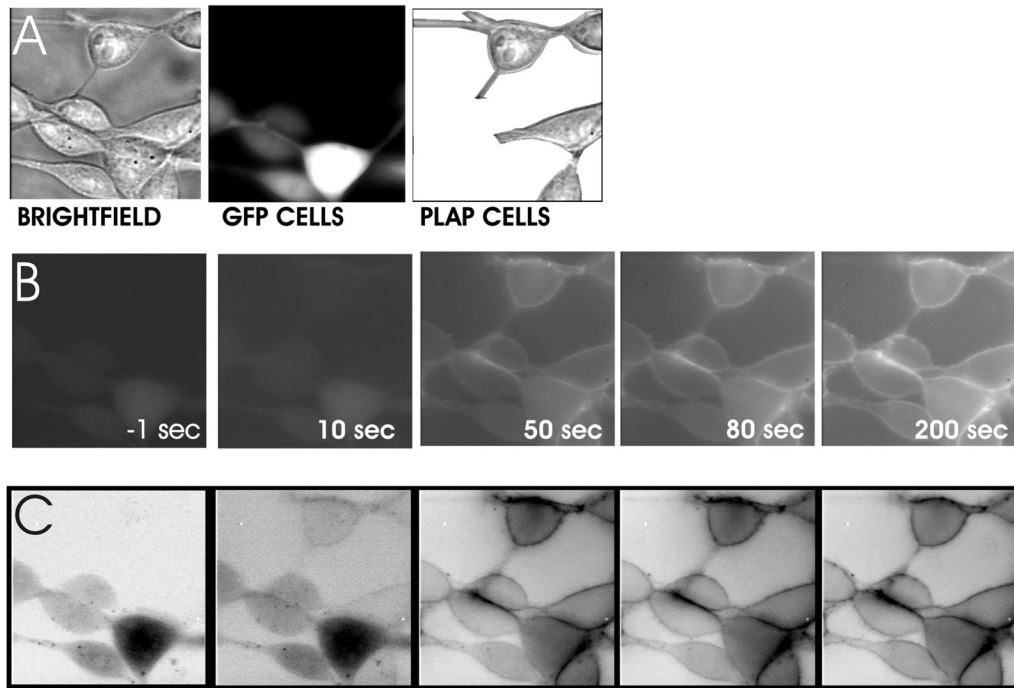


Figure 24. Enzyme Induced Staining with Di-10P-ASPBS. Cells expressing Phosphatase co-cultured with cells expressing cytosolic EGFP as a marker. (A) Illustration of Phosphatase expressing cells: Brightfield image of all cells on a dish; Fluorescence image of cells stably expressing cytosolic EGFP (excitation around 450 nm, emission at >510 nm); Cells stably expressing *ArtPlasMA AP*. (B) Enzyme Induced Staining. Fluorescence images of cells (excitation around 535 nm, emission around 610 nm) before (-1 sec) and after addition of Di-10P-ASPBS to a final concentration of 1 μ M. (C) Inverted and normalized images of row (B).

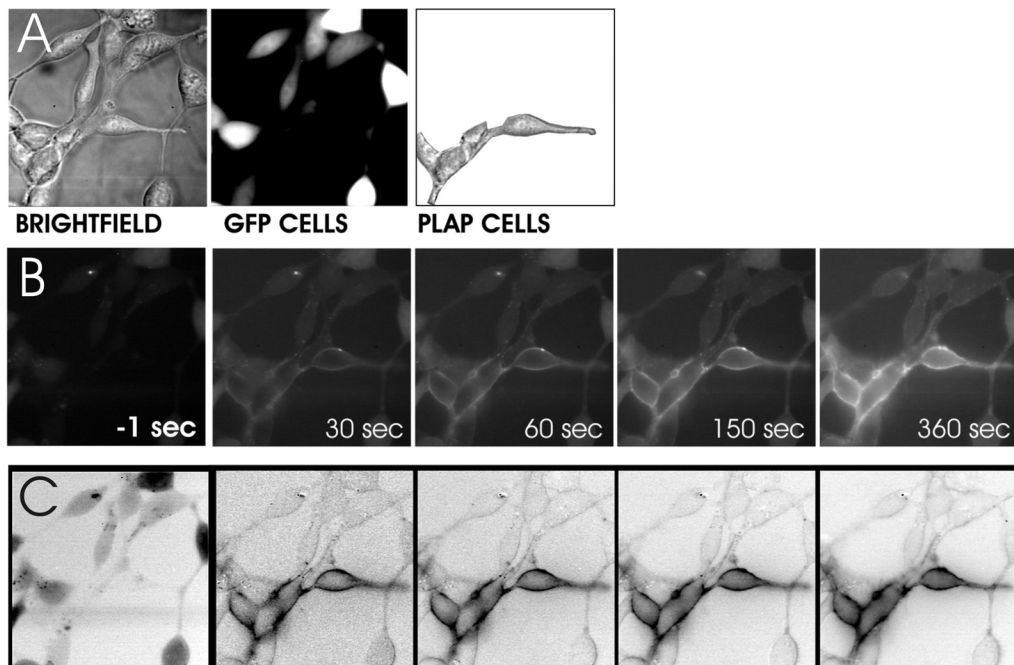


Figure 25. Enzyme Induced Staining with Di-12P-ASPBS. Cells expressing Phosphatase co-cultured with cells expressing cytosolic EGFP as a marker. (A) Illustration of Phosphatase expressing cells: Brightfield image of all cells on a dish; Fluorescence image of cells stably expressing cytosolic EGFP (excitation around 450 nm, emission at >510 nm); Cells stably expressing *ArtPlasMA AP*. (B) Enzyme Induced Staining. Fluorescence images of cells (excitation around 535 nm, emission around 610 nm) before (-1 sec) and after addition of Di-12P-ASPBS to a final concentration of 400 nM. (C) Inverted and normalized images of row (B).

5.2.3 Staining and Destaining after Removal of the Dye Precursor

In a similar experiment, the stable *ArtPlasMA AP* clone was co-cultured with native HEK293 cells. The cells were incubated for 30 sec with 100 nM Di-12P-ASPBS in buffer and washed twice in buffer without dye. A fluorescent marker of native cells was not necessary in this case. Fluorescence was therefore recorded with filter set “A”. Two minutes after staining and washing, a strong selective staining of certain cells is apparent (Figure 26A). With time, the membrane fluorescence declines due to diffusion of the dye from the cell membrane to the bulk medium. After renewed addition of Di-12P-ASPBS, the cells are again selectively stained with the voltage sensitive dye. The reaction is therefore fully reversible.

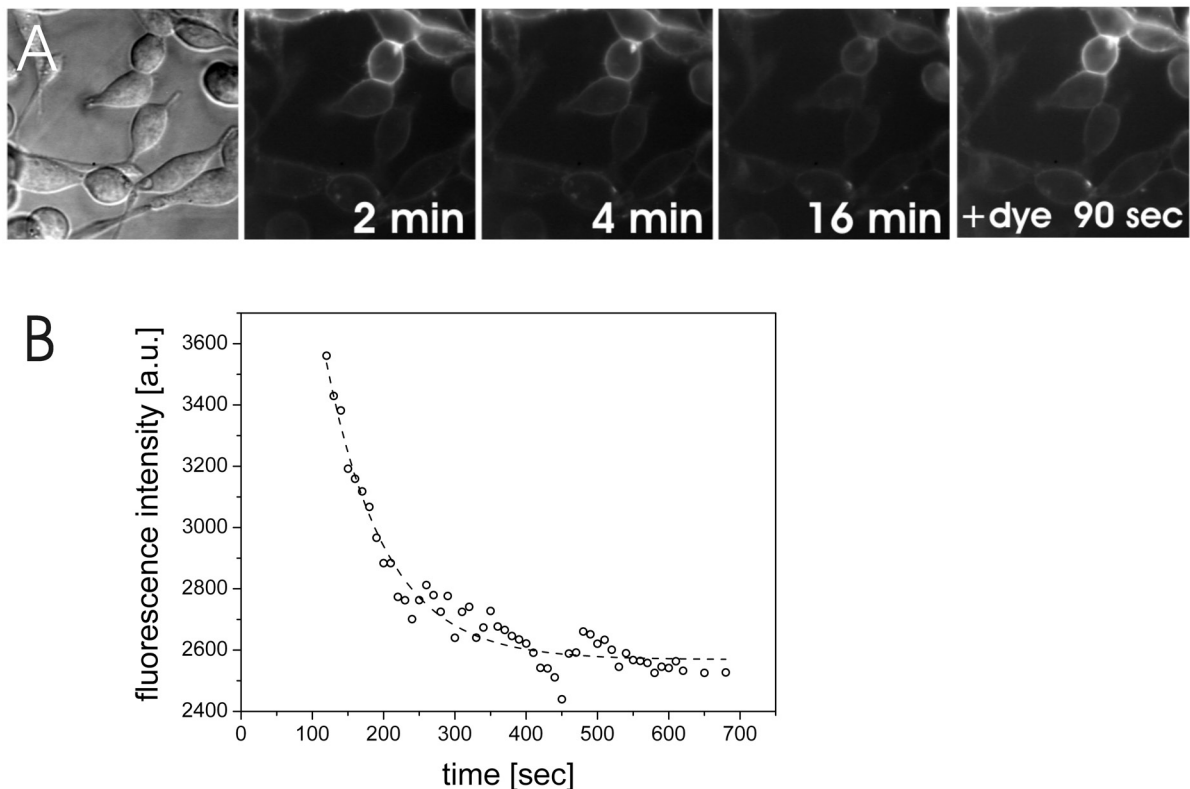


Figure 26. Destaining after Enzyme Induced Staining with Di-12P-ASPBS. Cells stably expressing Phosphatase co-cultured with native HEK293 cells. (A) Brightfield image of all cells on a dish; Fluorescence images (Filter set A, excitation around 450 nm, emission at >510 nm) of cells after 30 sec incubation with 100 nM Di-12P-ASPBS and washing twice with buffer containing no dye. Images were made 2, 4 and 16 minutes after washing and 90 sec after renewed addition of dye precursor.; Cells stably expressing *ArtPlasMA AP*. (B) Fluorescence intensity of a selected cell membrane (average of the peaks of the profile) versus time illustrating the decline of fluorescence after removing the dye precursor.

The time course of destaining as obtained by plotting the peak membrane fluorescence versus time indicates an exponential decay (Figure 26B). Fitting the data with the relation $A \exp(t / \tau_{destain}) + B$ yielded a time constant of destaining due to diffusion of $\tau_{destain} = 83 \text{ sec}$ (Figure 26B, dashed line). Carrying out the same destaining experiment with Di-10P-ASPBS was not possible due to the lack of selective staining and the fast destaining.

5.3 Enzyme Induced Staining: Profiles of Dye Diffusion

A close look at the fluorescence profiles of images Figure 22B and Figure 23B (section 5.1) reveals the development of a fluorescence signal in the region directly adjacent to the cell membrane. As experiments described in the following will show, performing the same experiments with the filter set B led to a very strong enhancement of this signal. The signal presumably originated from diffusing dye that subsequently bound to the plastic culture dish with a concomitant increase in quantum yield (cf. Discussion). Since membrane fluorescence is dominant and most of the observed surface of the dish was covered by the cells, this did not severely influence the results of the assay for selective staining (section 5.2). This is backed by the destaining experiment which was performed with filter set A (section 5.2.3.).

5.3.1 Di-10P-ASPBS

Figure 27A shows a sequence of images before and after the addition of 100 nM Di-10P-ASPBS to a group of two cells. As in the experiments described in section 5.1, the fluorescence of the cell membranes increased strongly due to binding activation of the dye. Using the filter set B, however, a strong fluorescence signal that developed in the vicinity of the cells is clearly discernible. The fluorescence profiles of one of the cells at selected points (Figure 27B) and a plot of the peak intensity versus time (Figure 27C) both show a clear saturation with time. However, the time constant of staining is not congruent to the one measured with filter set A (section 5.1), but amounts to $\tau_{stain(B)}^{10P} = 126 \text{ sec}$. The average of the plateau fluorescence minus the background was 820 a.u.. Note that due to the different filter set, fluorescence intensity can only be compared to the following experiment, but not to the values obtained in section 5.1.

5.3.2 Di-12P-ASPBS

With the precursor dye Di-12P-ASPBS, a development of fluorescence profiles assignable to dye diffusion and/or binding to the dish was observed as well (Figure 28). In this

experiment, however, the intensity of the profile fluorescence relative to the membrane fluorescence was significantly lower. Also here, the time constant of staining was higher than in the same experiment with filter set A (section 5.1.2) and amounted to $\tau_{stain(B)}^{12P} = 284 \text{ sec}$.

Within the observed time course, neither fluorescence profiles nor membrane fluorescence intensity saturated. The plateau fluorescence was therefore obtained from the exponential fit and amounted to 1250 a.u..

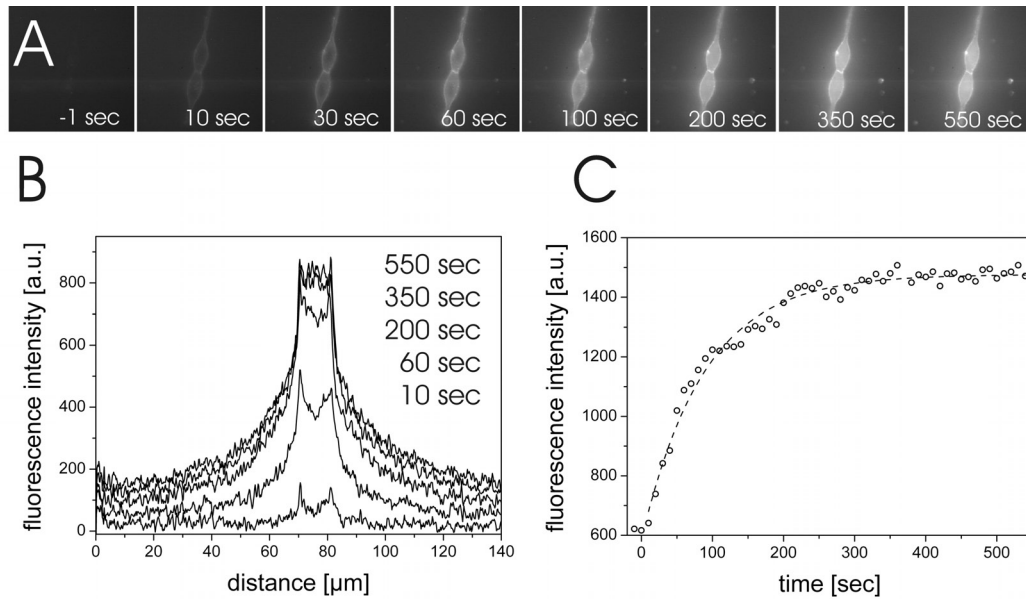


Figure 27. Enzyme Induced Staining on stably phosphatase-expressing HEK293 cells with the dye Di-10P-ASPBS and using filter set B (cf. Figure 22). (A) Fluorescence images (excitation around 535 nm, emission around 610 nm) of HEK293 cells before (-1 sec) and after addition of Di-10P-ASPBS at a final concentration of 100 nM. The image brightness was normalized to the same level for all images. Image contrast was enhanced by subtracting background fluorescence. (B) Profiles of fluorescence intensity minus background fluorescence (at -1 sec) across the diameter (approx. 15 μm) of a selected cell. (C) Fluorescence intensity of cell membrane (average of the peaks of the profile) versus time.

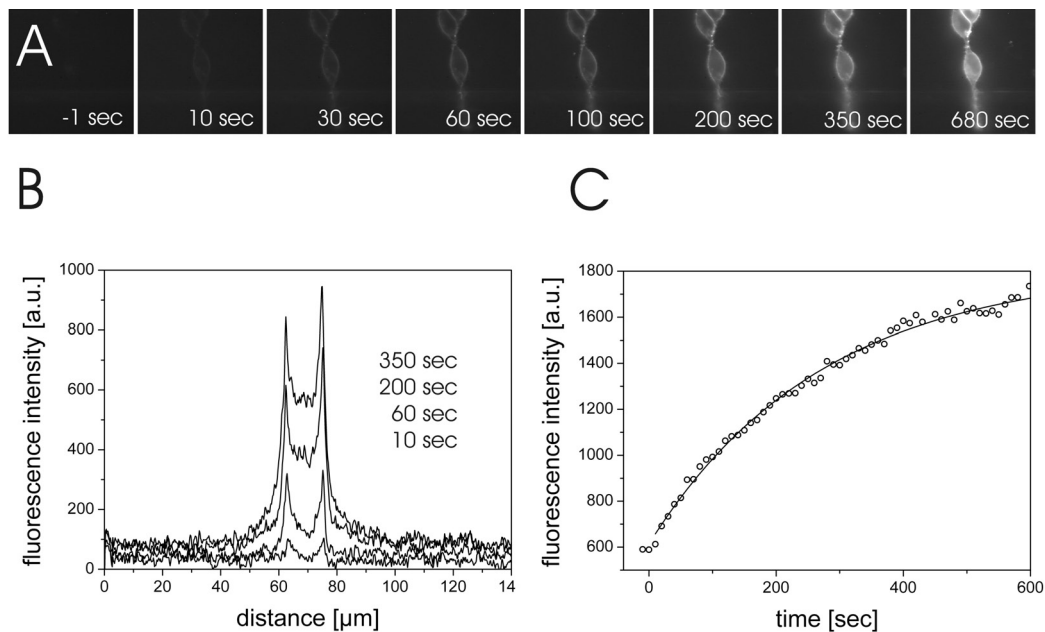


Figure 28. Enzyme Induced Staining on stably phosphatase-expressing HEK293 cells with the dye Di-12P-ASPBS and using filter set B (cf. Figure 23). (A) Fluorescence images (excitation around 535 nm, emission around 610 nm) of HEK293 cells before (-1 sec) and after addition of Di-12P-ASPBS at a final concentration of 100 nM. The image brightness was normalized to the same level for all images. Image contrast was enhanced by subtracting background fluorescence. (B) Profiles of fluorescence intensity minus the background fluorescence (at -1 sec) across the diameter (approx. 15 μm) of a selected cell. (C) Fluorescence intensity of cell membrane (average of the peaks of the profile) versus time.

5.4 Enzyme Induced Staining on MDCK Transiently Expressing Phosphatase

Now it was tested whether the approach could be transferred to other cell lines. It was also of interest to see whether the expression rates obtained by transient transfection would be sufficient to generate strong staining. For this purpose, MDCK cells were transiently transfected with ArtPlasMA AP and a fluorescent transfection marker. To facilitate discrimination between fluorescence originating from the membrane-bound dye and the marker, a cell nucleus-localized marker was used. This marker, called H2B-GFP, is a fusion construct of the histone 2B and EGFP.¹³² The nuclear localization of this marker and the weaker expression compared to the cytosolic EGFP marker, as well as the comparably strong staining of the cells allowed the use of filter set A.

To co-transfected cells, Di-10P-ASPBS or Di-12P-ASPBS were added at a final concentration of 200 nM and fluorescence was recorded (Figure 29A and B). In both cases, the transfected cells were selectively stained in the initial phase of the reaction. For Di-10P-ASPBS, however, a uniform, non-selective staining of all cells was apparent about three minutes after the addition. In contrast, the staining with Di-12P-ASPBS was selective, even ten minutes after precursor addition. Non-adjacent cells showed no visible staining at all, while directly adjacent cells were weakly stained at this point of time. The result with both precursor dyes on transiently transfected MDCK cells is therefore analogous to, but more distinct than the result obtained with stably transfected HEK293 cells.

The visual appearance of the staining of MDCK cells is different from that of HEK293 cells. While in HEK293 cells, the fluorescence is strongest along the outline of the cells, on MDCK cells a strong staining of the whole cell is apparent. This must be attributed to the different architectures of the cell membranes. While in HEK293 cells, the membrane is relatively smooth, the apical membrane of MDCK cells is rough due to the presence of so-called microvilli. This leads to a higher surface area of the apical membrane and therefore to stronger staining.

Two control experiments were carried out. Cells only transfected with the transfection marker H2B-GFP exhibited very weak and non-selective staining of cells, which can be attributed to staining with the precursor dye and low amounts of dye activated by the native phosphatase activity of the cells (Figure 29C). The staining is therefore not a result of the transfection process, like e.g. a change in membrane properties by the transfection reagent. In the second control experiment, the product of dye hydrolysis Di-10A-ASPBS was directly

added to cells co-transfected with phosphatase and marker. The resulting staining was clearly non-selective (Figure 29D). This showed that selective staining as shown in Figures 29A and B did not originate from binding of the dye to overexpressed phosphatase.

Enzyme Induced Staining obviously works not only on stably phosphatase expressing HEK293 cells, but also on transiently transfected MDCK. Nevertheless, the optical appearance of the stainings is rather peculiar. A closer inspection of the reaction on MDCK cells might bring clarity about the underlying reasons of this optical appearance.

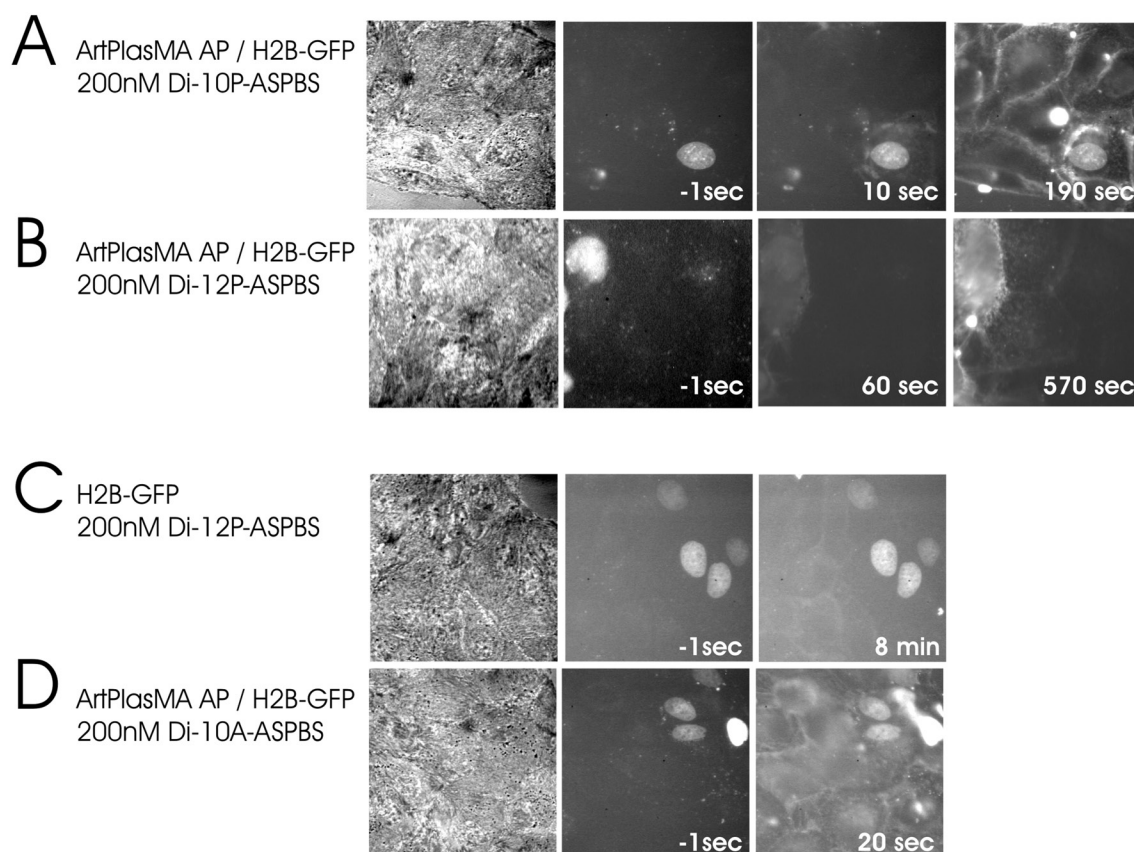


Figure 29. Enzyme Induced Staining of MDCK cells. Brightfield and fluorescence images (excitation around 450 nm, emission at >510 nm, filter set A). Fluorescence images after the addition of dye are normalized to the same level for each experiment. Fluorescence images before dye addition (-1 sec) are contrast enhanced where necessary to clearly show the transfection marker fluorescence. (A) Di-10P-ASPBS. Cells transiently transfected with ArtPlasMA AP and H2B-GFP as a nucleus-localized transfection marker. Dye precursor was added to a final concentration of 200 nM. (B) Di-12P-ASPBS. Analogous to (A). (C) Control. Cells were transfected with the transfection marker H2B-GFP alone and dye precursor was added to a final concentration of 200 nM. (D) Control. Cells transiently transfected with ArtPlasMA AP and H2B-GFP were incubated with the product of precursor hydrolysis Di-10A-ASPBS.

5.5 Model of Enzyme Induced Staining

In this section, a model for enzyme induced staining is introduced.¹³³ In this model, three zones are relevant: The stirred bulk aqueous phase with homogenous concentrations of dye precursor and produced dye, an unstirred Nernst layer¹³⁴ of thickness δ_N above the cell membrane in which mass transport takes place by diffusion, and the cell membrane. Both dye precursor and produced dye (in the following referred to as “dye”) bind to the membrane according to their partitioning constant, and it is assumed that no lateral diffusion of the dye in the membrane takes place. This assumption is backed by experiments performed with other styryl dyes.⁶⁰ Instead of the partition coefficient K_D (with dimension M^{-1}), an Ostwald-like distribution coefficient γ_D is used in the model.²⁶ γ_D is the proportionality constant of the surface density of the dye σ_D^M in the 2-dimensional membrane and the concentration of the dye in the aqueous phase with $\sigma_D^M = \gamma_D c_{D,f}$. It is linked to K_D via $\gamma_D = K_D / a_L$, with lipid area $a_L = 0.7 \text{ nm}^2$.

Cellular self-staining can be subdivided into four elementary steps (Figure 30): (i) Diffusion of the dye precursor from the stirred bulk phase ($c_{pre,f}^B$) to the unstirred layer above the reactive surface of the cell ($c_{dye,f}^B$) with diffusion constant D_{pre} . (ii) Conversion of the dye precursor to the dye by enzymatic hydrolysis with rate j_{dye}^E . (iii) Establishment of the dye partition equilibrium between membrane and unstirred layer with γ_{dye} . (iv) Diffusion of the dye from the unstirred layer to the bulk aqueous phase and diffusion to the surrounding area and cells within the unstirred layer.

Let us consider the simplified model of one-dimensional homogenous staining in an infinite active membrane.¹³³ One-dimensional diffusion implies that diffusion within the unstirred layer is not regarded. Depletion of the precursor dye in the unstirred layer and accumulation of the dye in the bulk aqueous phase are neglected.

The enzymatic production of the dye j_{dye}^E is balanced by an increase of local concentration of the dye $c_{dye,f}^{nernst}$ in the unstirred layer of thickness δ_N , by concomitant staining of the membrane with a density of σ_{dye} , and by diffusion of the dye to the bath. The latter is

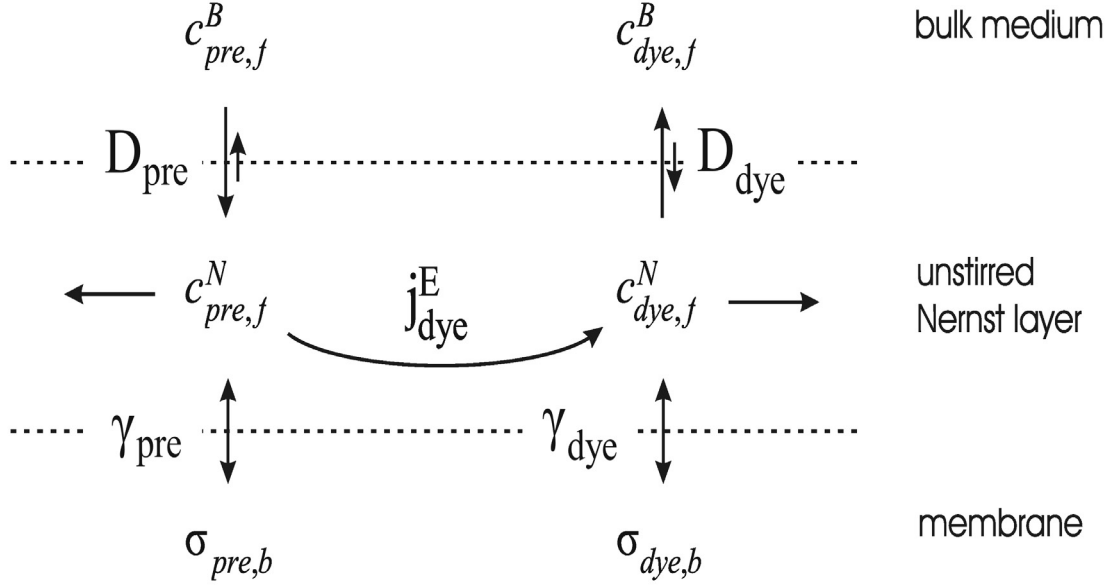


Figure 30. Reaction diagram of Enzyme Induced Staining. The three relevant zones are the stirred bulk aqueous medium, the unstirred Nernst layer above the cells and the cell membrane to which dye precursor and dye bind. The elementary steps are: (i) diffusion of the precursor from the bulk medium to the unstirred layer with diffusion coefficient D_{pre} . The precursor dye binds to the membrane in accordance with its binding coefficient γ_{pre}^{MW} . (ii) Enzymatic conversion of the dye precursor to the dye with the reaction rate j_{dye}^E . The dye binds to the cell membrane with γ_{dye}^{MW} . (iii) Diffusion of the dye from the active zone to the bulk aqueous medium and within the unstirred layer.

described by 1D diffusion with the dye's diffusion constant in water D_{dye} (eq 13). For simplicity, diffusion according to Fick's 1st law is replaced – in a one-compartment model – by diffusion from a hypothetical Nernst layer of thickness δ_N with homogenous concentration of dye $c_{dye,f}^N$ to the bulk phase with a dye concentration of $c_{dye,f}^B = 0$.

$$j_{dye}^E = \delta_N \frac{dc_{dye,f}^N}{dt} + \frac{d\sigma_{dye}}{dt} + \frac{D_{dye}}{\delta_N} c_{dye,f}^N \quad (13)$$

For equilibrated staining ($\sigma_{dye} = \gamma_{dye} c_{dye,f}^N$) and for large binding constants ($\gamma_{dye} \gg \delta_N$) one obtains:

$$j_{dye}^E = \frac{d\sigma_{dye}}{dt} + \frac{D_{dye}}{\gamma_{dye} \delta_N} \sigma_{dye} \quad (14)$$

Integration results in eq 15, with the time constant of staining τ_{stain} and membrane density of the dye in the stationary state $\bar{\sigma}_{dye}$:

$$\frac{\sigma_{dye}}{\bar{\sigma}_{dye}} = 1 - \exp\left(-\frac{t}{\tau_{Stain}}\right) \quad (15)$$

$$\tau_{Stain} = \gamma_{dye} \frac{\delta_N}{D_{dye}}, \quad \bar{\sigma}_{dye} = j_{dye}^E \tau_{Stain}$$

According to eq 15, the stationary staining $\bar{\sigma}_{dye}$ is dependent on the reaction rate j_{dye}^E and the time constant. τ_{stain} is determined by the diffusion velocity D_{dye}/δ_N to the bath and the binding coefficient γ_{dye} . While j_{dye}^E is linked to the dye concentration via the Michaelis-Menten kinetics (eq 11, cf. section 3.1.2), τ_{stain} is independent of the dye concentration. The time constants of staining and destaining are equal as deduced by integration of eq 14 with $j_D^E = 0$ which leads to $\sigma_D^M / \bar{\sigma}_D^M = \exp(-t / \tau_{destain})$.

5.6 Discussion

Time constant τ . The thickness of the Nernst layer and the diffusion coefficients should be equal for Di-10P-ASPBS and Di-12P-ASPBS. According to eq 15, the ratio of time constants τ^{12P} / τ^{10P} should therefore be equal to the ratio of the dye binding constants K_{12A} / K_{10A} as measured on lipid vesicles (cf. section 2.2). The expected ratio of the time constants for Di-12P-ASPBS and Di-10P-ASPBS is $\tau^{12P} / \tau^{10P} = K_{12A} / K_{10A} = 12$. The experimental ratio is considerably lower, with $\tau^{12P} / \tau^{10P} = 108\text{sec} / 48\text{sec} = 2.3$. This implies that the relative strength of dye binding to cell membranes $K_{12A}^{cell} / K_{10A}^{cell}$ is different from that measured on lipid vesicles. The binding constant of Di-12A-ASPBS to lipid vesicles was already lower than expected from a linear relationship between alkyl chain length and binding strength (cf. section 2.2), which would have led to $K_{12A} / K_{10A} = 30$. This further decreased value of $K_{12A}^{cell} / K_{10A}^{cell}$ is therefore likely to be due to deviations in the binding behaviour of Di-12A-

ASPBS. These results are disconcerting and might compromise a further optimization of the method.

Nevertheless, the model correctly reproduces that the time constants of staining are dependent of the binding constant of the dye. As predicted, the experimental time constants of staining and destaining are nearly the same, with values using the precursor dye Di-12P-ASPBS being $\tau_{stain}^{12P} = 108 \pm 18 \text{ sec}$ and $\tau_{destain}^{12P} = 83 \text{ sec}$.

Saturated staining $\bar{\sigma}_{dye}$. Preliminary investigations suggest that the rates of enzymatic hydrolysis j_D^E of Di-10P-ASPBS and Di-12P-ASPBS are similar (not shown).^e According to eq 15, the ratio of saturated staining densities for Di-12P-ASPBS and Di-10P-ASPBS should therefore be close to the measured ratios of τ_{stain} . This has indeed been found, with the experimental ratios using filter set A being $\bar{\sigma}_{12A} / \bar{\sigma}_{10A} = 2.6$.

With eq 15, one can estimate the order of magnitude of the density of saturated staining in an infinite active membrane. In the experiment on the dish, diffusion away from the cell can occur in three dimensions. Still, the area specific rate of enzymatic hydrolysis is not affected, and it can be assumed that the relation $\bar{\sigma}_{dye} = j_{dye}^E \tau_{Stain}$ still holds true in this case. The reaction rate depends on the substrate concentration according to eq 11. Inserting the enzyme kinetic constants determined for the dye Di-4-ASPPP^e (cf. section 3.1.2), the experimentally determined activity of the stably expressing HEK293 clone ($\tilde{\sigma}_E = 453 \text{ DEA Units} / m^2$, cf. section 4.3.4) and a substrate concentration of 100 nM, one obtains $j_D^E = 2 \times 10^3 \mu m^{-2} s^{-1}$.^f With the experimental time constants, a saturated staining therefore leads to a calculated density of $\bar{\sigma}_{10A} = 1.0 \times 10^5 / \mu m^2$ and $\bar{\sigma}_{12A} = 2.2 \times 10^5 / \mu m^2$, corresponding to a calculated ratio of dye to lipid of 0.14 (Di-10A-ASPBS) and 0.31 (Di-12A-ASPBS), respectively. Note that these values of the saturated staining density, just as the enzymatic activity of the plasma membrane (cf. section 3.1.2), must be viewed as an upper limit of the actual values.

^e For these experiments, the fluorescence increase accompanying hydrolysis of the dye precursors by PLAP in the presence of lipid vesicles was investigated in analogy to the experiments in section 3.2. The obtained rate constants were in the same range as the values obtained for Di-4-ASPPP.

^f In this approximation, it is assumed that the removal of the first phosphate group from the dye precursor is the rate limiting step.

Thickness of the Nernst layer δ_N . With eq 15, one can estimate the thickness of the unstirred Nernst layer. In the following computation, the parameters of Di-10A-ASPBS are used since the behaviour of Di-12A-ASPBS regarding lipid binding and cellular self-staining suggests that unknown effects play a role for this dye. With $\gamma_{10A} = 590\mu m$, $\tau_{stain}^{10P} = 48 \pm 14 \text{ sec}$ and a typical diffusion coefficient for small organic molecules of $D_{dye} = 0.5 \times 10^{-5} \text{ cm}^2 / \text{s}$,⁷³ one obtains a calculated thickness of the Nernst layer of $\delta_N \approx 40\mu m$. This is a reasonable value regarding that experimental ranges for δ_N have been reported to range from $0.5\mu m$ to $500\mu m$.¹³⁴ Using the relations of Vielstich¹³⁴ (cf. Materials and Methods), this would correspond to values for the characteristic length of the system of 1 mm and a velocity of the stirred medium of 3 cm/sec. A strict comparison with experimental values is not possible, since the parameters governing the flow of the medium in the reaction vessel were not well controlled. Nevertheless, the values are in a realistic range.

Selectivity. Unselective staining originates from: (i) staining by dye that is produced by the native enzymatic activity of the cells; (ii) staining by dye that diffuses away from enzymatically active cells; and (iii) staining by the dye precursor.

Qualitatively, it can be intuitively understood that selective staining is therefore promoted by (i) a high specific enzymatic activity at the membrane of the transfected cell; (ii) a large binding constant of the dye to minimize the concentration of free diffusible dye. This is strictly true only with the assumption that binding equilibration of the dye is fast; and (iii) weak binding of the dye precursor, i.e. $\gamma_{pre} \ll \gamma_{dye}$.

(i) *Enzyme activity.* As the experiments have shown, the phosphatase activity of stably transfected HEK293 cells exceeded the native activity by a factor of 70 (cf. section 4.3.4). A strong expression was also achieved in transiently transfected HEK293 and MDCK cells. Since reaction conditions can be further optimized, this issue does therefore not seem to be problematic.

(ii) *Diffusing dye.* In terms of the model of homogenous staining of an infinite active membrane, there are two relevant phases of the reaction (cf. eqs 14 and 15). In the initial phase of the reaction ($t < \tau$), most of the net flow of the produced dye binds to the membrane according to the binding equilibrium, increasing the staining density. In the saturated phase, where $t \gg \tau$, production of dye at the cell and diffusion away from the cell occur at the same rate. The net flow of produced dye is therefore lost by diffusion and does not contribute to increasing the staining density of the cell membrane.

These two phases can be assumed to also occur in the 3D environment of a real experiment. Selective staining therefore requires termination of the reaction in the initial phase where $t < \tau$. In practice, this is facilitated by a large τ_{stain} , and therefore a large binding constant, according to eq 15. This is reflected by the experimental data: (a) In the staining of MDCK cells (Figure 29A), and also on HEK293 cells (Figure 24), staining was selective with Di-10P-ASPBS only within the first tens of seconds of the reaction. (b) With Di-12P-ASPBS, staining was selective on HEK293 (Figure 25) and MDCK (Figure 29B) cells during the whole observed time course of up to 10 minutes. (c) The intensity of the fluorescence profile originating from diffusing dye at the same points of time was much higher for the more weakly binding Di-10P-ASPBS than for Di-12P-ASPBS (Figure 27 and 28; cf. *Profiles of Dye Diffusion* below).

(iii) *Dye precursor*. Background staining by the dye precursor during the reaction leads to a staining density of $\sigma_{pre}^M = \gamma_{pre} c_{pre,f}$. For $t_{stain} \ll \tau_{stain}$, one obtains $\sigma_{dye}^M = j_{dye}^E t$ from eq 15. Expressing j_{dye}^E by the Michaelis-Menten kinetics (eq 11) at low substrate concentrations with the membrane surface density of the enzyme $\tilde{\sigma}_E^M$, low background staining therefore requires $\gamma_{pre} K_M / \tilde{k}_{cat} \tilde{\sigma}_E^M \ll t_{stain}$. In order for enzyme induced staining to exceed background staining within a minimal time, one therefore requires a low γ_{pre} , a high capture rate of the enzyme¹³⁵ \tilde{k}_{cat} / K_M and a high $\tilde{\sigma}_E$. For the precursors used in this section, the term $\gamma_{pre} K_M / \tilde{k}_{cat} \tilde{\sigma}_E$ amounts to 7 msec (Di-10P-ASPBS) and 0.2 sec (Di-12P-ASPBS), respectively, using the determined enzyme kinetic constants determined for Di-4-ASPPP (cf. section 3.1.2) and the experimentally determined surface density of the enzyme (cf. section 4.3.4). In accordance with the experiments, background staining during the reaction is therefore not an issue when using these precursors. The following paragraph shows that background staining should also pose no problem when more strongly binding dyes are used.

Optimization of dyes with regard to destaining. For voltage-sensitive measurements with enzymatically stained cells, the experimental $\tau_{stain} = \tau_{destain}$ for the dyes Di-12A-ASPBS and Di-10A-ASPBS, being in the order of 100 sec, is too low to be practicable. Since selective staining requires terminating the reaction, i.e. removing the precursor dye, the fast destaining and the limited time window of selective staining would severely complicate voltage-sensitive measurements. Ideally, the dye would have a τ that lies in the order of hours or days. Using the same parameters for δ_N and D_{dye} as above and calculating τ_{stain} by eq 15, a binding

constant of 4.5×10^8 l/mol would correspond to $\tau_{stain} = 24$ h. Theoretically, this dye with $\gamma_{dye} = 2.1m$ would exhibit a dye/lipid ratio of approx. 0.4 at $t_{stain} = 300$ s. A precursor dye with a binding constant that is reduced by a factor of about 3×10^3 , as it was found for the phosphorylated dyes, would exhibit $\gamma_{pre} = 0.4mm$ and $\tau_{pre} = 28$ sec. During the reaction, background staining would therefore be quite high. On the HEK293 clone described in this section, it would take 15 sec for enzyme induced staining to reach the same intensity as background staining. After terminating the reaction, however, the precursor dye could easily be washed away due to its significantly smaller τ . This clearly shows that the difference in binding constants between a doubly tail-phosphorylated dye and its corresponding hydrolysis product should easily suffice to avoid background staining by the dye precursor. In addition, electrostatic repulsion should further reduce the effective binding constants and therefore background staining of very long-tail dye precursors (cf. section 2.3).

It is, however, not clear whether it is possible to obtain tail-modified dyes that exhibit very large binding constants on cell- and artificial membranes.

Profiles of dye diffusion. Using a filter set with red-shifted excitation and emission led to the appearance of intense profiles of fluorescence in the vicinity of the enzymatically active cells. This signal cannot have originated from dye in the aqueous phase, since then an increase of background fluorescence of comparable intensity would have been expected upon addition of precursor dye. The signal must therefore be due to diffusing dye that subsequently binds to the plastic culture dish with a concomitant increase in fluorescence quantum yield. In addition, binding to the substrate obviously leads to a red-shift in either fluorescence excitation or emission or both to produce the observed effect.

The time constants of staining as well as the ratio of saturated fluorescence intensity were different using the red-shifted filter set B as compared to the filter set A.

Concerning saturated fluorescence intensity, this may be explained by the fact that the overall fluorescence signal is a superposition of the signal of lipid bound dye and of substrate-bound dye. The saturated staining intensity is therefore severely influenced by the binding and spectral characteristics of substrate-bound dye. However, it can not be expected that the binding of Di-10A-ASPBS and Di-12A-ASPBS to the plastic culture dish occurs with the same binding constant as that on cell membranes.

A similar explanation could account for the difference in the time constants of staining. The observed time course not only includes the kinetics of enzymatic reaction and lipid binding

(as with filter set A), but also the kinetics of diffusion and binding to the substrate. An increase in the time constant of staining is therefore feasible.

Experiments clarifying this issue need to deal with the spectral and binding properties of dyes bound to the plastic culture dish.

Conclusion. The model of homogenous staining in an infinite enzymatically active membrane provides insight into some of the major properties of the system under study. The calculated time constants of staining and destaining are in the correct order of magnitude compared to the experimentally obtained values. The model also correctly predicts that the time constant of staining and the saturated staining density are connected since both depend on the binding coefficient γ_{dye} . With the model, estimates of the saturated staining density can be obtained. Predictions of dye properties towards higher time constants of staining show that this perspective is promising to implement enzyme induced selective staining by genetically targeted cells.

However, there are considerable discrepancies between model and experiment regarding the difference in the behaviour of Di-10A-ASPBS and Di-12A-ASPBS. This indicates that a more detailed investigation of the reaction as well as an application of more realistic models is required. A rigorous test of future, three-dimensional mathematical models will be greatly facilitated by the profiles of dye diffusion that can be observed using filter set B.

5.7 Materials and Methods

Enzyme Induced Staining on stably transfected HEK293 Cells. HEK293 cells were cultured as described in section 4.5. They were seeded at a low density (approx. 50000 cells per dish) to facilitate experiments on isolated groups of cells. In addition, this approach limits the overall enzymatic activity in the dish, which is necessary to exclude the possibility of precursor depletion during the time course of the experiment. 24-48 h after plating the culture medium was removed and cells were washed three times with buffer (20 mM HEPES, 150 mM NaCl, pH 7.5). This was done quickly, but thoroughly in order to remove any residual traces of the medium. Then, the cells were washed with Tris-Glucose buffer (20 mM Tris, 100 mM NaCl, 70 mM Glucose) and incubated in 4 ml of this buffer. An appropriate cell or group of cells was chosen under red light illumination, and dye precursors Di-10P-ASPBS or Di-12P-ASPBS were added to a final concentration of 100 nM. Fluorescence images were acquired every ten seconds with the setup and software described in section 3.5 and filter set A (band pass 450/50 nm; dichroic mirror 505 nm; long pass filter 510 nm or filter set B (band pass 535 nm/50, dichroic mirror 550 nm, band pass 610/75). The experiments were performed under continuous

stirring by pipetting with a 1 ml Eppendorf pipette at room temperature (20-25°C). Data analysis was carried out with the software described in section 3.5. Images were level normalized with Adobe Photoshop software.

For selective staining experiments, a stable clone of cells expressing cytosolic EGFP was obtained according to standard procedures¹¹⁸ using 400 µg/ml G418 for selection and 200µg/ml G418 for propagation of selected cells. The vector termed pcDNA3.EGFP(Kozak) was a gift from Jürgen Kupper. It consisted of pcDNA3 into which EGFP had been cloned using pEGFP-C1 (BD Biosciences Clontech, Palo Alto, CA, USA) as the source. The EGFP clone was seeded together with a clone stably expressing ArtPlasMA AP (cf. section 4) at a low density (overall approx. 150000 cells) and at a ratio of EGFP clones to ArtPlasMA AP clones of 2:1. 24-48 h after transfection, the cells were washed three times with 20mM HEPES, 150 mM NaCl, pH 7.5, once with Tris-Glucose pH 8.1 and incubated in 4 ml of this buffer. Then, dye was added to a final concentration of 1µM for Di-10P-ASPBS or 400 nM for Di-12P-ASPBS and images were acquired every ten seconds using filter set B (excitation 535/50 nm, dichroic mirror 535 nm, emission around >610/75 nm). Experiments were performed at room temperature (20-25°C) under continuous stirring by pipetting.

Destaining experiments were performed analogously on a co-culture of native HEK293 cells and a clone stably expressing ArtPlasMA AP. Cells were washed as described above, incubated for 30 sec in buffer containing 100 nM dye, washed twice in buffer without dye and fluorescence was recorded.

Enzyme Induced Staining on transiently transfected MDCK Cells. Madin-Darby Canine Kidney cell culture was performed as described in section 4.5. For selective staining experiments, cells were transiently transfected either with both or one of the plasmids coding for ArtPlasMA AP (pcDNA3 ArtPlasMA AP) and H2B-GFP (pBOS H2BGFP, BD Biosciences Pharmingen, San Diego, CA, USA) using Effectene (Qiagen) according to supplier's instructions. The ratio at which the plasmids pBOS H2BGFP and pcDNA3 ArtPlasMA were transfected was 1:10. 24 to 48 h post transfection, cells were washed three times in 20mM HEPES, 150 mM NaCl, pH 7.5. They were then washed once with Tris-Glucose pH 8.1 and incubated in 4 ml of this buffer. The dye Di-10P-ASPBS or Di-12P-ASPBS was added to a final concentration of 200 nM, and images were acquired every ten seconds using filter set A. The incubation medium was stirred continuously using a 1 ml Eppendorf-pipette.

Estimation of the depth of the unstirred layer. According to Vielstich¹³⁴, the mass transport of a reaction taking place at the boundary of a surface and a liquid medium can be described by diffusion from a hypothetical Nernst diffusion layer of thickness δ . The thickness of the Nernst layer is connected to the thickness of the Prandtl diffusion layer by $\delta_N = \text{Pr}^{\frac{1}{3}} \delta_{Pr}$. With Prandtl's number $\text{Pr} = \nu/D$ (ν kinematic viscosity, D diffusion coefficient) and Reynold's number $\text{Re} = vl/\nu$ (v velocity of the medium, l characteristic length), one obtains¹³⁴

$$\delta_N = \text{Pr}^{-\frac{1}{3}} \times 3l \text{Re}^{-\frac{1}{2}} = \left(\frac{\nu}{D}\right)^{-\frac{1}{3}} \times 3l \left(\frac{vl}{\nu}\right)^{-\frac{1}{2}}$$

The kinematic viscosity of water is $\nu_{H_2O} = 1 \times 10^{-6} \text{ m}^2/\text{s}$. A typical diffusion coefficient for medium sized molecules is $D = 0.5 \times 10^{-9} \text{ m}^2/\text{s}$.⁷³ At a given δ , one can therefore compute a set of the corresponding characteristic length of the system and the velocity of the streaming medium.

6 Final Conclusion and Outlook

The presented work introduces a novel approach to the selective staining of cells in tissue with Voltage Sensitive Dyes. These dyes are membrane-bound, optical probes of membrane potential. The envisaged concept relies on the activation of binding to the membrane of a genetically targeted cell.

To that end, weakly binding and water soluble precursor dyes were designed and synthesized. They were thoroughly characterized and employed for the enzyme induced staining of small lipid vesicles, giant lipid vesicles and erythrocytes using a soluble alkaline phosphatase. A membrane-bound version of this enzyme was produced by cloning a chimera of the phosphatase and a specially designed membrane anchor and targeting signal. This strategy facilitated a stable plasma membrane targeting, strong enzyme activity at the cell membrane and a detailed characterization of the chimera. Cells overexpressing this chimera were selectively stained, as compared to non-expressing cells, when they were incubated with the precursor dye Di-12P-ASPBS.

Starting from the very first steps of proving the principal feasibility of genetically targeted staining, the work presents the successful implementation of selective staining on cultured mammalian cells with a simple voltage sensitive dye.

In order to further improve the method, future work will have to address the following issues:

(i) Elucidation of the mechanism. There are considerable discrepancies between experimental results and theoretical considerations.

These concern on the one hand the sub-linear increase of binding constants for strongly binding tail-modified dyes with increasing length of the lipophilic tail (section 2.2). On the other hand, the difference in the time constants of cellular self-staining between the dyes Di-12P-ASPBS and Di-10P-ASPBS is significantly smaller than predicted by a theoretical model

of the reaction (section 5). This possibly originates from a further decrease of the difference of binding strengths of the dyes when binding to cell membranes.

More detailed investigations of dye binding to artificial and also natural membranes as well as of the formation of micelles and aggregates is necessary. The measurement of reaction kinetics under better defined reaction conditions and the application of more realistic models will provide further insight into the mechanism of enzyme induced binding.

(ii) Optimized dye properties. As described in more detail in section 5.5, the time constants of staining and destaining are dependent on the binding constant of the dye. An increase in binding strength of the dyes would be desirable to enhance the selectivity and stability of selective enzyme induced staining.

(iii) Highly sensitive dyes. To allow voltage sensitive measurements, the technique needs to be transferred to better voltage sensitive chromophores like the ANNINE dyes.^{1,2}

(iv) Faster Enzymes and Optimized Reaction Conditions. Using an alkaline phosphatase with higher reaction rates will enhance selectivity and/or allow the reduction of the staining buffer's pH (which is currently at pH 8.1) to more physiological conditions.

In addition, reaction conditions can be optimized. In this thesis, all experiments were performed under the same conditions using Tris-Buffer without divalent cations at pH 8.1/25°C. This was done in order to facilitate a comparison of results obtained in different systems. There is much room for enzymatic turnover increase, with variables being buffer type,¹³⁶ temperature, salt composition of the buffer and pH.

(v) Non-endogenous Enzymes. To further increase selectivity, it would be beneficial to use dye precursors with polar groups that are susceptible to enzymes not endogenously present in mammalian tissue. Primary work on targeting such enzymes to the plasma membrane of mammalian cells has been carried out (cf. appendix section 7.1.2.2).

The technology presented in this thesis, but transferred to a more sensitive dye, should already find valuable applications. One of these is reliable staining of nerve cells in general. To date, membrane staining with very hydrophobic dyes like ANNINE 6 is in some cases difficult, or it requires carrier compounds like *Pluronic F-127* and solvents like dimethylsulfoxide DMSO (cf. e.g.³). With the help of enzyme induced staining, be it with soluble or overexpressed enzyme, a strong staining can be produced that does not require high concentrations of possibly perturbing compounds. On cultured neurons, selective staining should be possible, which would facilitate optical recording of neurons in a monolayer of cells.

The method of enzyme activated binding of amphiphiles is of general interest also beyond applications with Voltage Sensitive Dyes. It might for example be interesting to modulate the binding of other amphiphilic compounds like labelled lipids, other membrane bound dyes or pharmaceutically active molecules. For example, a selective labelling of cancer cells with cytotoxic compounds *in vivo* might be feasible since phosphatases are prominent marker molecules of some types of cancer.

Voltage Sensitive Dyes exhibit a temporal and spatial resolution that is, at least in combination, not attainable with other techniques. Based on the results provided by the presented work and a theoretical model describing genetically targeted enzyme induced binding, a successful implementation of selective staining in nervous tissue seems feasible. A fully functional method of selective staining with Voltage Sensitive Dyes would allow previously impossible insights into the function of neuronal networks.

7 Appendix

7.1 Additional Experiments

7.1.1 A Study on Gene Synthesis: LCR vs. PCR and the Origin of Mutation

As mentioned in section 4.2.2, the extent of deletion mutations encountered in gene synthesis was much higher than expected. In the synthesis of an alternative membrane targeting signal termed *AsglypMA* (cf. next section), it was decided to explore the origin of these mutations, and a comparison of the two alternative methods LCR (coupled with PCR) and PCR was performed (cf. Figure 18). This work is included in the presented thesis since gene synthesis is a fundamental technique for protein engineering. It may be expected that future developments of targeted staining will rely on proteins with engineered properties.

In the literature, the reported error rates for deletion and mismatch errors in LCR and PCR based gene synthesis vary significantly. Insertion errors occur, but very rarely. In PCR based gene synthesis, deletion/insertion errors were reported to be 0/kB⁹⁸, 1.3-1.5/kB¹³⁷ and 0 - 2.9/kB¹⁰⁷. The latter value is from an extensive study by Hoover et al., who performed nine independent PCR gene syntheses, with an average deletion/insertion error rate of 0.9/kB. Rates for mismatch mutations in PCR based gene synthesis were reported to be 0.15/kB¹⁰⁵, 0.9/kB¹³⁷, 1.5/kb - 3.5/kb⁹⁸ and 0 - 4/kB (average: 0.9/kB), with the latter value again from the study by Hoover et al.

In LCR based gene synthesis, Chalmers¹⁰³ also reported a high occurrence of deletion errors, but did not provide exact values. In the original paper on LCR by Au et al.,¹⁰² no deletions are reported, and the average rate for base changes is 0.6/kB.

Obviously, the error rates are different from synthesis to synthesis, even when performed in the same lab. Although the exact protocols of the gene syntheses varied, including differences in oligonucleotide purification, no “magic recipe” has been provided so far. In principle, three possible explanations for the observed mutations exist: (i) The errors are introduced by the polymerase. (ii) The errors are introduced due to mis-hybridization. (iii) The errors are introduced by faulty oligonucleotides.

It has been found that keeping the number of PCR cycles down and using a proofreading polymerase had an effect on the purity of the product,^{138,139} hinting at polymerase introduced errors. In this case, LCR should be superior to PCR, since in this technique, the oligos are joined together unmodified to the full length product. However, it has been recognized in the literature that the rate of mutations is far higher than would be expected from the fidelity of the polymerases used,¹⁰⁷ and Hoover et al. have concluded that “the frequency of nucleotide errors is largely dependent on the quality of the oligonucleotides”.¹⁰⁷ So far, no evidence has been provided for this assumption, and no systematic study has been undertaken regarding either the origin of mutations or the superiority of either LCR or PCR.

7.1.1.1 Gene synthesis by LCR and PCR with Oligonucleotide Sets of Different Purity

An assay was performed using a set of 16 oligos to build up the artificial gene *AsglypMA* (cf. section 7.1.2.1). In contrast to the oligos used for *ArtPlasMA*, this set of oligos was not designed to be of equal length, but instead the length of the oligos was adjusted so that the opposing, hybridizing oligo sequences had an approximately equal melting temperature (T_M) throughout the whole construct. This was done to reduce the possibility of mishybridization “hot spots”,⁹⁸ although the necessity of this approach has so far not been proven. The gene sequence was obtained by backtranslation of the desired protein sequence regarding mammalian codon usage bias (cf. section 7.5.1). A Labview program was written that divided the gene into fragments of approximately equal melting temperature as computed by free base pairing energies determined by SantaLucia et al.¹⁴⁰ The T_M 's of the obtained oligos were compared to those calculated with free base pairing energies of Breslauer et al.¹⁴¹ and oligo lengths were readjusted to obtain the smallest achievable T_M window of 57°C to 66°C for both sets of parameters. The resulting set of oligos (cf. section 7.5.3) was ordered either with standard Reverse-Phase HPLC (RP-HPLC) purification, or with additional purification by PAGE. These oligonucleotides were then used without further modification in PCR gene synthesis using thermostable *Pfu* Polymerase, or they were phosphorylated and then used in gene synthesis relying on LCR with *Pfu* Ligase as the active enzyme. The product of LCR was subjected to preparative agarose gel electrophoresis and a band of the approximately appropriate size was excised and extracted from the gel. Both LCR and PCR products were then amplified in a PCR reaction with the outermost primers and cloned into the TA-cloning vector pCR2.1 (cf. map in section 7.6) after addition of adenosine residues with TAQ polymerase. Positive colonies were identified by blue/white selection and PCR screening. For

each of the four possible combinations (PCR with RP-HPLC purified oligos, PCR/PAGE, LCR/HPLC, LCR/PAGE), eight clones were propagated and sequenced.

7.1.1.2 Mutations in Gene Synthesis Products

The total number of sequence errors compared to the desired sequence is given in Table 4, a detailed assignment of these errors to the location in *AsglypMA* is depicted in Figure 31. The following observations were made: (i) the error rate decreased in the order

Method	clones correct/sequenced	overall mutations	deletions	insertions	base changes	error rate/kb
PCR HPLC	1/8	14	11	1	2	5,1
PCR PAGE	3/8	7	5	-	2	2,5
LCR HPLC	0/8	10	9	-	1	3,6
LCR PAGE	2/8	9	7	-	2	3,3

Table 4. Error rate encountered in the gene synthesis of *AsglypMA*.

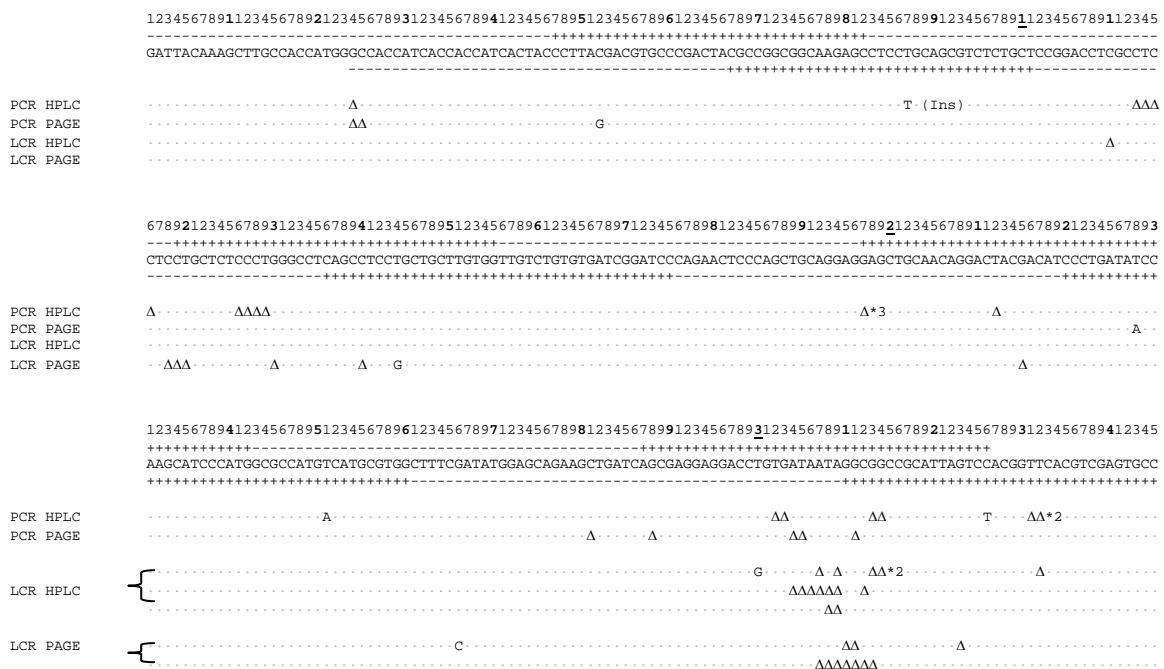


Figure 31. Error location in the gene synthesis of *AsglypMA*. The oligonucleotides that were used to build up the gene are symbolized by rows of minus and plus signs. Δ, ΔΔ: deletion of one or multiple bases; T (Ins): Base insertion; A,G,C,T: base exchange. Note that in some cases the exact location of the mutation, e.g. a single deletion in a row of the same bases, had to be assigned arbitrarily.

PCR/HPLC > LCR/HPLC \cong LCR/PAGE > PCR/PAGE from 5.1 errors/kb to 2.5 errors/kb. (ii) Mostly, the errors were deletions between 1 and 7 bp. Mismatch mutations occurred at an average rate of 0.6/kB, with no statistically discernible difference between the methods. (iii) Although some mutation “hot spots” are evident, the majority of the mutations occurred only once.

7.1.1.3 Investigation of Oligo Purity

To check the purity of the oligonucleotides used in the described gene synthesis, oligos were phosphorylated with [γ - 32 P]ATP and subjected to denaturing PAGE. The relative amount of impurities was assessed by autoradiography in a phosphoimager. Here, it was assumed that the most abundant product was the full length oligo. Figure 32 shows exemplary lanes of all the oligos used. For RP-HPLC purified oligos, the whole ladder of n-x (and in some cases, n+1) products can be discerned, for PAGE purified oligos, the amount of impurities at lengths below n-5 was usually smaller. A quantitative evaluation of the data showed that of the PAGE-purified oligos, an average of 76% had the correct size, while for HPLC-purified oligos, this value was 66%. The difference in purity mostly originated from products that were <n-4, since if these impurities were disregarded, the average purity of the PAGE-purified oligos amounted to 86%, while it was 83% for RP-HPLC-purified oligos. However, there was a great variance between different oligos, which ranged from 65 to 98% for PAGE purified oligos and from 51% to 96% for RP-HPLC-purified oligos.

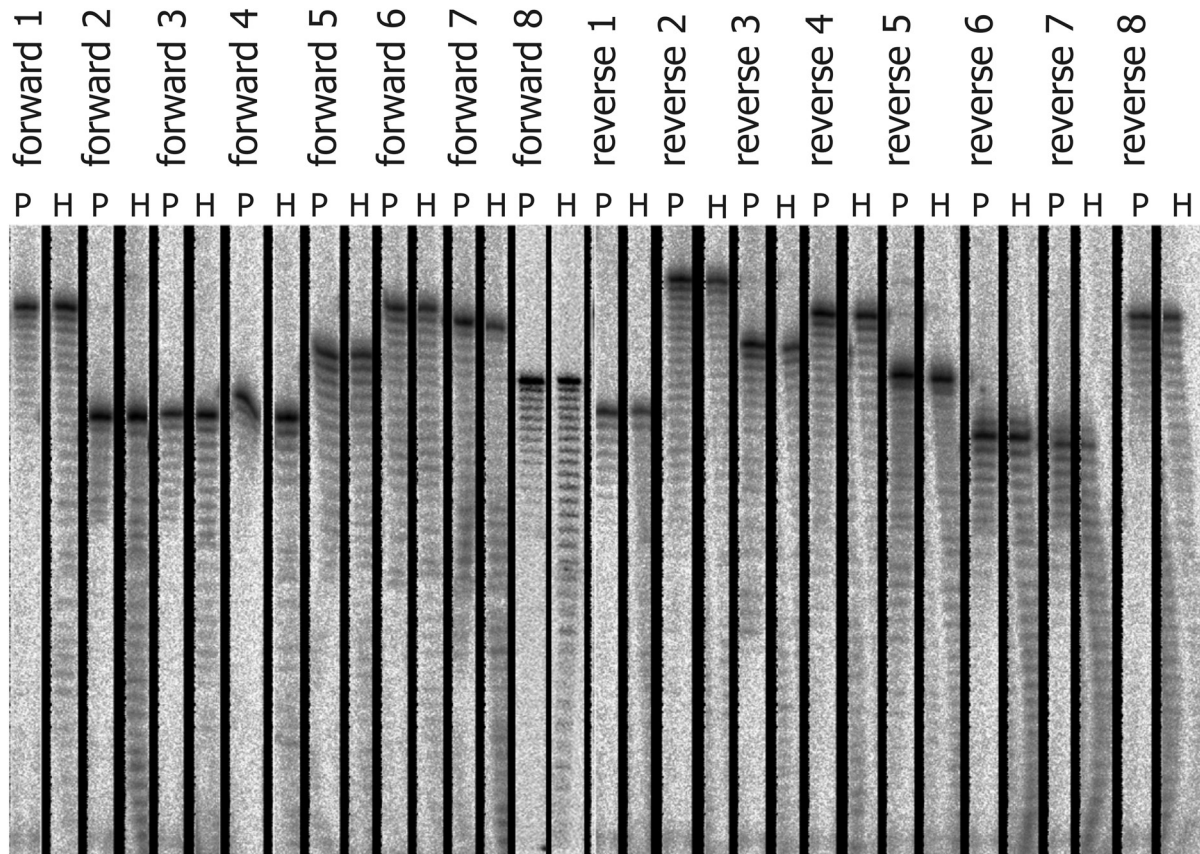


Figure 32. Autoradiographic analysis of oligonucleotides used for the gene synthesis of AsglypMA. Oligos were radioactively labelled with γ - ^{32}P by phosphorylation with T4 polynucleotidekinase using $[\gamma$ - ^{32}P]ATP. They were separated according to their size by electrophoresis on a denaturing polyacrylamide gel ($20 \times 40 \times 0.04$ mm). *forward1*, *forward2* etc.: Name of the oligonucleotide also indicating its position in the final gene (cf. section 7.5.3, Figure 31); Oligos that were ordered from the manufacturer with RP-HPLC purification are marked with an *H*. Oligos ordered with PAGE-purification are marked with a *P*.

7.1.1.4 Correlation of Errors with Oligo Purity

It was attempted to correlate the purity of the oligos to the occurrence of mutations seen in gene synthesis. Figure 32A to Figure 32D shows the number of deletion and insertion errors that occurred for each method in the 16 fragments of the gene, Figure 32E shows the cumulative errors that occurred for all methods of synthesis and the different oligo purities. Said fragments correspond to the respective overlapping sequences between sense and antisense oligo, which could both be the source of the observed error. In Figure 32F, the relative impurity for the *cleaner* of the opposing oligos is plotted versus the position in the gene. The values represent the percentage of byproducts from $n+1$ to $n-4$, normalized to the value of the most impure oligo. There is a clear correlation between purity and the number of errors observed, which is most striking when comparing the purity to the overall error rate

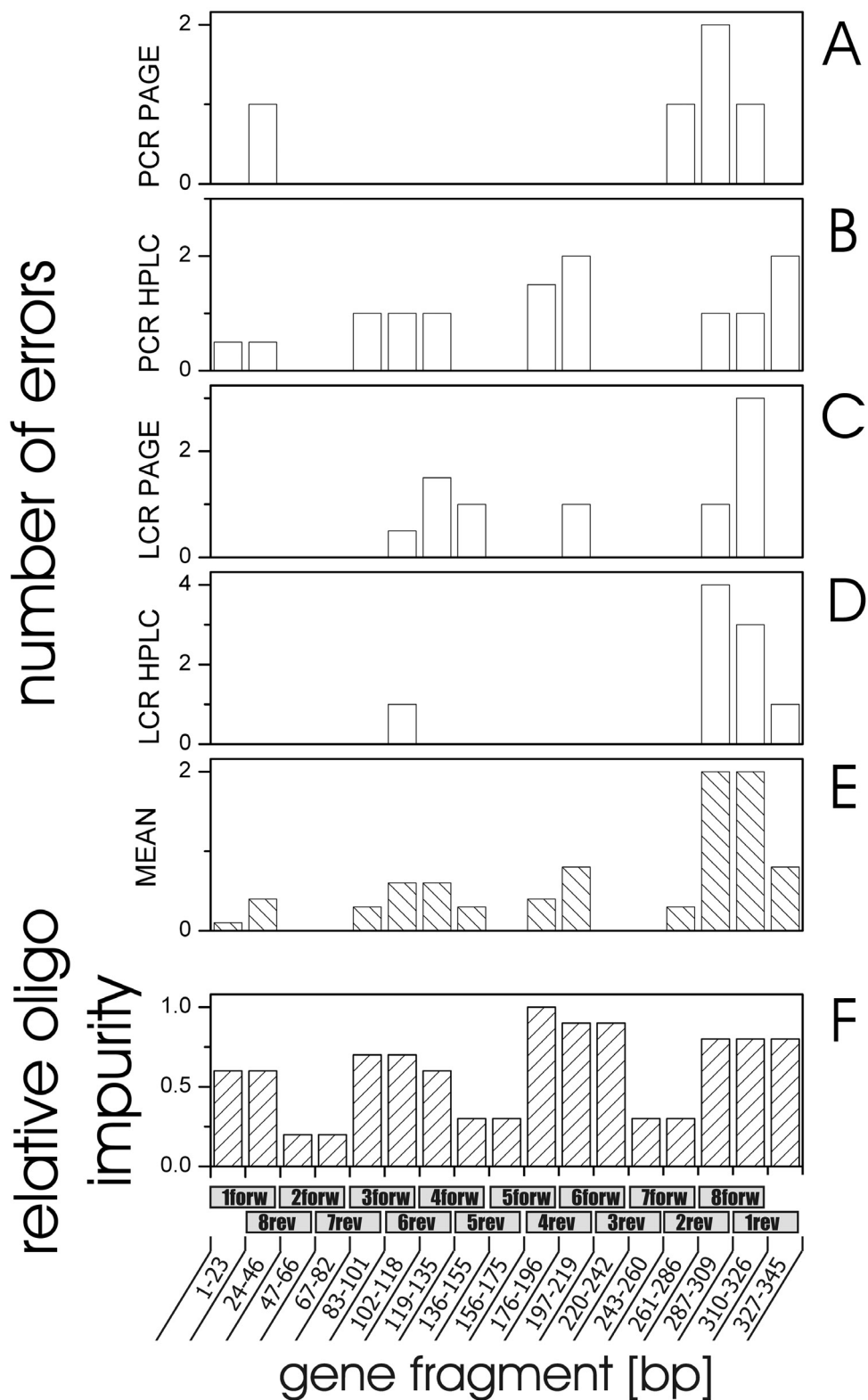


Figure 33. Location of deletion errors encountered in gene synthesis assigned to fragments corresponding to the respective overlapping sequences of oligonucleotides. In the cases where an error could not be unambiguously assigned to one of the fragments an error of 0.5 was assigned to the two involved oligos. The relative impurity corresponds to the percentage of impurities including n+1 and n-1 to n-4 by-products of oligo synthesis. For each fragment, the impurity of the purer oligo is depicted. The impurity data is normalized to the relative impurity of the oligo *4rev*.

($R^2 = 0.25$) and the error rate observed for PCR gene synthesis with HPLC purified oligos. From the data, it could be estimated that a purity >95% regarding the oligos down to n-4 products is necessary to get error free products.

There is no correlation to the average impurity of the opposing oligos ($R^2 = 0.04$, data not shown) or to the impurity of the less clean oligo ($R^2 = 0.00$; data not shown). There is also no correlation between the positional error rate and the overall impurity taking into account products with length <n-4. Also, no influence of the GC-content or individual length of the oligos could be discerned (data not shown).

7.1.1.5 Discussion

The overall error rate in PCR based gene synthesis decreased from 5.1/kb for HPLC-purified oligos to 2.5/kB for PAGE-purified oligos. For the combined LCR/PCR method, no significant dependence on oligo purification was observed, and the error rate was about 3.5/kB. Mismatch errors on average occurred at 0.6/kB, with no statistically relevant difference between the different methods. The predominant mutations were deletions (and one 1bp insertion) of up to 4 bp in PCR and of up to 7 bp in LCR based gene synthesis. The high occurrence of deletion errors was also observed in the synthesis of *ArtPlasMA* (cf. section 4.2.2). The observed deletion rate is high compared to literature values, but the mismatch mutation rate lies in the lower range of literature values. By electrophoresis and autoradiography of [γ - 32 P]ATP-phosphorylated oligos their purity was assessed with regard to the overall length, and it was found that both PAGE and RP-HPLC purified oligos contained a large number of n-x products, and that the purity of PAGE and RP-HPLC purified oligos differed only in the amount of n-x products that were smaller than n-4. The occurrence of deletion errors in the 16 fragments of the gene was correlated to oligo purity, and it was found that there was a significant correlation of the purity of the cleaner oligo with the error rate.

The following questions need to be discussed: i) can the observed errors in gene synthesis be explained either by polymerase errors, mispriming of fully matched oligonucleotides, or correct priming of mismatched oligos? ii) How could faulty oligonucleotides be incorporated in the products of gene syntheses? iii) Which amount and nature of impurities are to be expected for synthetically obtained oligonucleotides? iv) Why does PCR-based gene synthesis depend on oligo purity, but not the LCR-based method? v) Why is there a correlation of errors with the minimal primer purity, but not the medium purity of both primers or the purity of the oligo that was less clean? (vi) What are the consequences of the findings of this work? The following sections deal with these questions.

(i) Since the gene synthesis product obtained by LCR needs to be amplified by PCR, both LCR and PCR mediated gene synthesis errors could arise from mutations generated via PCR. The errors introduced during PCR are, however, mainly base changes,¹⁴² and in this respect the fidelity of Pfu has been reported to be 6.5×10^{-7} errors per base per doubling,¹⁴³ or according to a different report $1.3 - 5 \times 10^{-6}$,¹⁴⁴ depending on Mg^{2+} concentration. If, under non-optimal conditions, a minimal fidelity of Pfu of 1×10^{-5} errors/bp \times doubling is assumed, mismatch mutations at a calculated rate of 0.2/kb (20 doublings) or 0.3/kB (30 doublings) could be expected. This is close to the experimentally observed mismatch rate, but can not account for all mismatch mutations observed. There is also no significant correlation of the mismatch mutations observed (CG \rightarrow GC, TA \rightarrow GC, TA \rightarrow AT, CG \rightarrow TA) with published mutation “hotspots” reported for Pfu (GC \rightarrow TA, AT \rightarrow TA, AT \rightarrow CG, AT \rightarrow CG).¹⁴³ Deletions are in general rarely observed in PCR products, but could occur by *replication slippage* on homopolymeric runs¹⁴³ or when two direct sequence repeats are linked by a stable secondary structure.¹⁴⁵ The product of such a PCR induced mutation would be a shortening of the homopolymeric run or a sequence missing one of the direct repeats and the stable secondary structure, respectively. However, none of these possible errors can be observed for the synthesis of *AsglypMA*.

Mispriming could lead to deletions in cases where there are more ways than one in which template and primer can hybridize stably, as was observed in the synthesis of *ArtPlasMA* (cf. section 4.2.2.). No error in *AsglypMA* synthesis can be traced back to this origin, however.

The observed mutations must therefore originate from faulty oligonucleotides, an assumption that is also supported by the correlation between oligo purity and observed positional error rate. The possibility that both primers contain the same deletion, especially deletions that are larger than 1 bp, is rather small, however. Let us therefore turn to the ability of both Ligases and Polymerases to tolerate mismatches between primer and template.

(ii) The ability of polymerases to ignore mismatches is the basis for in-vitro site-directed mutagenesis via PCR methods. In protocols describing this method, usually matching sequences of 10 bases around a 3 bp sequence that is to be deleted are sufficient to allow for PCR to proceed efficiently.¹⁴⁶ Mutations in the eight nucleotides closest to the 3' end have been reported to affect the efficiency of the primer,¹⁴⁷ but they can be incorporated into the

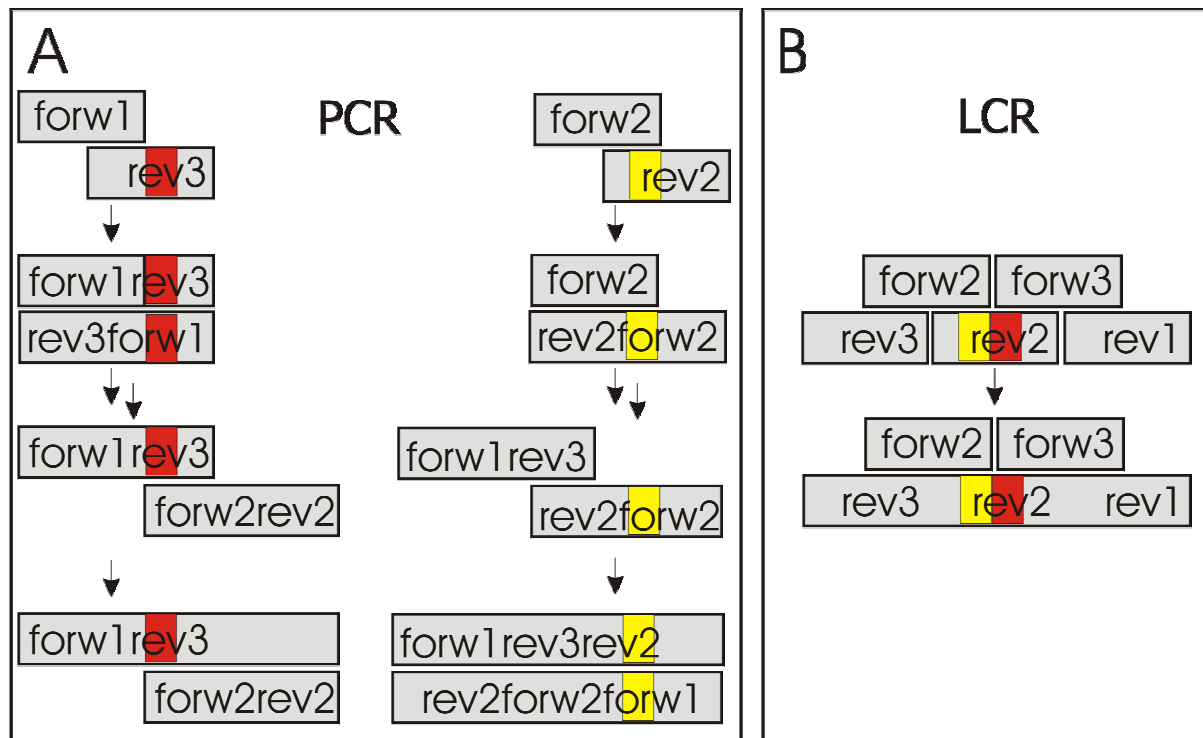


Figure 34. Schematic view of the integration of faulty oligonucleotides into the final product of gene synthesis. (A) PCR. The region that contains the mutation is shown in red or yellow. The forward oligonucleotides are termed forw1, forw2 etc., the reverse primers are named rev1, rev2 etc. Intermediate products of PCR are named by the contributing oligos, e.g. the products of forw1 and rev3 are forw1rev3 and rev3forw1. (B) LCR.

PCR product. Some polymerases, e.g. *Tth*, will even accept a mismatch at the 3' end of the primer.¹⁴⁸

Ligases also are fairly tolerant towards non-fully complementary oligos *in vitro*. At positions more than 9 bp away from the point of ligation, *Tth* Ligase does no longer discriminate between correctly and incorrectly paired bases.^{149,150} Other Ligases only “see” 6 bp of the ligated strand.¹⁵¹ Oligonucleotides with mismatched bases that are closer than 9 bp to the point of ligation can still be incorporated with efficiencies of up to 10 % compared to a perfectly matched oligo.^{149,150} Even mismatches directly adjacent to the nick (i.e. the open link between adjacent oligos), especially at the 5' phosphate donor terminus, can be ligated.¹⁵²

Incorporation of faulty oligonucleotides into a synthesized gene is therefore easily possible for both LCR and PCR based methods. It is feasible even with large mismatches or deletions, when the error is situated at a sufficient distance from the 5' and 3' primer ends, as is depicted in Figure 34A and B. This means that in principle, every observed error can be explained by an insertion of a faulty oligonucleotide.

Together with the fact that errors are correlated to oligo purity, this work provides good evidence that oligonucleotides are the source of the errors. The observation that keeping the number of PCR cycles down is beneficial for product purity is probably a kinetic effect due to competition: Mismatched oligos have a disadvantage due to their suboptimal hybridizing properties. In principle, the full length product of a gene made up of 16 oligos could be produced after 4 (16/4) PCR cycles. With an increasing number of cycles, the chance increases that one of the products containing a faulty oligo reaches full length.

(iii) Phosphodiester oligonucleotides are almost exclusively synthesized by the phosphoramidite method.^{96,153} Nucleoside monomers are typically attached to the growing chain one at a time in a repeated series of phosphoramidite coupling, oxidation or oxidative sulfurization, acyl capping and acidic detritylation reactions. The stepwise yield for each nucleoside addition is 98.6% to 99%, depending on the internucleotide linkage type. Nucleotide deletion occurs due to failure to couple and subsequent failure to cap or to failure to detritylate or to remain detritylated. The resulting crude oligo mixture contains all possible deletion sequences and also capped sequences. The purity of the final product therefore depends on additional purification steps, of which cartridge methods, RP-HPLC and PAGE are the most common.¹⁵⁴ To check whether the major product of oligo synthesis corresponds to the desired product, the most suitable method is mass spectrometry.¹⁵⁴ Deletion and insertion products can be quantified by autoradiographic PAGE. It is difficult to quantify the amount of oligo byproducts containing mismatched bases. HPLC is the preferred quality proof of oligo manufacturers and HPLC traces are sometimes supplied with the oligo. According to the experience of the author, this quality control is not suitable, however.

In the literature it has been reported that deletion mutants (up to 4bp) can be present in PAGE purified oligos, and reported values were 9/kB¹⁵⁵ (for ~100mers) and 3/kB¹⁵⁶ (for ~80mers). Applied to a 40mer these values correspond to 64% or 88% purity, respectively. It is interesting to note that in the first study, primarily deletion mutants were found, while in the second study mismatch mutations were prevalent. Two reports dealing with the nature of the n-1 impurities have been published, and they have come to different results: A method employing cloning the purified n-1 products and amplifying them in transformed bacteria came to the conclusion that there was a strong bias of deletions occurring closer to the 3'-end where chemical synthesis starts.¹⁵⁷ A different method relying on hybridization of the ³⁵S-labeled n-1 fraction of an oligo synthesis to complementary, immobilized oligonucleotides on a DNA array came to the conclusion that the occurrence of deletions was uniform throughout

the sequence.¹⁵⁸ This indicates that not only the prevalence of either mismatch or deletion errors is variable, but that there is also no clear trend as to where deletions are primarily located.

The oligo supplying company Thermo-Hyaid, which synthesized the oligos used in this study, claims that the purity of their 30mer oligos is in the range of 80 to 90 % for RP-HPLC purified oligos and >90 -98 % for PAGE purified oligos.¹⁵⁹ The oligos that were delivered (34 to 49mers) must therefore be considered to spectacularly fail the company's own specifications, with an average overall purity regarding deletions of 66% (83% n+1 to n-4) for RP-HPLC purified oligos and 76% (86% n+1 to n-4) for PAGE purified oligos.

(iv) Although RP-HPLC and PAGE purified oligos have been shown to be of equal purity regarding the products down to n-4, there is a clear decrease in error rate for PCR based gene synthesis when PAGE purified oligos are used, while this is not the case in combined LCR/PCR gene synthesis. This might be assigned to the fact that in PCR, also smaller fragments can still be incorporated into the full length product provided they can anneal properly. In this case, an oligo that was not "counted" as an impurity might still contribute to errors in the final product.

(v) There is a clear correlation between the purity of the cleaner of the opposing oligos and the observed error rate, i.e. when one of the oligos is relatively pure, the chance that the final product contains a mutation in this region is significantly decreased. Such a behavior would normally indicate that errors can only occur if both oligos contain the same mutation. This, however, is very improbable. Also in this case, the origin of the correlation must be sought in kinetic effects due to competition between perfectly annealing and mutated oligos. If oligos that are mutated would be incorporated into the final product with equal efficiency as correct oligos, one would expect an error rate of $0.15 \times 16 \times 2/345 \text{ bp} = 13.9/\text{kB}$ (with oligos of 85% purity regarding deletion byproducts down to n-4). If it is assumed that oligos containing a mutation close to the 3' or 5' end are not incorporated, this error rate is approximately halved to 7.0/kB. This value is still significantly higher than the observed ones, indicating that mutated oligos are discriminated against in the gene synthesis process.

(vi) As the error analysis of the gene synthesis of *AsglypMA* and oligo synthesis itself indicates, the mutations are usually randomly distributed. This has important consequences, since in this case the probability to obtain an error-free clone follows a binomial distribution (cf. Materials and Methods). Table 5 shows the number of clones that need to be sequenced to obtain a correct clone with appreciable probability (>70%) in dependence on error rate and length of the gene. There is a steep dependence of this probability on the length: while e.g. for

an error rate of 3/kB and a length of 520 bp only 5 clones need to be sequenced, this number increases to 24 at a length of 1000 bp. By first obtaining two correct clones of the smaller fragments and subsequently assembling these, the number of clones to be sequenced can therefore be more than halved in this case.

That the assumption of a random distribution is applicable in practice can be seen by evaluating the number of correct clones in dependence on length and error rate for the gene syntheses of *AsglypMA* (cf. Table 4). For this synthesis, the number of correct clones out of eight corresponds to the most probable number as computed by the binomial distribution, with the only exception of LCR with HPLC purified oligos, where 2 out of 8 correct clones would have been the highest probability and zero out of 8 was the experimental value.

Number of sequenced clones necessary to obtain one correct clone with a probability >70%	2 errors/kB	3 errors/kB	5 errors/kB
270 bp	2	2	4
520 bp	3	5	16
1000 bp	9	24	180

Table 5. Gene synthesis and statistical error probability in dependence of overall error rate and gene length. The table depicts the number of sequenced clones necessary to obtain one correct clone with a probability >70% as computed by a binomial distribution.

7.1.1.6 Conclusion

In this work, evidence is provided that the most significant source of mutations in gene synthesis is faulty oligonucleotides. PCR and combined LCR/PCR based gene synthesis lead to errors that are approximately in the same range, but LCR seems to be less sensitive to byproducts in oligonucleotide synthesis that are <n-4. Considerations regarding the mechanism of PCR and LCR strongly indicate that polymerase errors or misligation very probably contribute only little to mutations, and mispriming can be avoided by carefully designing the oligos. Optimizing reaction conditions with regard to annealing temperature and number of cycles might reduce the number of errors, but will probably not help if oligos are impure. To reliably obtain an error-free gene, oligonucleotides of the highest purity must be used. Since the number of mutations in a given segment of the gene was correlated only to the

relative purity of the cleaner oligo, it is possibly sufficient that only one of the two strands is made up of high-purity oligos. From the data of this work, it was estimated that a purity >95% regarding the oligos down to n-4 products is necessary to get error free products. A feasible strategy for gene synthesis that does not necessitate proof of oligo purity by PAGE or mass spectrometry is described in the following, and it is also applicable to non-purified oligos, albeit at the cost of a little extra work:

- (i) Design gene and oligos with regard to codon bias and avoidance of excessive single base or sequence repeats. Include unique restriction sites at equal distances of about 500 bp to allow building up the gene from its fragments (see below). Taking into account equal melting temperature of the overlaps might be beneficial, but the necessity of this approach has not been proven so far.
- (ii) Make a test gene synthesis of the full-length gene by PCR. Cloning of the product by TA-cloning is beneficial since the presence of the correct restriction sites in the gene synthesis product is not necessary. Pick and sequence three colonies.
- (iii) Check for errors that could originate from mispriming or polymerase slippage. If these are present, try to obtain the gene by LCR or redesign oligos. Check for errors that occur in the same position or region for all colonies. Have these oligos resynthesized or purified. Calculate error rate and, with regard to a binomial distribution, determine the optimal length of gene fragments that ensures that an error free product can be obtained with the minimal number of colonies to pick and sequence.
- (iv) Synthesize and clone fragments. Use restriction sites to obtain error-free fragments and synthesize the full length gene by PCR or by ligation.

One caveat in this strategy is that for the outermost primers, a higher possibility of incorporation of errors into the final product is probable since these do not have to “grow” in two directions. This could be circumvented by using highly purified oligos for the outermost positions, or, more easily, by positioning restriction sites needed for subcloning at a sensible distance away from 3' and 5' end, respectively.

7.1.1.7 Outlook

The performance of gene synthesis could be enhanced by removing erroneous sequences before cloning. This could in principle be done by electrophoresis, since heteroduplexes (obtained by melting and reannealing of purified PCR or LCR product) show a different

behavior than homoduplexes.¹⁶⁰ It is also feasible to use enzymes like Endonuclease VII,¹⁶¹ T7 endonuclease I¹⁶⁰ or other structure specific endonucleases^{162,163} that recognize and cut heteroduplex DNA at the site of mismatch. Both approaches, however, lead to an increase in hands-on time and cost.

7.1.1.8 Materials and Methods

Design. The 345 bp gene corresponding to *AsglypMA* was subdivided into 16 fragments of approximately equal melting temperature, with all containing a G or C residue at the 3'-terminus. This was done with the software *gene hackman*, which was written in cooperation with Christian Figger. Melting temperatures (T_M) were computed with free base pairing energies determined by SantaLucia et al.¹⁴⁰ With the sequence and a desired range of T_M as input, the program cut the gene into fragments of approximately equal melting temperature. As an additional parameter, each second fragment was made to contain a G or C residue at both 5' and 3' end, if the T_M window was large enough to allow for it. From the fragments, the respective forward and reverse primers were assembled. Due to each second fragment containing G' or C' ends, this strategy leads to all forward and reverse oligos containing a G' or C' at the 3'-terminus ("3'-C/G-clamp"). Since the base pairing energy of G and C is higher than for A and T, it is generally believed that primers with a G/C-clamp perform better in PCR or sequencing.¹⁶⁴ Therefore this feature was included although experimental data seems to contradict this belief.¹⁶⁴ The T_M 's of the obtained fragments were compared to those calculated with the software *OMIGA* (Accelrys, Cambridge, England), which uses free base pairing energies of Breslauer et al.¹⁴¹ Fragment lengths were adjusted to obtain a relatively small T_M window of 57°C to 66°C for both sets of parameters. Two fragments each corresponded to one oligonucleotide. All Forward and Reverse primers together covered the whole length of the sense and antisense strand except for the first and last fragment of the gene, which was built up only by the Forward1 and the Reverse1 primers, respectively.

Gene Synthesis of *AsglypMA* by PCR. The gene was obtained by two PCR steps from 16 primers of varying length (cf. 7.5.3), being either HPLC or PAGE-purified, with a Robocycler Gradient 40 (Stratagene). To guarantee equal reaction conditions, the experiment was performed synchronously with both sets of primers. In the first step, the gene was assembled in the buffer supplied for the polymerase containing 0.02 μ M of each primer, 1 mM Mg^{2+} , 0.2 mM of each dNTP, and 50U/ml Pfu Polymerase. The PCR program consisted of 2 min initial denaturation and 25 cycles of 30 sec denaturation at 94°C, 30 sec annealing at 51°C and 120 sec elongation at 72°C. To amplify the full size product in a second round of PCR, the product was diluted 1:10 in Pfu Polymerase buffer containing 0.2 μ M of the outermost primers, 50 U/ml Pfu Polymerase, 0.2 mM of each dNTP and 1 mM Mg^{2+} . PCR parameters were 2 min initial denaturation, 15 cycles of 45°sec at 94°C, 45 sec at 51°C and 5 min at 72°C with a final elongation step of 10 min at 72°C. The final PCR product was purified by agarose gel electrophoresis and gel elution with the Qiaquick Spin Columns kit. Before cloning into the vector pCR2.1 using the Topo-TA cloning kit., adenosine residues were added using TAQ polymerase at 72°C (20-30 ng/ μ l PCR product, 0.8mM dNTPs, 6mM Mg^{2+} , 33 U/ml TAQ polymerase in TAQ buffer; reaction time 10 min). Positive colonies were identified by blue-white selection¹¹⁸ and PCR screening with primers Forw2 and Rev2 (cf. 7.5.2). Eight clones each for HPLC respectively PAGE-purified primers with the approximately correct size were sequenced.

Gene Synthesis of AsglypMA by LCR. The following protocol was performed synchronously with HPLC-purified and PAGE-purified primers. In the first step, all primers except for Forw1 and Rev1 were phosphorylated (13 μ M of each primer, 1.4 U/ μ l T4 polynucleotidkinase (Fermentas), 3.6 mM rATP, BSA, buffer supplied by the manufacturer). The mixture was incubated for 2 h at 37°C and inactivated for 10 min at 75°C. Ligation of all primers including Forw1 and Rev1 was performed in a thermocycler, with primer concentration being 6.5 μ M each, 0.2 U/ μ l thermostable Pfu DNA Ligase (Stratagene) and the buffer supplied by the manufacturer. Cycling parameters were 60°sec initial denaturation at 95°C, 40 cycles of 30 sec at 95°C, 90 sec at 50°C, 90 sec at 70°C and a final step of 120 sec at 72°C. The intermediate product was gel purified (Qiaquick) to remove nonligated primers. To amplify the full length product, the gel purified LCR product was diluted 1:50 into buffer containing 0.2 μ M of the outermost primers, 1 mM MgCl₂, 0.2 mM of each dNTP and 0.1U/ μ l Pfu native Polymerase. Cycling parameters were 2 min initial denaturation at 94°C, 25 cycles of 45 sec at 94°C, 45 sec at 55°C and 5 min at 72°C, with a final elongation step of 10 min at 72°C. Purification, addition of A-residues and cloning was performed as described in the preceding paragraph.

Assessment of oligo purity. One microliter of 10 μ M oligonucleotide containing solution was added to 9 μ l of a solution containing 100 μ M Tris-HCl, 10 mM MgCl₂, 5 mM DTT, 10 μ M ATP, 100 nCi/ μ l [γ -³²P]ATP and 0.1 units of T4 polynucleotidkinase. The mixture was incubated for 15 min at 37°C, supplemented with 10 μ l of formamide and applied onto a 12% acrylamide gel (20x40x0.04 mm) containing 8 M urea and TBE buffer. Electrophoresis was performed at 2000 V for 2 hours (bromophenol blue migrated about 30 cm) and exposed to a BAS-IIISphosphoimager plate (Fuji Photo Film Co., Tokyo, Japan) for 15 min. The phosphoimager plate was evaluated with a Bas2000 scanner and the intensities of the bands were quantified with ImageGauge 3.3 software (both Fuji Photo Film Co.).

Statistics. If the error rate of a given gene synthesis is , say, 3/kB, then the probability that a gene of x bp length contains no error is $p = 0.997^x$, and the probability that it contains an error is $p = 1 - 0.997^x$. If one sequences n clones, then the probability that k correct clones are obtained is given by the binomial distribution:

$$W_p^n(k) = \binom{n}{k} p^k (1-p)^{n-k} \quad ; \quad \binom{n}{k} = \frac{n!}{k!(n-k)!}$$

For example, at an error rate of 3/kB and a length of the gene of 1000 bp, the probability that out of ten clones all contain at least one error ($k = 0$) is 60.1%. The probability to obtain an error free clone is therefore 39.9%. In order to have a 70% chance of obtaining an error free clone, one would have to sequence 24 clones. This, of course, applies only if the errors are statistically distributed. To test this, one can calculate the probability to obtain k correct clones at a given error rate when n clones are sequenced ($k=0, 1, 2, n$) (cf. section 7.1.1.5.). For example, at an error rate of 2.5/kB as it was observed with PCR based gene synthesis and HPLC purified oligos, the most probable number of correct clones out of 8 clones sequenced is 3, in accordance with the experimental result.

7.1.2 Comparison of an Artificial and a Natural Targeting Signal

When the work on this thesis was started, it was not clear whether the strategy of using a poly-Leucine membrane targeting signal would be successful in making a plasma-membrane transport-competent and stably anchored PLAP fusion protein. For this reason, the construct *AsglypMA*, which is similar to *ArtPlasMA*, but which contains a naturally occurring targeting signal, was also designed and synthesized.

As mentioned above, using a Phosphatase for enzyme induced staining is not ideal, since many cells including those in the nervous tissue show ectopic phosphatase activity. One of the aims of making *ArtPlasMA* was also to target an enzyme exhibiting hydrolytic activity that is normally not encountered in native mammalian tissue at the extracellular side of the plasma membrane. The ideal candidate for this would be a β -Galactosidase, as will be explained below.

This section first describes the design of *AsglypMA* and provides background information about BIF3, a putatively extracellular bacterial β -Galactosidase. A fragment of BIF3 was used to make chimeras with *ArtPlasMA* and *AsglypMA*. Immunofluorescence experiments performed with these constructs as well as with a chimera of *AsglypMA* are presented in the following section. These experiments are by no means complete, but they are included in this work in order to make them available for future developments.

7.1.2.1 The Membrane Anchor Construct *AsglypMA* and the Fusion Protein *AsglypMA AP*

The Asialoglycoproteinreceptor is a type II cell-surface protein expressed by hepatocytes.⁸³ A construct similar to *ArtPlasMA* was made with the 22 Leucine targeting signal replaced by that of the Asialoglycoproteinreceptor (Figure 35). In addition, it contains a slightly modified multiple cloning site that contains two cleavage sites for the restriction enzyme *XcmI*. This design allows the use of the so-called TA-cloning technique, an efficient method for the cloning of PCR products.^{110,165} The *XcmI*-cleavage site has the further advantage that, due to its long recognition sequence, it is very unlikely to occur in natural DNA sequences. The construct was made by gene synthesis as described in section 7.1.1. It was then used to make a chimera with PLAP analogous to the procedure described in section 4.3.

immunofluorescence images are shown Figure 36B. As expected, the immunofluorescence staining is strong for both *anti-HA* and *anti-cmyc* antibodies, and it is distributed evenly throughout the cytoplasm. Under permeabilizing conditions, no drop-like structures are discernible. The pattern observed for *AsglypMA AP* therefore hints at a preferred localization at a membrane of the secretory pathway, presumably the ER membrane. The dissolution of the web-like structure under permeabilizing conditions very likely originates from the detergent action of Triton X-100. However, no similar phenomenon could be found in the literature, and more extensive experiments need to be performed to clarify this issue.

Although the immunofluorescence experiments did not show any protein to reside at the plasma membrane of HEK cells, a histochemical staining (cf. section 4.3.3) of overexpressed *AsglypMA AP* in HEK293 and MDCK cells showed that some of the protein is transported to the cell membrane in active form (Figure 36C). However, the staining develops much more slowly, i.e. the activity is much smaller than in the same experiment conducted with *ArtPlasMA AP* (cf. Figure 21). Although this is just a qualitative assay, it nevertheless together with the immunofluorescence images indicates that *AsglypMA* is inferior to *ArtPlasMA* in conferring the correct topology and plasma membrane transport competence in a chimera. The fact that no unique topology is created might result from the fact that the native Asialoglycoproteinreceptor-TM domain was modified by the addition of the HA and 6His-tags at the N-terminus. Since the strategy to introduce a row of positively charged amino acid residues (K₄; cf. 4.2.1) was not used here, this modification might be detrimental to the correct insertion of the TM domain in the ER membrane. The reason for decreased plasma membrane transport competence is unclear at the moment. Note, however, that this experiment clearly shows that immunofluorescence as performed in this study is not a perfectly suitable method to assay whether a fraction of overexpressed protein is transported to the cell surface.

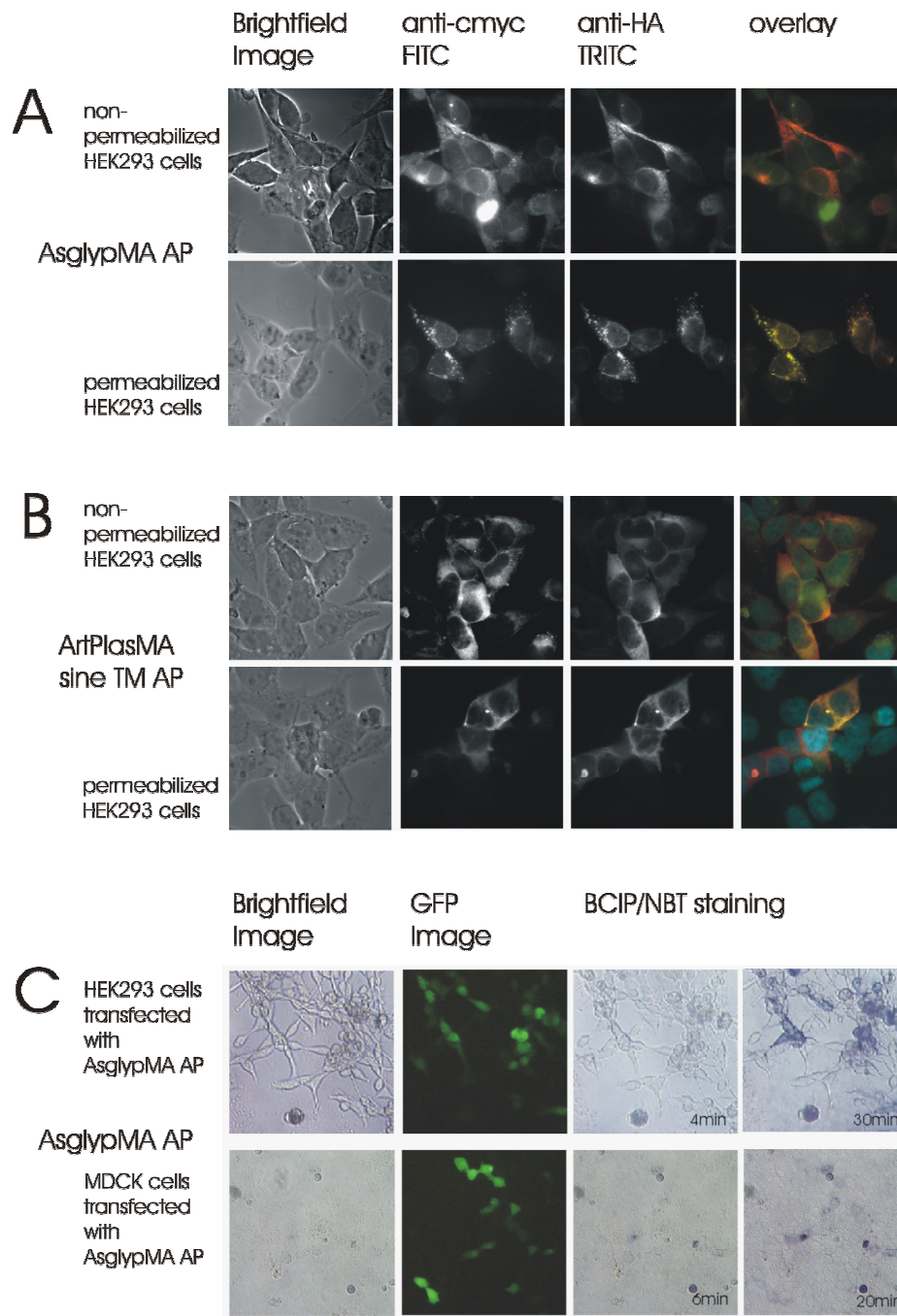


Figure 36. Localization and functional detection of *AsglypMA* AP and *ArtPlasMA* sine TM AP. (A) Immunofluorescence of HEK293 cells stably transfected with *AsglypMA* AP. Immunofluorescence images of formaldehyde-fixed HEK293 cells incubated with fluorescently labeled antibodies *anti-cmyc* and *anti-HA*. Cell nucleus counterstaining was achieved with the dye *Hoechst 33258*. Experiments were performed with (second row) and without (first row) Triton X-100 treatment. Fluorescence images were digitally edited by normalization to the maximum intensity and subtraction of background fluorescence. (B) Analogous to (A), but with the construct *ArtPlasMA* sineTM AP. (C) Histochemical staining of HEK293 and MDCK cells transiently transfected with *AsglypMA* AP. Cells were incubated with the chromogenic phosphatase detection reagents BCIP and NBT (columns 1,3,4). GFP was used as a transfection marker (fluorescence image column 2).

7.1.2.2 BIF3, an Extracellular β -Galactosidase in Bacteria

The target of β -Galactosidase is a half acetale of the highly polar sugar β -Galactose and an alcohol residue. β -Galactosidase contains five polar alcohol moieties as a half acetale. When attached to voltage sensitive dyes, it should therefore be able to increase their solubility and decrease their membrane binding strength to a similar extent as phosphates. Since β -Galactosidases are not expressed ectopically in mammalian tissue, galactose-modified voltage sensitive dyes should be ideal candidates as precursors for enzyme induced staining. The problem that needs to be overcome is to make a mammalian cell express a β -Galactosidase at its cell surface. The widely used reporter protein bacterial lacZ β -Galactosidase can however not be expressed as an active ectopic (respectively periplasmic) enzyme due to incorrect folding.^{124,166} An extensive literature research did not reveal any cloned secreted or ectopic mammalian β -Galactosidase. Secreted β -Galactosidases from fungi exhibit an acidic pH-optimum (see e.g. ref.¹⁶⁷) which is inappropriate for staining of live cells. Also in bacteria, no secreted or periplasmic β -Galactosidase has so far been unambiguously identified. However, it has been reported that *Bifidobacterium bifidum* expresses a putatively extracellular enzyme termed *BIF3* and its DNA has been cloned (GeneBank Acc.# AJ224435).^{168,169} The DNA was obtained from Peter Stougaard as a generous gift.

The coding sequence of BIF3 is rather large (5256 bp) and therefore difficult to clone. In addition, also smaller fragments of the gene have been found to exhibit enzymatic activity when overexpressed in bacteria.¹⁶⁹ Consequently, it was attempted to make a chimera of a smaller fragment of BIF3 with *ArtPlasMA* and *AsglypMA*. This fragment corresponds to a region of high homology to other known β -Galactosidases as found by a BLAST search,¹⁷⁰ namely bases 96 to 1787 of the coding sequence. The first 96 bases encode the putative signal sequence of the protein and were therefore truncated.

The resulting constructs termed *ArtPlasMA bGal/small* and *AsglypMA bGal/small* were overexpressed in HEK293 cells and examined by immunofluorescence methods. Figure 37 shows immunofluorescence images of the fusion proteins.

The appearance is quite similar to the immunofluorescence images of *AsglypMA AP*, indicating an accumulation of the constructs in the ER. For *ArtPlasMA bGal/small* under non-permeabilizing conditions, no signal for *anti-cmyc* exceeding background fluorescence could be detected, indicating an efficient insertion into the ER as a *type II* transmembrane protein. For *AsglypMA bGal/small*, a strong signal against *anti-cmyc* was found both under permeabilizing and non-permeabilizing conditions, indicating, as it was found with *AsglypMA*

AP, that *type II* insertion was not exclusive. Note that expression of the nonpermeabilized *AsglypMA bGal/small* is very strong, reflecting the fact that a stable clone was used for immunofluorescence in this case.

It is still possible that some of the constructs are transported to the plasma membrane as the experiments with *AsglypMA AP* have shown. Further experiments that might prove cell surface expression have so far not been conducted.

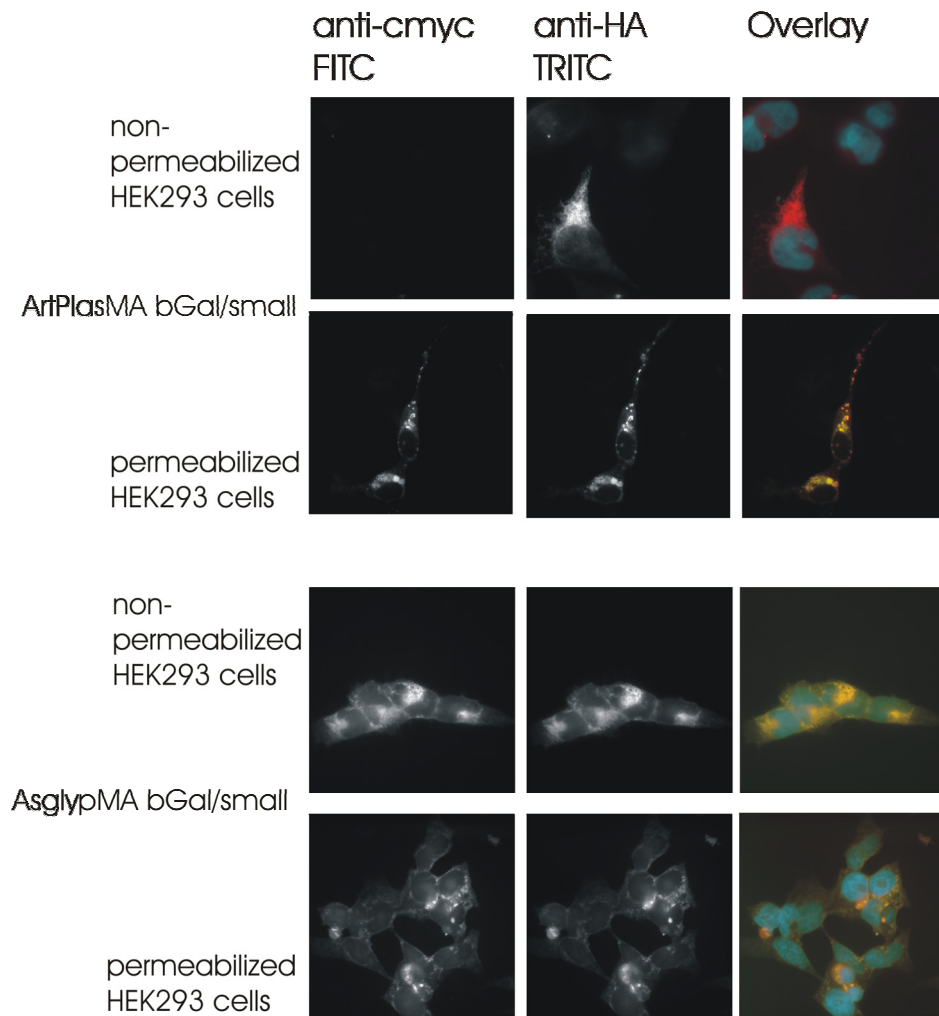


Figure 37. Localization of *ArtPlasMA bGal/small* and *AsglypMA bGal/small* by immunofluorescence of transiently transfected HEK293 cells. Immunofluorescence images of formaldehyde-fixed HEK293 cells incubated with fluorescently labeled antibodies *anti-cmyc* and *anti-HA*. Cell nucleus counterstaining was achieved with the dye *Hoechst 33258*. Experiments were performed with (second row) and without (first row) Triton X-100 treatment. Fluorescence images were digitally edited by normalization to the maximum intensity and subtraction of background fluorescence.

7.1.2.3 Materials and Methods.

Cloning of pcDNA3 AsglypMA AP and pcDNA3 ArtPlasMA sineTM AP, Cell culture, Immunofluorescence and Histochemical detection was performed exactly analogous to the procedure for pcDNA3 ArtPlasMA AP described in section 4.5.

Gene synthesis of ArtPlasMA sine TM. The gene was obtained by two PCR steps from 10 primers of 40 bp length (cf. sections 4.5, 7.5.2) with a Robocycler Gradient 40 (Stratagene). In the first step, the gene was assembled in the buffer supplied for the polymerase containing 0.2 μ M of each Primer, 1.2mM Mg^{2+} , 0.2 mM of each dNTP, and 50U/ml Pfu Polymerase, with an overall volume of 50 μ l. The PCR program consisted of 60 sec initial denaturation and 30 cycles of 30 sec denaturation at 94°C, 30 sec annealing at 52°C and 120 sec elongation at 73°C. To amplify the full size product in a second round of PCR, the product was diluted 1:10 in Pfu Polymerase buffer containing 1 μ M of the outermost primers, 50 U/ml Pfu Polymerase, 0.2 mM of each dNTP and 2.5 mM Mg^{2+} (overall volume 100 μ l). PCR parameters were 1 min initial denaturation, 25 cycles of 45°sec at 94°C, 45 sec at 68°C and 300 sec at 73°C with a final elongation step of 10 min at 73°C. The final PCR product was purified by agarose gel electrophoresis and gel elution with the Qiaquick Spin Columns kit. To facilitate cloning into the vector pCR2.1 using the Topo-TA cloning kit., adenosine residues were added using TAQ polymerase at 72°C (1mM dNTPs, 7mM Mg^{2+} , 30 U/ml TAQ polymerase in TAQ buffer; reaction time ten minutes). TA-cloning was performed according to supplier's instructions using Top Ten transformation competent bacterial strains (Invitrogen). Positive colonies were identified by blue-white selection¹¹⁸ and PCR screening with primers Forw2 and Rev1 (cf. 7.5.2) and sequenced. One clone with the correct sequence was subcloned into pcDNA3 using the restriction sites *HindIII* and *NotI*.

Cloning of ArtPlasMA/bGal small and AsglypMA/bGal small. The DNA of the bacterial Galactosidase *BIF3*^{168,169} (GeneBank Acc.# AJ224435) from *Bifidobacterium bifidum* was obtained from Peter Stougaard. A fragment of the N-terminal part of the gene corresponding to bases 33 to 599 was cloned was amplified with forward primer 5'-GTCGAGGACGCCACCCGATCCG-3' and reverse primer 5'-GGAATTGTCATAGCTGGTCAG-3 using standard procedures and Pfu Polymerase. The PCR product was gel purified (Qiaquick) and cloned into the EcoRV site of pcDNA3 ArtPlasMA and pcDNA3 AsglypMA via blunt cut ligation following the protocol described in section 4.5.

7.2 Expanded Background

7.2.1 Lipids and Vesicles

Lipids are the main structural component of the membranes of cells, which form microenvironments in the cell and in its compartments, like e.g. the nucleus, mitochondria, endoplasmic reticulum and so on. Recently, it has been found that they do not only serve as a passive barrier, but that they also actively take part in processes like cell signaling.⁵¹ To examine processes at cell membranes, a well-defined model system with manifold uses are lipid vesicles, which are spherical bilayers usually made of chemically synthesized lipids. This section shall provide an introduction to the area of lipids, lipid membranes and vesicles. Topics and literature cited deal with the kinds of lipids, the synthesis, characterization and stability of vesicles and some special topics like membrane permeability and charge.

Kinds of Lipids. The most abundant types of lipids in cell membranes are the neutral sphingomyelins, phosphatidylcholines and phosphatidylethanolamine as well as the negatively charged phosphatidylserines and phosphatidylinositols. Apart from their basic structure, different subtypes exist that contain fatty acid chains of varying length and degree of saturation. There is, for example, a general trend that phosphatidylserines have longer and more unsaturated fatty acid chains than phosphatidylcholines.⁵¹ There is great variation in the lipid composition of the membranes in a cell. In addition, each membrane is asymmetrical in that the inner and outer leaflet of the lipid double layer of plasma membrane and organelles are very different in their relative lipid content. For example, the negatively charged lipids reside almost exclusively on the cytoplasmic side of erythrocyte plasma membranes. Conclusively, the membranes of different organelles and even both leaflets of the same membrane are distinctly different in their physicochemical properties.

Lipid Vesicles. The main characteristics of lipid vesicles are their size, the number of double layers that make up the membrane (i.e. uni-, oligo- or multilamellar) and the kind or kinds of lipids used in their synthesis. With lyophilized, solid lipids as a starting material, Small (diameter < 100 nm⁷¹) and Large Vesicles can be made from suspensions in buffer by ultrasonication, „freeze and thaw“ methods, or extrusion. The latter method uses polymer filters with a defined pore size. In combination with freeze thawing, to eliminate smaller vesicles, this technique leads to small or large unilamellar vesicles (SUV/LUV) with a

defined, unimodal size distribution. The exact size depends on the kind of lipid used and the applied pressure, but it is close to the pore diameter of the filter.¹⁷¹ A different method employs solutions of lipids in organic solvents. The solvents are removed under reduced pressure and the resulting adsorbed layer of lipids forms vesicles when it gets in contact with aqueous buffer. This method can be applied to the formation of giant unilamellar vesicles (GUV, diameter 0.5 – 300 μm) when lipids are adsorbed on a conductive substrate and AC voltage is applied. Here, usually indium tin oxide (ITO)⁷⁹ or platinum electrodes (see e.g. ref.¹⁷²) are used.

The structure of lipid membranes can be probed by X-Ray and Neutron-Diffraction as well as by NMR. It is also an active area of research of computational simulations.¹⁷³ Parameters that are of interest in this respect are e.g. the area per lipid, the density and order parameters for lipid chains.

Depending on the kind of lipid, the double membrane has a characteristic transition temperature from a well ordered gel state (L_{β}) to the liquid crystalline state (L_{α}). Apart from the structure, these phases also differ in physicochemical properties like e.g. membrane permeability (see below). Vesicle synthesis and storage should be performed above the transition temperature of the respective lipid, which for example is $-2.5 \pm 2.4^{\circ}\text{C}$ for POPC.¹⁷⁴

Quality Control. The purity of lipids can best be assessed by two-dimensional thin layer chromatography.¹⁷⁵ The size of vesicles is commonly determined by quasi-elastic light scattering (QELS), which is based on the analysis of the intensity fluctuations of light scattered by particles in solution performing Brownian Motions. The information eventually extracted is the translational diffusion coefficient D and the corresponding Stokes-Einstein-Diameter of the particle.¹⁷¹ Freeze-fracture electron microscopy delivers in addition information about the number of lamellas that make up the vesicle membrane.¹⁷⁶ The lipid content, which is a crucial parameter if binding experiments need to be performed, can be determined by elementary analysis or specific enzymatic reactions. The analysis of POPC concentration, for example, can be performed by chemical liberation of inorganic phosphate and the subsequent quantization of its concentration. A number of inorganic determination methods are available, mostly based on the formation of a phosphomolybdate complex which is chemically reduced and can be quantized spectroscopically. The basic protocol was presented by Chen et al.¹⁷⁷, and further developments use additional reagents like malachite green¹⁷⁸⁻¹⁸⁰ or Triton X-100¹⁸¹ to increase sensitivity. Other methods make use of chromogenic coupled enzymatic reactions^{182,183}, some of which are available commercially as

a kit. The decisive advantage of the latter method is that no additional special equipment and no chemical liberation of inorganic phosphate are necessary. This would involve the use of the potentially dangerous perchloric acid.

Stability. Phospholipid vesicles are unstable against hydrolysis, oxidation and fusion or aggregation. While hydrolysis is independent of ionic strength and oxygen content, its strong pH-dependence is V-shaped with the minimum at pH 6.5.⁷⁷ High buffer concentrations also increase the rate of hydrolysis. The products of this reaction are free fatty acids, lysophospholipids and glycerophosphocompounds (see ref.¹⁸⁴ and refs. cited therein). These compounds have been reported to be fusogenic,⁷¹ and naturally, a high content of these compounds will change the physicochemical properties of the vesicles and might compromise e.g. binding data. The rate of lysolecithin formation in liquid form stored at 4°C can be as high as 5-20%/month.⁵³ Bivalent cations also induce fusion.¹⁷⁵ Liposomes which lack a net electrical charge tend to be less stable towards aggregation than charged liposomes.⁷⁷

Unsaturated lipids are sensitive to oxidation. This can be excluded by storage at low temperatures and protection from light and oxygen. For long term storage like e.g. in pharmaceutical applications, antioxidants and cholesterol are added to lipid vesicles.¹⁸⁵

The “freshness” of vesicles can be tested by ³¹P-NMR,¹⁸⁴ osmolarity⁷⁷ and turbidity measurements.

Membrane permeation. Various parameters influencing permeability have been reported: Permeability increases with vesicle size; small contaminations with some amphiphilic or hydrophobic molecules can increase the permeability by one or two orders of magnitude;⁵³ the addition of cholesterol to liposomes renders them more impermeable to water, electrolytes and non-ionic molecules.¹⁷⁵ It has been found that in general, leakage of drugs from gel state is slower than from liquid crystalline state. However, storage around the phase transition temperature enhances the permeability of gel state bilayers.⁷⁷

7.2.2 Human Alkaline Phosphatases

Alkaline Phosphatases are ubiquitary *ectopic* membrane enzymes, i.e. their active site faces the extracellular space. Currently, four specific subtypes are known in mammals. Since their nomenclature is quite confusing, the alternative names are given in brackets: 1. Germ-cell like (ALPPL, PPBN, Nagao Isozyme, GCAP), 2. Placental (PLAP, ALPP, PPB1, Regan Isozyme), 3. Intestinal (ALPI, PPBI, IAP) and 4. Tissue Non-Specific (APT NAP, TNSALP, PPBT, ALPL, NSAP).¹²¹ Some mammalian phosphatases require Mg²⁺ to achieve maximum

activity. Those from bovine kidney, brain and bone marrow are strongly activated by this metal, while the intestinal and placental enzymes are less influenced.¹⁸⁶ PLAP, the enzyme which is used in this thesis, is anchored to the membrane by a GPI-anchor, and it forms dimers in vivo and in this form shows allosteric control of hydrolysis when the enzyme is fully metalized.¹²¹ However, also the monomer is active in hydrolysis. The enzyme is inhibited e.g. by phosphate, pyrophosphate and arsenate,²² L-amino acids (L-Phe, L-Trp, L-Leu),¹²¹ okadaic acid¹⁸⁷ or Zn^{2+} .¹⁸⁶ Four different alleles of PLAP with slightly different kinetic behaviour have been found in humans.¹⁸⁸ Alkaline Phosphatases show maximum activity in vitro at a pH of about 9.8, and the enzyme has a wide range of substrate specificity.^{22,136,189,190} In fact, since APs show very little preference toward any specific substrate, the target for each human AP remains unknown so far.¹²¹ PLAP is one of the known markers of cancer cells where it is ectopically expressed, i.e. bound to the extracellular side of the cell wall.¹²¹ The structure of dimeric PLAP has been determined by crystallography.¹²¹

7.3 Tables

7.3.1 Human and Yeast Codon Usage

	H	Y		H	Y		H	Y		H	Y					
Ala	GCU	17	38	Cys	UGU	32	63	Leu	CUU	5	17	Ser	UCU	13	26	
	GCC	53	22		UGC	68	37		CUC	26	5		UCC	28	16	
	GCA	13	29	Gln	CAA	12	69		CUA	3	13		UCA	5	21	
	GCG	17	11		CAG	88	31		CUG	58	10		UCG	9	10	
Arg	CGU	7	14	Glu	GAA	25	71	UUA	2	28	AGU		10	16		
	CGC	37	6		GAG	75	29	UUG	6	28	AGC		34	11		
	CGA	6	7	Gly	GGU	12	48	Lys	AAA	18	58	Thr	ACU	14	35	
	CGG	21	4		GGA	14	21		AAG	82	42		ACC	57	20	
	AGA	10	48		GGA	14	21	Pro	CCU	19	31		ACA	14	31	
	AGG	18	21		GGG	24	12		CCC	48	15		ACG	15	14	
Asn	AAU	22	59	His	CAU	21	63	Tyr	UAU	26	56	Val	GUU	7	39	
	AAC	78	41		CAC	79	37		UAC	74	44		GUC	25	21	
Asp	GAU	25	63		Phe	UUU	20	60	Val	GUA	5		21	GUG	64	19
	GAC	75	37			UUC	80	40		GUG	64		19			

Data taken from ref.⁹⁵

7.3.2 Oligonucleotides used for the Synthesis of *ArtPlasMA*

The sequence is written from 5' to 3'.

```

1forw  GATTACAGGTACCGCCACCATGGGCCACCATCACCACCAT
2forw  CACTACCCCTACGACGTGCCCCGACTACGCCGGCGGCAAGA
3forw  AGAAGAAGCTGCTGCTCCTGCTCCTGCTGCTCCTCCTGCT
4forw  GCTCCTGCTCCTGCTGCTGCTGCTCCTGCTCCTCGTGCAG
5forw  CAACAGGACTACGACATCCCCACCACCGCCAGCCGCGGCC
6forw  AGGCCCGGGCGGATCCCGAATTCGATATCGAGCAGAAGCT
7forw  GATCAGCGAGGAGGACCTGTGATAATAGGCGGCCGCATTA

0rev   ACTCGACGTGAACCGTGGACTAATGCGGCCGCCTATTATC
1rev   ACAGGTCTCTCGCTGATCAGCTTCTGCTCGATATCGAA
2rev   TTCGGGATCCGCCCGGGCCTGGCCGCGGCTGGCTGTGGTG
3rev   GGGATGTCGTAGTCCTGTTGCTGCACGAGGAGCAGGAGCA

```

4rev GCAGCAGCAGGAGCAGGAGCAGCAGCAGGAGCAGCAGGAG
5rev CAGGAGCAGCAGCTTCTTCTTCTTGCCGCCGGCGTAGTCG
6rev GGCACGTCGTAGGGGTAGTGATGGTGGTGGTGGTGGCCCA

7.3.3 Oligonucleotides used for the Synthesis of *AsglypMA*

Forw 1 GATTACAAAGCTTGCCACCATGGGCCACCATCACCACCATCACTAC
Forw 2 CCTTACGACGTGCCCGACTACGCCGGCGGCAAGAGC
Forw 3 CTCCTGCAGCGTCTCTGCTCCGGACCTCGCCTCCTC
Forw 4 CTGCTCTCCCTGGGCCTCAGCCTCCTGCTGCTTGTGG
Forw 5 TTGTCTGTGTGATCGGATCCCAGAACTCCCAGCTGCAGGAG
Forw 6 GAGCTGCAACAGGACTACGACATCCCTGATATCCAAGCATCCCATG
Forw 7 GCGCCATGTCATGCGTGGCTTTCGATATGGAGCAGAAGCTGATC
Forw 8 AGCGAGGAGGACCTGTGATAAATAGGCGGCCGATTAGTCC

Rev 1 GGC ACTCGACGTGAACCGTGGACTAATGCGGCCGCC
Rev 2 TATTATCACAGGTCCTCCTCGCTGATCAGCTTCTGCTCCATATCGAAAG
Rev 3 CCACGCATGACATGGCGCCATGGGATGCTTGGATATCAGGG
Rev 4 ATGTCGTAGTCCTGTTGCAGCTCCTCCTGCAGCTGGGAGTTCTG
Rev 5 GGATCCGATCACACAGACAACCACAAGCAGCAGGAGGCTG
Rev 6 AGGCCAGGGAGAGCAGGAGGAGGCGAGGTCCGG
Rev 7 AGCAGAGACGCTGCAGGAGGCTCTTGCCGCCGGCG
Rev 8 TAGTCGGGCACGTCGTAAGGGTAGTGATGGTGGTGGTGGC

7.3.4 Oligonucleotides used for the Synthesis of *ArtPlasMA sine TM*

Forw 1 ATTAGACAAGCTTGCCACCATGGGCCACCATCACCACCAT
Forw 2 CACTACCCCTACGACGTGCCCGACTACGCCGGCGGCAAGA (ArtP. Forw 2)
Forw 3 CAACAGGACTACGACATCCCTCCAAGGATGTCATGGTCCG
Forw 4 GAGCCAGGCTAGCTGTGGCGTTCGATATCGAGCAGAAGCT
Forw 5 GATCAGCGAGGAGGACCTGTGATAAATAGGCGGCCGCATTA (ArtP. Forw 7)

Rev 1 ACTCGACGTGAACCGTGGACTAATGCGGCCGCCTATTATC (ArtP. Rev 0)
Rev 2 ACTCGACGTGAACCGTGGACTAATGCGGCCGCCTATTATC (ArtP. Rev 1)
Rev 3 CGCCACAGCTAGCCTGGCTCCGGACCATGACATCCTTGGA
Rev 4 GGGATGTCGTAGTCCTGTTGGCTCTTGCCGCCGGCGTAGTCG
Rev 5 GGCACGTCGTAGGGGTAGTGATGGTGGTGGTGGTGGCCCA (ArtP. Rev 6)

7.4 Vector Maps

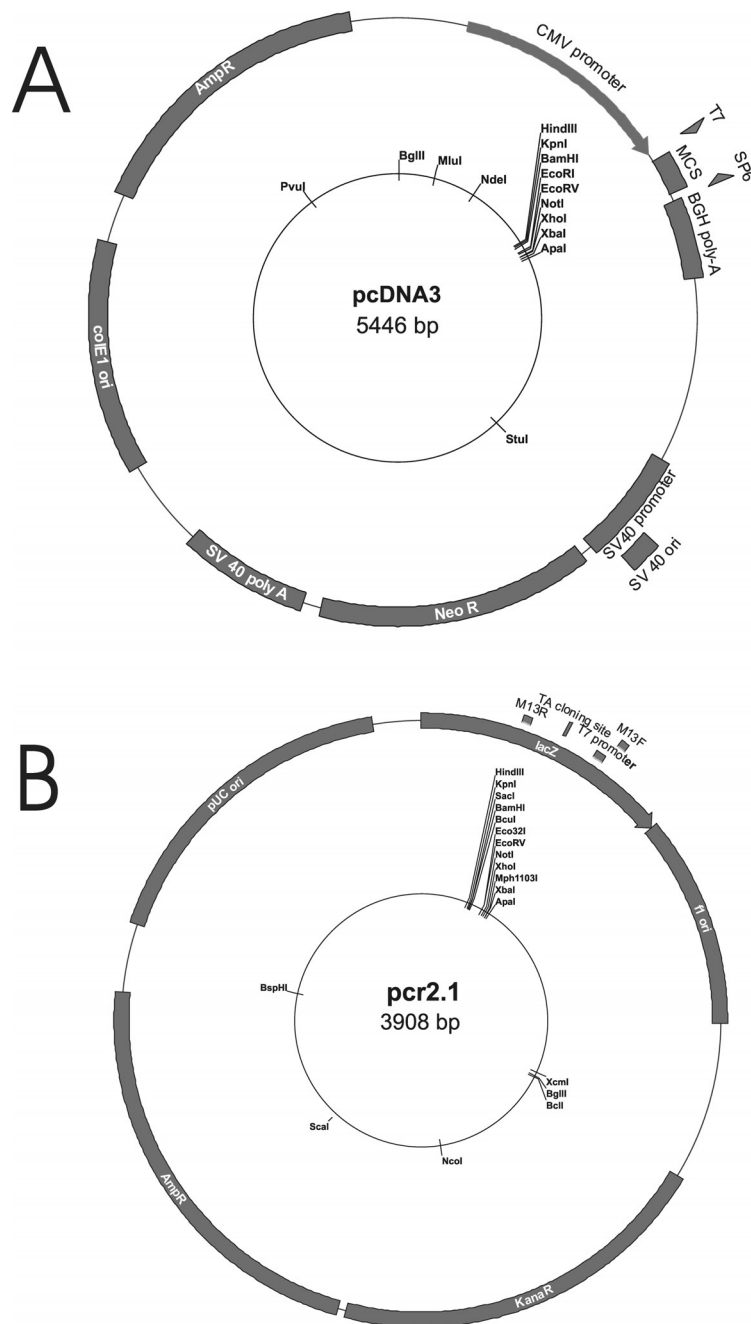


Figure 38. Vector maps. (A) pcDNA3. Features include ampicillin resistance (ampR, expression of β -Lactamase), neomycin/G418 resistance (NeoR, aminoglycosid-phosphotransferase), E.Coli origin of replication (colE1 ori, leading to 15 to 20 plasmid copies/bacterial cell), CMV-promoter for strong eukaryotic expression, SV40-promoter, Bovine Growth Hormone poly-A addition sequence and T7 and Sp6 bacteriophage promoters for in-vitro translation. (B) pCR2.1. Features include Ampicillin (ampR) and Kanamycin (KanR) resistance, the lacZ α -gene necessary for blue/white selection, the pUC origin of replication (high copy number) and f1 origin for single stranded DNA production. The vector contains a TA-cloning site.

7.5 Abbreviations

7.5.1 General Abbreviations

8-ANS	8-anilinonaphtalenesulfonate
AA	amino acid
ANNINE	annelated hemicyanine (dye)
ArtPlasMA	artificial plasma membrane anchor
ArtPlasMA AP	artificial plasma membrane anchor and alkaline phosphatase
AsglypMA	asialoglycoprotein-receptor membrane anchor
AsglypMA AP	asialoglycoprotein-receptor membrane anchor and alkaline phosphatase
ATP	adenosine triphosphate
bp	basepair or basepairs
BCIP	5-bromo-4-chloro-3-indolyl-phosphate
BIF	<i>Bifidobacterium bifidum</i>
DEA	diethanolamine
dec.	decomposition
DMEM	Dulbecco's modified Eagle medium
DNA	deoxyribonucleic acid
ECL	enhanced chemiluminescence
EGFP	enhanced green fluorescent protein
ER	endoplasmic reticulum
FITC	fluorescein isothiocyanate
GFP	green fluorescent protein
GPI	glycosyl phosphatidylinositol
GUV	giant unilamellar vesicles
H2B	histone 2B
HEK293	human embryonic kidney (mammalian cell line)
HPLC	high performance liquid chromatography
HRP	horse radish peroxidase
ITC	isothermal titration calorimetry
ITO	indium tin oxide
kDa	kilodalton
LCR	ligase chain reaction
LUV	large unilamellar vesicles
MDCK	Madin Darby Canine Kidney (mammalian cell line)
NBT	Nitro-Blue Tetrazolium Chloride
NMR	nuclear magnetic resonance
PAGE	polyacrylamide gel electrophoresis
PCR	polymerase chain reaction
<i>Pfu</i>	<i>Pyrococcus furiosus</i>

PLAP	Placental Alkaline Phosphatase
<i>p</i> -NPP	<i>para</i> -nitrophenylphosphate
POPC	palmitoyl-oleoyl-phosphatidylcholine
QELS	quasi-elastic light scattering
RP-HPLC	reversed phase high performance liquid chromatography
SDS	sodium dodecyl sulfate
SUV	small unilamellar vesicle
<i>Taq</i>	<i>Thermus aquaticus</i>
TGN	trans-Golgi network
TLC	thin layer chromatography
T _M	melting temperature
TM domain	transmembrane domain
TRITC	tetramethylrhodamine isothiocyanate
U	Unit
UV/Vis	ultraviolet/visible

7.5.2 Nomenclature of the Dyes

The short names are oriented at the nomenclature given in ref.¹² Only one dye of each structural subclass is given as an example.

Di-4-ASPBS	Di-butyl-AminoStyrylPyridinium ButylSulfonate
Di-6-ASPBS	Di-hexyl-AminoStyrylPyridinium ButylSulfonate
Di-4-ASPPA	Di-butyl-AminoStyrylPyridinium-PropylAlcohol;
Di-4-ASPPP	Di-butyl-AminoStyrylPyridinium-PropylPhosphate
Di-4-ASPP(PP)	Di-butyl-AminoStyrylPyridinium-Propyl-DiPhosphate
Di-4-ASPPiHA ₂	Di-butyl-AminoStyrylPyridinium-isoohexyl-DiAlcohol
Di-4-ASPPiHP ₂	Di-butyl-AminoStyrylPyridinium-isoohexyl-DiAlcohol phosphoric acid ester
Di-10P-ASPBS	Di-phosphatodecyl-AminoStyrylPyridinium ButylSulfonate
Di-10A-ASPBS	Di-hydroxydecyl-AminoStyrylPyridinium ButylSulfonate
Di-4-ASP Dication	Di-butyl-AminoStyrylPyridinium-Propyl(trimethyl-)ammonium

8 Literature

- (1) Hübener, G.; Lambacher, A.; Fromherz, P. *Anellated Hemicyanine Dyes with Large Symmetrical Solvatochromism of Absorption and Fluorescence*. *J. Phys. Chem. B* **2003**, *107*, 7896-7902.
- (2) Kuhn, B.; Fromherz, P. *Anellated Hemicyanine Dyes in a Neuron Membrane: Molecular Stark Effect and Optical Voltage Recording*. *J. Phys. Chem. B* **2003**, *107*, 7903-7913.
- (3) Kuhn, B.; Fromherz, P.; Denk, W. *High Sensitivity of Stark-Shift Voltage-Sensing Dyes by One- or Two-Photon Excitation Near the Red Spectral Edge*. *Biophys. J.* **2004**, *87*, 631-639.
- (4) Bullen, A.; Saggau, P. *Optical Recording from Individual Neurons in Culture*. In *Modern Techniques in Neuroscience Research*; 1st ed.; Johannson, H., Ed.; Springer: Berlin, 1999; pp 89.
- (5) Sinha, S. R.; Saggau, P. *Optical Recording from Populations of Neurons in Brain Slices*. In *Modern Techniques in Neuroscience Research*; 1st ed.; Johannson, H., Ed.; Springer: Berlin, 1999; pp 459.
- (6) Grinvald, A.; Shoham, D.; Shmuel, A.; Glaser, D.; Vanzetta, I.; Shtoyerman, E.; Slovov, H.; Wijnbergen, C.; Hildesheim, R.; Arieli, A. *In Vivo Optical Imaging of Cortical Architecture and Dynamics*. In *Modern Techniques in Neuroscience Research*; Johannson, H., Ed.; Springer: Berlin, 1999; Vol. 1; pp 893.
- (7) Tasaki, I.; Watanabe, A.; Sandlin, R.; Carnay, L. *Changes in Fluorescence, Turbidity, And Birefringence Associated with Nerve Excitation*. *Proc. Natl. Acad. Sci. U. S. A.* **1968**, *61*, 883-888.
- (8) Cohen, L. B.; Salzberg, B. M.; Davila, H. V.; Ross, W. N.; Landowne, D.; Waggoner, A. S.; Wang, C. H. *Changes in axon fluorescence during activity - molecular probes of membrane-potential*. *J. Membr. Biol.* **1974**, *19*, 1-36.
- (9) Cohen, L. B.; Salzberg, B. M. *Optical measurement of membrane potential*. *Rev. Physiol. Biochem. Pharmacol.* **1978**, *83*, 35-88.
- (10) Loew, L. M.; Bonneville, G. W.; Surow, J. *Charge shift optical probes of membrane potential. Theory*. *Biochemistry* **1978**, *17*, 4065-4071.
- (11) Loew, L. M.; Simpson, L. L. *Charge-shift probes of membrane potential: a probable electrochromic mechanism for p-aminostyrylpyridinium probes on a hemispherical lipid bilayer*. *Biophys. J.* **1981**, *34*, 353-365.

- (12) Fluhler, E.; Burnham, V. G.; Loew, L. M. *Spectra, membrane binding, and potentiometric responses of new charge shift probes*. *Biochemistry* **1985**, *24*, 5749-5755.
- (13) Grinvald, A.; Hildesheim, R.; Farber, I. C.; Anglister, L. *Improved fluorescent probes for the measurement of rapid changes in membrane potential*. *Biophys. J.* **1982**, *39*, 301-308.
- (14) Grinvald, A.; Fine, A.; Farber, I. C.; Hildesheim, R. *Fluorescence monitoring of electrical responses from small neurons and their processes*. *Biophys. J.* **1983**, *42*, 195-198.
- (15) Grinvald, A.; Salzberg, B. M.; Lev-Ram, V.; Hildesheim, R. *Optical recording of synaptic potentials from processes of single neurons using intracellular potentiometric dyes*. *Biophys. J.* **1987**, *51*, 643-651.
- (16) Antic, S.; Zecevic, D. *Optical Signals from Neurons with Internally Applied Voltage-Sensitive Dyes*. *J. Neurosci.* **1995**, *15*, 1392-1405.
- (17) Siegel, M. S.; Isacoff, E. Y. *A Genetically Encoded Probe of Membrane Voltage*. *Neuron* **1997**, *19*, 735-741.
- (18) Sakai, R.; Canonigo, V. R.; Raj, C. D.; Knöpfel, T. *Design and Characterization of a DNA-encoded, voltage-sensitive fluorescent protein*. *Eur. J. Neurosci.* **2001**, *13*, 2314-2318.
- (19) Hinner, M. J.; Hübener, G.; Fromherz, P. *Enzyme-Induced Staining of Biomembranes with Voltage-Sensitive Fluorescent Dyes*. *J. Phys. Chem. B* **2004**, *108*, 2445-2453.
- (20) Hassner, A.; Birnbaum, D.; Loew, L. M. *Charge-Shift Probes of Membrane Potential. Synthesis*. *J. Org. Chem.* **1984**, *49*, 2546-2551.
- (21) Massoud, S. S.; Sigel, H. *Metal ion coordinating properties of pyrimidine-nucleoside 5'-monophosphates (CMP, UMP, TMP) and of simple phosphate monoesters, including D-ribose 5'-monophosphate - establishment of relations between complex stability and phosphate basicity*. *Inorg. Chem.* **1988**, *27*, 1447-1453.
- (22) Georgatsos, J. G. *Specificity and phosphotransferase activity of purified placental alkaline phosphatase*. *Arch. Biochem. Biophys.* **1967**, *121*, 619-624.
- (23) Skynner, M. J.; Drage, D. J.; Dean, W. L.; Turner, S.; Watt, D. J.; Allen, N. D. *Transgenic mice ubiquitously expressing Human Placental Alkaline Phosphatase (PLAP): an additional reporter gene for use in tandem with beta-galactosidase (lacZ)*. *Int. J. Dev. Biol.* **1999**, *43*, 85-90.
- (24) Fromherz, P. *Monopole-Dipole Model for Symmetrical Solvatochromism of Hemicyanine Dyes*. *J. Phys. Chem.* **1995**, *99*, 7188-7192.
- (25) Siano, D. B.; Metzler, D. E. *Band Shapes of the Electronic Spectra of Complex Molecules*. *J. Chem. Phys.* **1969**, *51*, 1856-1861.
- (26) Fromherz, P.; Röcker, C. *Staining of Biomembranes with Amphiphilic Hemicyanine Dyes*. *Ber. Bunsenges. Phys. Chem.* **1994**, *98*, 128-131.

-
- (27) Lasch, J. *Interaction of detergents with lipid vesicles*. Biochim. Biophys. Acta **1995**, *1241*, 269-292.
- (28) Tan, A.; Ziegler, A.; Steinbauer, B.; Seelig, J. *Thermodynamics of sodium dodecyl sulfate partitioning into lipid membranes*. Biophys. J. **2002**, *83*, 1547-1556.
- (29) McLaughlin, S. *Electrostatic Potentials at Membrane-Solution Interfaces*. Curr. Top. Membr. Transp. **1977**, *9*, 71-144.
- (30) Wiseman, T.; Williston, S.; Brandts, J. F.; Lin, L. N. *Rapid measurement of binding constants and heats of binding using a new titration calorimeter*. Anal. Biochem. **1989**, *179*, 131-137.
- (31) Seelig, J. *Titration calorimetry of lipid-peptide interactions*. Biochim. Biophys. Acta **1997**, *1331*, 103-116.
- (32) Heerklotz, H.; Seelig, J. *Titration calorimetry of surfactant-membrane partitioning and membrane solubilization*. Biochim. Biophys. Acta **2000**, *1508*, 69-85.
- (33) Demant, E. J.; Friche, E. *Equilibrium binding of anthracycline cytostatics to serum albumin and small unilamellar phospholipid vesicles as measured by gel filtration*. Biochem. Pharmacol. **1998**, *55*, 27-32.
- (34) Buser, C. A.; McLaughlin, S. *Ultracentrifugation technique for measuring the binding of peptides and proteins to sucrose-loaded phospholipid vesicles*. Methods Mol. Biol. **1998**, *84*, 267-281.
- (35) Kalinin, S. V.; Molotkovsky, J. G. *Anion binding to lipid bilayers: determination using fluorescent membrane probe by direct quenching or by competitive displacement approaches*. J. Biochem. Biophys. Methods **2000**, *46*, 39-51.
- (36) Santos, N. C.; Prieto, M.; Castanho, M. A. *Quantifying molecular partition into model systems of biomembranes: an emphasis on optical spectroscopic methods*. Biochim. Biophys. Acta **2003**, *1612*, 123-135.
- (37) Danielsson, L.-G.; Zhang, Y.-H. *Methods for Determining n-octanol-water partition constants*. Trends Anal. Chem. **1996**, *15*, 188-196.
- (38) Bouchard, G.; Carrupt, P. A.; Testa, B.; Gobry, V.; Girault, H. H. *Lipophilicity and solvation of anionic drugs*. Chemistry **2002**, *8*, 3478-3484.
- (39) Rogachev, I.; Serra, C.; Farran, A.; Cortina, J. L.; Gressel, J.; Warshawsky, A. *Prediction of the octanol-water distribution of dithiocarbamate derivatives*. React. Funct. Pol. **2003**, *54*, 17-24.
- (40) Ephardt, H.; Fromherz, P. *Fluorescence and Photoisomerization of an Amphiphilic Aminostilbazolium Dye As Controlled by The Sensitivity of Radiationless Deactivation to Polarity and Viscosity*. J. Phys. Chem. **1989**, *93*, 7717-7725.
- (41) Fromherz, P.; Schenk, O. *Voltage-Sensitive fluorescence of amphiphilic hemicyanine dyes in a black lipid membrane of glycerol monooleate*. Biochim. Biophys. Acta **1993**, *1191*, 299-308.

- (42) Schote, U.; Seelig, A. *Interaction of the neuronal marker dye FM1-43 with lipid membranes - Thermodynamics and lipid ordering*. *Biochim. Biophys. Acta* **1998**, *1415*, 135-146.
- (43) Fernández, M. S.; Fromherz, P. *Lipoid pH Indicators as Probes of Electrical Potential and Polarity in Micelles*. *J. Phys. Chem.* **1977**, *81*, 1755.
- (44) Born, M. *Volumen und Hydratationswärme der Ionen*. *Z. Physik* **1920**, *1*, 45-48.
- (45) Shannon, R. D. *Revised Effective Ionic Radii and Systematic Studies of Interatomic Distances in Halides and Chalcogenides*. *Acta Crystallogr. A.* **1976**, *32*, 751-767.
- (46) Abraham, M. H.; Whiting, G. S. *Thermodynamics of Solute Transfer from Water to Hexadecane*. *J. Chem. Soc. [Perkin. 2]*. **1990**, *2*, 291-300.
- (47) Cheong, W. J. *A Study of the Gas Liquid Partition Coefficients of Eleven Normal, Branched and Cyclic Alkanes in Sixty Nine Common Organic Liquids: The Effect of Solute Structure*. *Bull. Korean Chem. Soc.* **2002**, *23*, 459-468.
- (48) Seelig, A.; Allegrini, P. R.; Seelig, J. *Partitioning of local anesthetics into membranes: surface charge effects monitored by the phospholipid head-group*. *Biochim. Biophys. Acta* **1988**, *939*, 267-276.
- (49) Seelig, J.; Nebel, S.; Ganz, P.; Bruns, C. *Electrostatic and nonpolar peptide-membrane interactions. Lipid binding and functional properties of somatostatin analogues of charge $z = +1$ to $z = +3$* . *Biochemistry* **1993**, *32*, 9714-9721.
- (50) Irvine, J. D.; Takahashi, L.; Lockhart, K.; Cheong, J.; Tolan, J. W.; Selick, H. E.; Grove, J. R. *MDCK (Madin-Darby canine kidney) cells: A tool for membrane permeability screening*. *J. Pharm. Sci.* **1999**, *88*, 28-33.
- (51) Zachowski, A. *Phospholipids in animal eukaryotic membranes: transverse asymmetry and movement*. *Biochem. J.* **1993**, *294*, 1-14.
- (52) Cullis, P. R.; Hope, M. J.; Bally, M. B.; Madden, T. D.; Mayer, L. D.; Fenske, D. B. *Influence of pH gradients on the transbilayer transport of drugs, lipids, peptides and metal ions into large unilamellar vesicles*. *Biochim. Biophys. Acta* **1997**, *1331*, 187-211.
- (53) Lasic, D. D. *Liposomes - from Physics to Applications*; Elsevier: Amsterdam, 1993.
- (54) Graham, F. L.; Smiley, J.; Russell, W. C.; Nairn, R. *Characteristics of a Human Cell Line Transformed by DNA from Human Adenovirus Type-5*. *J. Gen. Virol.* **1977**, *36*, 59-72.
- (55) Kleinfeld, A. M.; Chu, P.; Storch, J. *Flip-flop is slow and rate limiting for the movement of long chain anthroyloxy fatty acids across lipid vesicles*. *Biochemistry* **1997**, *36*, 5702-5711.
- (56) Ries, R. S.; Choi, H.; Blunck, R.; Bezanilla, F.; Heath, J. R. *Black Lipid Membranes: Visualizing the Structure, Dynamics and Substrate Dependence of Membranes*. *J. Phys. Chem. B* **2004**, *108*, 16040-16049.

- (57) Melikyan, G. B.; Deriy, B. N.; Ok, D. C.; Cohen, F. S. *Voltage-dependent translocation of R18 and DiI across lipid bilayers leads to fluorescence changes*. *Biophys. J.* **1996**, *71*, 2680-2691.
- (58) Thomas, R. M.; Baici, A.; Werder, M.; Schulthess, G.; Hauser, H. *Kinetics and Mechanism of Long-Chain Fatty Acid Transport into Phosphatidylcholine Vesicles from Various Donor Systems*. *Biochemistry* **2002**, *41*, 1591-1601.
- (59) Visser, N. V.; van Hoek, A.; Visser, A. J.; Frank, J.; Apell, H. J.; Clarke, R. J. *Time-resolved fluorescence investigations of the interaction of the voltage-sensitive probe RH421 with lipid membranes and proteins*. *Biochemistry* **1995**, *34*, 11777-11784.
- (60) Knippenberg, C. *Spannungsabhängige Fluoreszenzspektroskopie an Neuronen mittels Förster Energieübertragung*. Diploma thesis, Universität Ulm, 1993.
- (61) Mellman, I. *Endocytosis and Molecular Sorting*. *Annu. Rev. Cell Dev. Biol.* **1996**, *12*, 575-625.
- (62) Grinvald, A.; Frostig, R. D.; Lieke, E.; Hildesheim, R. *Optical imaging of neuronal activity*. *Physiol. Rev.* **1988**, *68*, 1285-1366.
- (63) Axelrod, D. *Carbocyanine dye orientation in red cell membrane studied by microscopic fluorescence polarization*. *Biophys. J.* **1979**, *26*, 557-573.
- (64) Lambacher, A.; Fromherz, P. *Orientation of Hemicyanine Dye in Lipid Membrane Measured by Fluorescence Interferometry on a Silicon Chip*. *J. Phys. Chem. B* **2001**, *105*, 343-346.
- (65) Tisato, F.; Maina, T.; Shao, L. R.; Heeg, M. J.; Deutsch, E. *Cationic [Tc-99m(III)(DIARS)(2)(SR)(2)](+) complexes as potential myocardial perfusion imaging agents (DIARS equals o-phenylene(dimethylarsine); SR(-) equals thioilate)*. *J. Med. Chem.* **1996**, *39*, 1253-1261.
- (66) Leuchs, H. *Über eine verbesserte Darstellung monosubstituierter Malonester und Acetessigester*. *Chem. Ber.* **1911**, 1507-1511.
- (67) Hands, A. R.; Mercer, A. J. H. *Reactions of sodium hydride with omega-hydroxyalkylphosphonium -aesonium and -ammonium salts*. *J. Chem. Soc. [C - Organic]* **1968**, *11*, 1331-1337.
- (68) Abe, M.; Hayashikoshi, T.; Kurata, T. *A new synthetic method of macrocyclic lactones from omega-iodoalkylacrylates*. *Chem. Lett.* **1994**, *10*, 1789-1792.
- (69) Burger, A.; Clark, J. E.; Nishimoto, M.; Muerhoff, A. S.; Masters, B. S. S.; De Montellano, P. R. O. *Mechanism-based inhibitors of prostaglandin omega-hydroxylase-(R)-12-hydroxy-16-heptadecynoic and (S)-12-hydroxy-16-heptadecynoic acid and 2,2-dimethyl-12-hydroxy-16-heptadecynoic acid*. *J. Med. Chem.* **1993**, *36*, 1418-1424.
- (70) Ainscow, T. A.; Belmont, M. R.; Henshall, J. L.; Hooper, R. M.; Simmonds, D. J. *Synthesis of 4 n-alkanes with terminal dipolar substituents*. *Tetrahedron* **1987**, *43*, 115-122.

- (71) Gregoriadis, G. *Liposome Technology: Preparation of Liposomes: 001*; CRC: Boca Raton, 1984; Vol. 1.
- (72) MacDonald, R. C.; MacDonald, R. I.; Menco, B. P. M.; Takeshita, K.; Subbarao, N. K.; Hu, L. R. *Small-volume extrusion apparatus for preparation of large, unilamellar vesicles*. *Biochim. Biophys. Acta* **1991**, *1061*, 297-303.
- (73) Atkins, P. W. *Physical Chemistry*, 6th ed.; Oxford University Press: Oxford, 1998.
- (74) Todd, M. J.; Gomez, J. *Enzyme kinetics determined using calorimetry: a general assay for enzyme activity?* *Anal. Biochem.* **2001**, *296*, 179-187.
- (75) Tewari, Y. B.; Steckler, D. K.; Goldberg, R. N.; Gitomer, W. L. *Thermodynamics of hydrolysis of sugar phosphates*. *J. Biol. Chem.* **1988**, *263*, 3670-3675.
- (76) Eriksson, H. J. C.; Somsen, G. W.; Hinrichs, W. L. J.; Frijlink, H. W.; de Jong, G. J. *Characterization of human placental alkaline phosphatase by activity and protein assays, capillary electrophoresis and matrix-assisted laser desorption/ionization time-of-flight mass spectrometry*. *J. Chromatogr. B* **2001**, *755*, 311-319.
- (77) Grit, M.; Crommelin, D. J. *Chemical stability of liposomes: implications for their physical stability*. *Chem. Phys. Lipids* **1993**, *64*, 3-18.
- (78) Dimitrov, D. S.; Angelova, M. I. *Lipid swelling and liposome formation mediated by electric fields*. *Bioelectrochem. Bioenerg.* **1988**, *19*, 323-336.
- (79) Angelova, M. I.; Soleau, S.; Meleard, P.; Faucon, J. F.; Bothorel, P. *Preparation of giant vesicles by external AC electric fields. Kinetics and Applications*. *Prog. Coll. Pol. Sci.* **1992**, *89*, 127-131.
- (80) Fromherz, P.; Kiessling, V.; Kottig, K.; Zeck, G. *Membrane transistor with giant lipid vesicle touching a silicon chip*. *Appl. Phys. A* **1999**, *69*, 571-576.
- (81) Schwoch, G.; Passow, H. *Preparation and properties of human erythrocyte ghosts*. *Mol. Cell. Biochem.* **1973**, *2*, 197-218.
- (82) Nielsen, H.; Engelbrecht, J.; Brunak, S.; von Heijne, G. *Identification of prokaryotic and eukaryotic signal peptides and prediction of their cleavage sites*. *Protein Eng.* **1997**, *10*, 1-6.
- (83) Spiess, M.; Lodish, H. F. *An internal signal sequence: the asialoglycoprotein receptor membrane anchor*. *Cell* **1986**, *44*, 1103-1112.
- (84) Munro, S.; Pelham, H. R. *A C-terminal signal prevents secretion of luminal ER proteins*. *Cell* **1987**, *48*, 899-907.
- (85) Munro, S. *Localization of proteins to the Golgi apparatus*. *Trends Cell Biol.* **1998**, *8*, 11-15.
- (86) Munro, S. *An Investigation of the Role of Transmembrane Domains in Golgi Protein Retention*. *EMBO J.* **1995**, *14*, 4695-4704.
- (87) Ma, D.; Zerangue, N.; Lin, Y. F.; Collins, A.; Yu, M.; Jan, Y. N.; Jan, L. Y. *Role of ER export signals in controlling surface potassium channel numbers*. *Science* **2001**, *291*, 316-319.

- (88) Rothman, J. E.; Orci, L. *Molecular dissection of the secretory pathway*. Nature **1992**, 355, 409-415.
- (89) Englund, P. T. *The Structure and Biosynthesis of Glycosyl Phosphatidylinositol Protein Anchors*. Annu. Rev. Biochem. **1993**, 62, 121-138.
- (90) von Heijne, G. *Sequence Analysis in Molecular Biology: Treasure Trove or Trivial Pursuit*; Academic Press: San Diego, 1987.
- (91) von Heijne, G., personal communication.
- (92) Sakaguchi, M. *Mutational Analysis of Signal-Anchor and Stop-Transfer Sequences in Membrane Proteins*. In *Membrane Protein Assembly*; von Heijne, G., Ed.; Springer: New York, 1997; pp 270.
- (93) Spector, D. L. *Detection of beta-Galactosidase and Alkaline Phosphatase Activity in Tissues*. In *Cells: A Laboratory Manual*; Spector, D. L., Goldman, R. D., Leinwand, L. A., Eds.; CSHL Press: Plainview, 1998; Vol. 3.
- (94) Rigaut, G.; Shevchenko, A.; Rutz, B.; Wilm, M.; Mann, M.; Seraphin, B. *A generic protein purification method for protein complex characterization and proteome exploration*. Nat. Biotechnol. **1999**, 17, 1030-1032.
- (95) Kim, C. H.; Oh, Y.; Lee, T. H. *Codon optimization for high-level expression of human erythropoietin (EPO) in mammalian cells*. Gene **1997**, 199, 293-301.
- (96) Beaucage, S. L. *Synthesis of Unmodified Oligonucleotides*. In *Current Protocols in Nucleic Acid Chemistry*; Beaucage, S. L., Bergstrom, D. E., Glick, G. D., Jones, R. A., Eds.; John Wiley & Sons, Inc.: New York, 2003.
- (97) Withers-Martinez, C.; Carpenter, E. P.; Hackett, F.; Ely, B.; Sajid, M.; Grainger, M.; Blackman, M. J. *PCR-based Gene Synthesis as an efficient approach for expression of the A+T-rich malaria genome*. Protein Eng. **1999**, 12, 1113-1120.
- (98) Martinez, C. W.; Blackman, M. J.; et al. *PCR-based Gene Synthesis as an efficient approach for expression of the A+T-rich malaria genome*. Protein Engineering **1999**, 12(12), 1113-1120.
- (99) Kozak, M. *An analysis of 5'-noncoding sequences from 699 vertebrate messenger RNAs*. Nucleic Acids Res. **1987**, 15, 8125-8148.
- (100) Makrides, S. C. *Strategies for achieving High-Level Expression of Genes in Escherichia coli*. Microbiol. Rev. **1996**, 60, 512-538.
- (101) Ciccarelli, R. B.; Gunyuzlu, P.; Huang, J.; Scott, C.; Oakes, F. T. *Construction of synthetic genes using PCR after automated DNA synthesis of their entire top and bottom strands*. Nucleic Acids Res. **1991**, 19, 6007-6013.
- (102) Au, L. C.; Yang, F. Y.; Yang, W. J.; Lo, S. H.; Kao, C. F. *Gene Synthesis by a LCR-based approach: high-level production of leptin-L54 using synthetic gene in Escherichia coli*. Biochem. Biophys. Res. Commun. **1998**, 248, 200-203.
- (103) Chalmers, F. M.; Curnow, K. M. *Scaling up the ligase chain reaction-based approach to Gene Synthesis*. Biotechniques **2001**, 30, 249-252.

- (104) Casimiro, D. R.; Wright, P. E.; Dyson, H. J. *PCR-based Gene Synthesis and protein NMR spectroscopy*. *Structure* **1997**, *5*, 1407-1412.
- (105) Prodromou, C.; Pearl, L. H. *Recursive PCR: a novel technique for total Gene Synthesis*. *Protein Eng.* **1992**, *5*, 827-829.
- (106) Stemmer, W. P. C.; Cramer, A.; Ha, K. D.; Brennan, T. M.; Heyneker, H. L. *Single-step assembly of a gene and entire plasmid from large numbers of oligodeoxyribonucleotides*. *Gene* **1995**, *164*, 49-53.
- (107) Hoover, D. M.; Lubkowsky, J. *DNAWorks: an automated method for designing oligonucleotides for PCR-based Gene Synthesis*. *Nucleic Acids Res.* **2002**, *30*, e43.
- (108) Zuker, M. *Mfold web server for nucleic acid folding and hybridization prediction*. *Nucleic Acids Res.* **2003**, *31*, 3406-3415.
- (109) SantaLucia, J. *A unified view of polymer, dumbbell, and oligonucleotide DNA nearest-neighbor thermodynamics*. *Proc. Natl. Acad. Sci. U. S. A.* **1998**, *95*.
- (110) Chuang, S. E.; Wang, K. C.; L., C. A. *Single-step direct cloning of PCR products*. *Trends Genet.* **1995**, *11*, 7-8.
- (111) *Characterization of Cellular Proteins (Chapter 5)*. In *Current Protocols in Cell Biology*; Bonifacino, J. S., Dasso, M., Harford, J. B., Lippincott-Schwartz, J., Yamada, K. M., Eds.; John Wiley & Sons, Inc.: New York, 2000; Vol. 1.
- (112) Oohashi, T.; Zhou, X. H.; Feng, K.; Richter, B.; Morgelin, M.; Perez, M. T.; Su, W. D.; Chiquet-Ehrismann, R.; Rauch, U.; Fässler, R. *Mouse Ten-m/Odz Is a new family of Dimeric Type II Transmembrane Proteins expressed in many tissues*. *J. Cell Biol.* **1999**, *145*, 563-577.
- (113) Flanagan, J. G.; Leder, P. *The kit ligand: a cell surface molecule altered in steel mutant fibroblasts*. *Cell* **1990**, *63*, 185-194.
- (114) Hinners, I.; Moschner, J.; Nolte, N.; Hille-Rehfeld, A. *The orientation of membrane proteins determined in situ by immunofluorescence staining*. *Anal. Biochem.* **1999**, *276*, 1-7.
- (115) *Organelle atlas (Chapter 4A)*. In *Current Protocols in Cell Biology*; Bonifacino, J. S., Dasso, M., Harford, J. B., Lippincott-Schwartz, J., Yamada, K. M., Eds.; John Wiley & Sons, Inc.: New York, 2000; Vol. 1.
- (116) Johnston, J. A.; Ward, C. L.; Kopito, R. R. *Aggresomes: A Cellular Response to Misfolded Proteins*. *J. Cell Biol.* **1998**, *143*, 1883-1889.
- (117) García-Mata, R.; Bebök, Z.; Sorscher, E. J.; Sztul, E. S. *Characterization and Dynamics of Aggresome Formation by a Cytosolic GFP-Chimera*. *J. Cell Biol.* **1999**, *146*, 1239-1254.
- (118) Sambrook, J.; Russell, D. W. *Molecular Cloning: A Laboratory Manual*, 3rd ed.; CSHL Press: Cold Spring Harbor, 2001.
- (119) Rozengurt, E.; Heppel, A. H. *A specific effect of external ATP on the permeability of transformed 3T3 cells*. *Biochem. Biophys. Res. Commun.* **1975**, *67*, 1581-1588.

- (120) Tokumitsu, S.; Fishman, W. H. *Alkaline Phosphatase Biosynthesis in the Endoplasmic Reticulum and Its Transport Through the Golgi Apparatus to the Plasma Membrane*. *J. Histochem. Cytochem.* **1983**, *31*, 647-655.
- (121) Le Du, M. H.; Stigbrand, T.; Taussig, M. J.; Menez, A.; Stura, E. A. *Crystal Structure of Alkaline Phosphatase from Human Placenta at 1.8 Å Resolution - Implication for a substrate specificity*. *J. Biol. Chem.* **2001**, *276*, 9158-9165.
- (122) Wahlberg, J. M.; Spiess, M. *Multiple determinants direct the orientation of signal-anchor proteins: the topogenic role of the hydrophobic signal domain*. *J. Cell Biol.* **1997**, *137*, 555-562.
- (123) Cottet, S.; Corthésy, B. *Cellular processing limits the heterologous expression of secretory component in mammalian cells*. *Eur. J. Biochem.* **1997**, *246*, 23-31.
- (124) Boyd, D. *Use of Gene Fusions to Determine Membrane Protein Topology*. In *Membrane Protein Structure: Experimental Approaches*; White, S. H., Ed.; Oxford Univ. Press: New York, 1994; pp 395.
- (125) Prinz, W. A.; Beckwith, J. *Gene fusion analysis of membrane protein topology: a direct comparison of alkaline phosphatase and beta-Lactamase fusions*. *J. Bacteriol.* **1994**, *176*, 6410-6413.
- (126) Wessels, H. P.; Beltzer, J. P.; Spiess, M. *Analysis of Protein topology in the endoplasmic reticulum*. *Methods Cell Biol.* **1991**, *34*, 287-302.
- (127) Gaush, C. R.; Hard, W. L.; Smith, C. F. *Characterization of an established line of canine kidney cells (MDCK)*. *Proc. Soc. Exp. Biol. Med.* **1966**, *122*, 931-935.
- (128) Mülhardt, C. *Der Experimentator: Molekularbiologie, Genomics*, 3 ed.; Spektrum: Heidelberg, 2002.
- (129) Freshney, R. I. *Culture of Animal Cells: A Manual of Basic Technique*; Wiley-Liss: New York, 1994.
- (130) Laemmli, U. K. *Cleavage of structural proteins during assembly of head of bacteriophage T-7*. *Nature* **1970**, *227*, 680-685.
- (131) Cormack, B. P.; Valdivia, R. H.; Falkow, S. *FACS-optimized mutants of the green fluorescent protein (GFP)*. *Gene* **1996**, *173*, 33-38.
- (132) Kanda, T.; Sullivan, K. F.; Wahl, G. M. *Histone-GFP fusion protein enables sensitive analysis of chromosome dynamics in living cells*. *Curr. Biol.* **1998**, *8*, 377-385.
- (133) Fromherz, P., unpublished results.
- (134) Vielstich, W. *Der Zusammenhang zwischen Nernstscher Diffusionsschicht und Prandtlscher Strömungsgrenzschicht*. *Z. Elektrochem.* **1953**, *57*, 646-655.
- (135) Northrop, D. B. *On the meaning of K_m and V/K in Enzyme kinetics*. *J. Chem. Educ.* **1998**, *75*, 1153-1157.
- (136) Stinson, R. A. *Kinetic Parameters for the Cleaved Substrate, and Enzyme and Substrate Stability, Vary with the Phosphoacceptor in Alkaline Phosphatase Catalysis*. *Clin. Chem.* **1993**, *39*, 2293-2297.

- (137) Chen, G. Q.; Choi, I.; Ramachandran, B.; Gouaux, J. E. *Total Gene Synthesis: Novel Single-Step and Convergent Strategies Applied to the Construction of a 779 Base Pair Bacteriorhodopsin Gene*. *J. Am. Chem. Soc.* **1994**, *116*, 8799-8800.
- (138) Chalmers, F., personal communication.
- (139) Blackman, M. J., personal communication.
- (140) SantaLucia, J., Jr; Allawi, H. T.; Seneviratne, P. A. *Improved Nearest-Neighbour Parameters for Predicting DNA Duplex Stability*. *Biochemistry* **1996**, *35*, 3555-3562.
- (141) Breslauer, K. J.; Frank, R.; Blöcker, H.; Marky, L. A. *Predicting DNA duplex stability from the base sequence*. *Proc. Natl. Acad. Sci. U. S. A.* **1986**, *83*, 3746-3750.
- (142) Keohavong, P.; Thilly, W. G. *Fidelity of DNA polymerases in DNA amplification*. *Proc. Natl. Acad. Sci. U. S. A.* **1989**, *86*, 9253-9257.
- (143) Andre, P.; Kim, A.; Khrapko, K.; Thilly, W. G. *Fidelity and mutational spectrum of Pfu DNA polymerase on a human mitochondrial DNA sequence*. *Genome Res.* **1997**, *7*, 843-852.
- (144) Cline, J.; Braman, J. C.; Hogrefe, H. H. *PCR fidelity of pfu DNA polymerase and other thermostable DNA polymerases*. *Nucleic Acids Res.* **1996**, *24*, 3546-3551.
- (145) Viguera, E.; Canceill, D.; Ehrlich, S. D. *In vitro replication slippage by DNA polymerases from thermophilic organisms*. *J. Mol. Biol.* **2001**, *312*, 323-333.
- (146) Zhu, L. *In Vitro Site-Directed Mutagenesis Using the Unique Restriction Site Elimination (USE) Method*. In *In Vitro Mutagenesis Protocols*; 1st ed.; Trower, M. K., Ed.; Humana: Totowa, 1996; pp 390.
- (147) Watkins, B. A.; Reitz Jr., M. S. *Using PCR for Rapid Site-Specific Mutagenesis in Large Plasmids*. In *In Vitro Mutagenesis Protocols*; Trower, M. K., Ed.; Humana: Totowa, 1996; pp 390.
- (148) Ignatov, K. B.; Kramarov, V. M.; Uznadze, O. L.; Miroshnikov, A. I. *DNA polymerase mediated amplification of DNA fragments using primers with mismatches in the 3'-region*. *Bioorg. Khim.* **1997**, *23*, 817-822.
- (149) Housby, J. N.; Southern, E. M. *Thermus scotoductus and Rhodothermus marinus DNA ligases have higher ligation efficiencies than thermus thermophilus DNA ligase*. *Anal. Biochem.* **2002**, *302*, 88-94.
- (150) Housby, J. N.; Southern, E. M. *Fidelity of DNA ligation: a novel experimental approach based on the polymerisation of libraries of oligonucleotides*. *Nucleic Acids Res.* **1998**, *26*, 4259-4266.
- (151) Pritchard, C. E.; Southern, E. M. *Effects of base mismatches on joining of short oligodeoxynucleotides by DNA ligases*. *Nucleic Acids Res.* **1997**, *25*, 3403-3407.
- (152) Shuman, S. *Vaccinia virus DNA ligase: specificity, fidelity, and inhibition*. *Biochemistry* **1995**, *34*, 16138-16147.

- (153) Beaucage, S. L.; Caruthers, M. H. *Deoxynucleoside phosphoramidites - a new class of key intermediates for deoxypolynucleotide synthesis*. *Tetrahedron Lett.* **1981**, *22*, 1859-1862.
- (154) Bergstrom, D. E. *Purification and Analysis of Synthetic Nucleic Acids and Components (Chapter 10)*. In *Current Protocols in Nucleic Acid Chemistry*; Beaucage, S. L., Bergstrom, D. E., Glick, G. D., Jones, R. A., Eds.; John Wiley & Sons, Inc., 2003.
- (155) Hecker, K. H.; Rill, R. L. *Error analysis of chemically synthesized polynucleotides*. *Biotechniques* **1998**, *24*, 256-260.
- (156) McClain, W. H.; Foss, K.; Mittelstadt, K. L.; Schneider, J. *Variants in clones of gene-machine-synthesized oligodeoxynucleotides*. *Nucleic Acids Res.* **1986**, *14*, 6770.
- (157) Tamsamani, J.; Kubert, M.; Agrawal, S. *Sequence Identity of the n-1 product of a synthetic oligonucleotide*. *Nucleic Acids Res.* **1995**, *23*, 1841-1844.
- (158) Chen, D.; Yan, Z.; Cole, D. L.; Srivatsa, G. S. *Analysis of internal (n-1)mer deletion sequences in synthetic oligodeoxyribonucleotides by hybridization to an immobilized probe array*. *Nucleic Acids Res.* **1999**, *27*, 389-395.
- (159) *Why are we performing Reversed Phase HPLC as a standard purification?*; Thermo Electron GmbH **2004**;
http://www.thermo.com/eThermo/CMA/PDFs/Various/File_19397.pdf. (in possession of the author).
- (160) Qiu, X. Y.; Wu, L. Y.; Huang, H. S.; McDonel, P. E.; Palumbo, A. V.; Tiedje, J. M.; Zhou, J. Z. *Evaluation of PCR-generated chimeras, mutations, and heteroduplexes with 16S rRNA gene-based cloning*. *Appl. Environ. Microbiol.* **2001**, *67*, 880-887.
- (161) Del Tito, B. J.; Poff, H. E.; Novotny, M. A.; Cartledge, D. M.; Walker, R. I.; Earl, C. D.; Bailey, A. L. *Automated fluorescent analysis procedure for enzymatic mutation detection*. *Clin. Chem.* **1998**, *44*, 731-739.
- (162) Demchinskaya, A. V.; Shilov, I. A.; Karyagina, A. S.; Lunin, V. G.; Sergienko, O. V.; Voronina, O. L.; Leiser, M.; Plobner, L. *A new approach for point mutation detection based on a ligase chain reaction*. *J. Biochem. Biophys. Methods* **2001**, *50*, 79-89.
- (163) Oleykowski, C. A.; Bronson Mullins, C. R.; Godwin, A. K.; Yeung, A. T. *Mutation detection using a novel plant endonuclease*. *Nucleic Acids Res.* **1998**, *26*, 4597-4602.
- (164) Buck, G. A.; Fox, J. W.; Gunthorpe, M.; Hager, K. M.; Naeve, C. W.; Pon, R. T.; Adams, P. S.; Rush, J. *Design Strategies and Performance of Custom DNA Sequencing Primers*. *Biotechniques* **1999**, *27*, 528-536.
- (165) Rivkin, M. I. *XcmI-Containing Vector for Direct Cloning of PCR products*. *Biotechniques* **1997**, *22*, 812-814.
- (166) Snyder, W. B.; Silhavy, T. J. *Beta-Galactosidase is inactivated by Intermolecular Disulfide Bonds and is Toxic when Secreted to the periplasm of Escherichia Coli*. *J. Bacteriol.* **1995**, *177*, 953-963.

- (167) Domingues, L.; Teixeira, J. A.; Penttilä, M.; Lima, N. *Construction of a flocculent Saccaromyces Cerevisiae strain secreting high levels of Aspergillus Niger beta-Galactosidase*. Appl. Microbiol. Biotechnol. **2002**, *58*, 645-650.
- (168) Moller, P. L.; Jorgensen, F.; Hansen, O. C.; Madsen, S. M.; Stougaard, P. *Intra- and Extracellular beta-Galactosidases from Bifidobacterium bifidum and B infantis: Molecular Cloning, Heterologous Expression, and Comparative Characterization*. Appl. Environ. Microbiol. **2001**, *67*, 2276-2283.
- (169) Jorgensen, F.; Hansen, O. C.; Stougaard, P. *High-efficiency synthesis of oligosaccharides with a truncated beta-galactosidase from Bifidobacterium bifidum*. Appl. Microbiol. Biotechnol. **2001**, *57*, 647-652.
- (170) Altschul, S. F.; Gish, W.; Miller, W.; Meyers, E. W.; Lipman, D. J. *Basic local alignment search tool*. J. Mol. Biol. **1990**, *215*, 403-410.
- (171) Kölchens, S.; Ramaswami, V.; Birgenheier, J.; Nett, L.; O'Brien, D. F. *Quasi-elastic light-scattering determination of the size distribution of extruded vesicles*. Chem. Phys. Lipids **1993**, *65*, 1-10.
- (172) Higashi, K.; Suzuki, S.; Fujii, H.; Kirino, Y. *Preparation and Some Properties of Giant Liposomes and Proteoliposomes*. J. Biochem. (Tokyo). **1987**, *101*, 433-440.
- (173) Tieleman, D. P.; Marrink, S. J.; Berendsen, H. J. *A computer perspective of membranes: molecular dynamics studies of lipid bilayer systems*. Biochim. Biophys. Acta **1997**, *1331*, 235-270.
- (174) Koynova, R.; Caffrey, M. *Phases and phase transitions of the phosphatidylcholines*. Biochim. Biophys. Acta **1998**, *1376*, 91-145.
- (175) Prasad, R. *Manual on Membrane Lipids*; Springer: Berlin, 1996.
- (176) Traikia, M.; Warschawski, D. E.; Recouvreux, M.; Cartaud, J.; Devaux, P. F. *Formation of unilamellar vesicles by repetitive freeze-thaw cycles: characterization by electron microscopy and ³¹P-nuclear magnetic resonance*. Eur. Biophys. J. **2000**, *29*, 184-195.
- (177) Chen, P. S.; Toribara, T. Y.; Warner, H. *Microdetermination of Phosphorus*. Anal. Chem. **1956**, *28*, 1756.
- (178) Xi, Z.; Gilbert, A. *Improved procedures for the determination of lipid phosphorus by malachite green*. J. Lipid Res. **1992**, *33*, 1233.
- (179) Chalvardjian, A.; Rudnicki, E. *Determination of lipid phosphorus in the nanomolar range*. Anal. Biochem. **1970**, *36*, 225-226.
- (180) Itaya, K.; Ui, M. *A new micromethod for the colorimetric determination of inorganic phosphate*. Clin. Chim. Acta **1966**, *14*, 361-366.
- (181) Kyaw, A.; Maung, U. K.; Toe, T. *Determination of inorganic phosphate with molybdate and Triton X-100 without reduction*. Anal. Biochem. **1985**, *145*, 230-234.
- (182) de Groot, H.; Noll, T. *Enzymic determination of inorganic phosphates, organic phosphates and phosphate-liberating Enzymes by use of nucleoside phosphorylase*

- xanthine oxidase (dehydrogenase)-coupled reactions*. *Biochem. J.* **1985**, *230*, 255-260.
- (183) Takayama, M.; Itoh, S.; Nagasaki, T.; Tanimizu, I. *New Enzymatic Method for Determination of Serum Choline-Containing Phospholipids*. *Clin. Chim. Acta* **1977**, *79*, 93-98.
- (184) Zuidam, N. J.; Gouw, H. K.; Barenholz, Y.; Crommelin, D. J. *Physical (in) stability of liposomes upon chemical hydrolysis: the role of lysophospholipids and fatty acids*. *Biochim. Biophys. Acta* **1995**, *1240*, 101-110.
- (185) Pietzyk, B.; Henschke, K. *Degradation of phosphatidylcholine in liposomes containing carboplatin in dependence on composition and storage conditions*. *Int. J. Pharm.* **2000**, *196*, 215-218.
- (186) Hung, H. C.; Chang, G. G. *Differentiation of the slow-binding mechanism for magnesium ion activation and zinc ion inhibition of human placental alkaline phosphatase*. *Protein Sci.* **2001**, *10*, 34-45.
- (187) Mestrovic, V.; Pavela-Vrancic, M. *Inhibition of alkaline phosphatase activity by okadaic acid, a protein phosphatase inhibitor*. *Biochimie* **2003**, *85*, 647-650.
- (188) Wennberg, C.; Kozlenkov, A.; Di Mauro, S.; Frohlander, N.; Beckman, L.; Hoylaerts, M. F.; Millan, J. L. *Structure, genomic DNA typing, and kinetic characterization of the D allozyme of placental alkaline phosphatase (PLAP/ALPP)*. *Hum. Mutat.* **2002**, *19*, 258-267.
- (189) O'Brien, P. J.; Herschlag, D. *Alkaline phosphatase revisited: hydrolysis of alkyl phosphates*. *Biochemistry* **2002**, *41*, 3207-3225.
- (190) Stinson, R. A.; Gainer, A. L.; Chai, J.; Chan, J. A. *Substrate specificity of alkaline phosphatase from human polymorphonuclear leukocytes*. *Clin. Chim. Acta* **1986**, *161*, 283-291.

ACKNOWLEDGMENTS

The work on this thesis was carried out in the Max-Planck-Institute for Biochemistry in Munich, under the supervision of Prof. Dr. Peter Fromherz.

I am deeply indebted to:

Prof. Dr. Peter Fromherz for creative and continuous supervision, incredible support, superb ideas and the development of the theoretical model describing enzyme induced staining (cf. section 5.5).

Prof. Dr. Thorsten Bach for his generous readiness to be a referee of this work.

Dr. Gerd Hübener with assistants Stephanie Stumhofer, Sonja Golla and Birgit Haringer for the synthesis of the dyes and the fruitful collaboration.

Michaela Morawetz for never-tiring technical assistance in molecular biology, cell biology and spectroscopy.

Doris Eckerlein and Heidi Simeunovic for cell culturing.

Monika Negenborn for dealing with the bureaucratic matters of science.

Dr. Christian Figger-Reccius for quick and expert programming of labview programs used in this work, for helpful advice and help in diverse matters as well as for interesting discussions and friendship.

Dr. Max Ulbrich for interesting discussions and help on mathematica programming.

Dr. Raimund Gleixner for help on dye orientation experiments and jelly smurfs.

Dr. Armin Lambacher for help and discussions regarding all topics of spectroscopy and his readiness to help in many other matters of science, including critical reading.

Dr. Evgeny Zaichikov for performing the autoradiographic PAGE of oligonucleotides,

Dr. Bernd Kuhn for teaching me to patch and for interesting discussions,

Janosch Lichtenberger, Ingmar Peitz, Alexander Kaul, Dr. Matthias Brittinger-Python, Evgeny Gutyrchik, and Frank Wallrapp for discussions as well as for help in „smaller“ matters.

Many people outside of our department were of invaluable aid to me, among those:

Dr. Tanja Buesgen and Dr. Matthias Grimmmler for their patient and especially helpful advice for a molecular and cell biology newcomer – I kept coming and they almost never complained,

Dr. Matthias Grimmmler in addition for critical reading,

Elisabeth „Lissy“ Weyher-Stingl for her knowledgeable and motivated help in HPLC and ITC,

Anna Le Bris and Peter Reichelt for teaching me SDS-PAGE and Western Blotting,

ACKNOWLEDGMENTS

Prof. Dr. Frauke Melchior for helpful advice and the permission to use her department's equipment (and to tap the knowledge of her group's people),

Dr. med. Monika Sommer for taking the blood samples,

Florian Kiendl, Annette Flotho, Dr. Erik Schleicher, Dr. Susanne Witt, Dr. Matthias Pfeiffer and Dr. Uwe Köhler for molecular, gene synthesis and cell biology advice,

Dr. Ina Hinner, Dr. Michael J. Blackman, Dr. Felicity Dunlop, Prof. Gunnar von Heijne, Dr. Susanne Witt, Dr. Bernd Lorenz, Dr. Peter Stougaard, Dr. Jürgen Kupper, Dr. Nick Housby, Prof. Reinhardt Fässler for advice via email and/or donation of constructs,

Scott Bruce Balaban for english proofreading,

Ricarda Henke for her loving support in the last years,

And finally,

Maria Hinner-Kärtner and Harald Hinner for their mental and financial support during the last thirty years and for being there all my life.